



Marisa Abreu Rodrigues

**HIGH-THROUGHPUT SCREENING OF HYDROCHLOROTHIAZIDE
COCRYSTALS BY VIBRATIONAL SPECTROSCOPY**

Dissertação do 2º Ciclo de Estudos Conducente ao Grau de Mestre em Controlo
de Qualidade na especialidade de Fármacos e Plantas Medicinais

Trabalho realizado sob orientação de:
Doutora Mafalda Cruz Sarraguça

julho
2019

É autorizada a reprodução integral desta tese apenas para efeitos de investigação, mediante declaração escrita do interessado que a tal se compromete.

Marisa Abreu Rodrigues

ACKNOWLEDGEMENTS

No final deste intenso percurso, com um misto de sentimentos no coração, gostava humildemente de agradecer a todas as pessoas que tornaram possível este trabalho. Se o consegui foi graças à sua ajuda, preocupação, dedicação, afeto e humanidade.

Agradeço, antes de mais, à pessoa mais ativa nesta minha jornada, sem a qual este trabalho não seria possível, nem tão construtivo quanto foi. Obrigada, Mafalda, não só pelo teu bom profissionalismo, por toda a ajuda, sugestões e tempo despendido em mim. Mas, sobretudo, agradeço por demonstrares genuína preocupação por mim, por partilhares comigo as felicidades e infelicidades deste trabalho e pelo apoio que sempre me deste.

Agradeço ao grupo de Química Aplicada e à Faculdade de Farmácia da Universidade do Porto, por me permitirem desenvolver este trabalho.

Agradeço ao Professor João Lopes da Faculdade de Farmácia da Universidade de Lisboa e à sua equipa pela disponibilidade e ajuda para o desenvolvimento do trabalho em DSC aqui apresentado.

Agradeço ao Professor João Figueirinhas e Carlos Cruz do Instituto Superior Técnico por disponibilizarem o equipamento PXRD e por toda a preocupação e ajuda.

Agradeço a Professora Alexandra Guedes da Faculdade de Ciências da Universidade do Porto por disponibilizar o equipamento de microespetroscopia Raman e por toda a preocupação e ajuda.

Agradeço à Anton Paar (<https://www.anton-paar.com/corp-en/>) e à MTBrandão (<http://www.mtbrandao.com/>) por providenciarem o espectrómetro Raman.

Um obrigada a todos os membros da unidade LAQV-REQUIMTE da Faculdade de Farmácia da Universidade do Porto que, de uma forma ou de outra, tornaram a minha estadia mais agradável. Agradeço à D. Manuela e à Vânia, por fazerem tudo funcionar nestes laboratórios, mesmo quando não parece possível.

Um especial agradecimento à acolhedora equipa da unidade SpeChem com quem tive o prazer de trabalhar.

Muito obrigada às meninas do mestrado em Controlo de Qualidade, Adelaide, Flávia e Sarah, que me acompanharam ao longo deste percurso e nunca me falharam com um bom conselho.

Às minhas companheiras da casa, Kata e Joana, obrigada pelos bons serões depois de longos dias de trabalho.

Um muito especial agradecimento aos amigos que esta cidade me deu, Alice, Ana Gomes, Ana Moura, Beatriz, João e Samuel. Espero que continuemos a partilhar e enfrentar juntos todas as jornadas que nos advém.

Às minhas amigas de infância, Inês, Lau, Márcia e Susana, agradeço imensamente por me terem acompanhado em mais uma superação, como sempre o têm feito. Que a distância nunca nos separe.

Ao Tiago, um especial agradecimento, pelo apoio incondicional, por toda a ajuda, por acreditar em mim, por estar sempre presente na minha vida, mesmo estando longe. Pela contínua demonstração de amor, obrigada.

E, finalmente, agradeço à minha família, que sempre foi o meu suporte, o meu porto de abrigo. Sem vocês, nunca teria conseguido. Obrigada, pai, mãe e Simão, espero que se orgulhem de mim como eu sempre me orgulhei de vocês.

ABSTRACT

A recurrent problem faced by the pharmaceutical industry is new active pharmaceutical ingredients (APIs) that display desirable pharmaceutical activity but unfavorable physicochemical properties, such as solubility and bioavailability. Cocrystals, which are crystalline materials comprising at least two components, solid at room temperature and held together by non-covalent bonds, are growing up as a possible approach to overcome this problem. The increasing interest on these compounds is steadily demanding faster, simpler and more reliable methods for screening new cocrystals.

In this work, a high-throughput screening procedure is performed using 96-well plates, through an ultrasound assisted cocrystallization method. Hydrochlorothiazide (HTZ) was the API used and eleven different coformers were tested in two different API:coformer ratios (1:1 and 1:2) and nine solvents. The cocrystallization products were analyzed at-line by near and mid infrared spectroscopy and Raman spectroscopy and *in-situ* by Raman microspectroscopy.

Vibrational spectroscopy techniques with multivariate analysis were able to provide information regarding to API:coformer ratio and solvent with the greatest performance. Despite of being performed at-line, mid infrared spectroscopy was the technique that provided more valuable and complete information, about API:coformer ratio, solvent influence and chemical groups involved on cocrystal formation. Other techniques fail presenting information, mainly regarding to groups involved in cocrystal and to samples with fluorescence problems.

A cocrystallization by solvent evaporation was made to obtain cocrystals in a higher scale and with high purity to be further characterized by vibrational spectroscopy techniques, differential scanning calorimetry and powder X-ray diffraction and to perform solubility assays. Three new cocrystals with tromethamine, adenine and D(-)-mannitol as coformers were obtained and characterized. Also, cocrystals with nicotinamide and *p*-aminobenzoic acid were produced and new information about their apparent solubility was obtained. All the cocrystals improved API's solubility. Cocrystal with tromethamine presents the higher apparent solubility value, improving solubility in 1.7 fold. A crystalline-amorphous hydrated mixture between L(+)-arginine in amorphous form and HTZ in crystalline form was obtained and apparent solubility value is one of the highest of the tested systems, with an increase of 1.4 fold for the 1:2 ratio.

Keywords: hydrochlorothiazide, cocrystal, high-throughput screening, vibrational spectroscopy

RESUMO

Na indústria farmacêutica, os ingredientes farmacêuticos ativos com uma atividade desejada, porém, com propriedades físico-químicas desfavoráveis, tais como, solubilidade e biodisponibilidade, são um recorrente problema. Os cocristais, que são materiais cristalinos constituídos por pelo menos dois componentes, sólidos à temperatura ambiente e ligados por ligações não covalentes, estão a crescer como uma possível solução para ultrapassar este problema. Desta forma, é essencial o desenvolvimento de métodos de triagem mais rápidos, simples e fidedignos para rastrear novos cocristais.

Neste trabalho, é aplicado um método de triagem de alto rendimento com placas de 96 poços, usando o método de cocrystalização assistida por ultrassons. O ingrediente farmacêutico ativo usado foi a hidroclorotiazida, que foi testada com onze coformadores em duas proporções diferentes (1:1 e 1:2) e nove solventes. Os produtos da cocrystalização foram analisados at-line por espectroscopia no infravermelho médio e próximo, espectroscopia Raman e *in-situ* por microespectroscopia Raman.

As técnicas de espectroscopia vibracional, juntamente com análise multivariada, foram capazes de providenciar informação quanto à proporção de ingrediente ativo e coformador e ao solvente com melhor desempenho. Apesar de ser realizada at-line, a espectroscopia no infravermelho médio foi a técnica que forneceu informação mais completa acerca das proporções do cocrystal e da sua pureza, da influência do solvente e dos grupos químicos envolvidos na formação do cocrystal. As outras técnicas apresentaram falhas, por exemplo, quanto aos grupos químicos envolvidos na formação do cocrystal e no que toca a amostras que apresentam problemas de fluorescência.

Para obter os cocristais em maior quantidade e com uma maior pureza, aplicou-se o método de cocrystalização por evaporação de solvente e os seus produtos foram caracterizados por técnicas de espectroscopia vibracional, calorimetria diferencial de varrimento e difração de raios X de pós e submetidos a ensaios de solubilidade. Foram obtidos e caracterizados três novos cocristais com os coformadores trometamina, adenina e D(-)-manitol. Também foram produzidos cocristais com nicotinamida e ácido *p*-aminobenzóico e nova informação quanto à sua solubilidade foi obtida. Todos os cocristais melhoraram a solubilidade do ingrediente ativo. O cocrystal com trometamina apresentou a maior solubilidade aparente, melhorando a solubilidade 1.7 vezes. Uma mistura cristalino-amorfa hidratada foi produzida com o coformador L(+)-arginina, cuja solubilidade foi uma das maiores, com um aumento de 1.4 vezes para a proporção de 1:2

Palavras-chave: hidroclorotiazida, cocrystal, triagem de alto rendimento, espectroscopia vibracional

CONTENTS

Acknowledgements	iv
Abstract.....	vi
Resumo.....	vii
Contents.....	viii
List of figures.....	xi
List of tables	xvi
List of abbreviation	xvii
1. Motivation, Objectives and Outline	1
1.1. Motivation.....	1
1.2. Objectives	2
1.3. Outline	3
2. Introduction	4
2.1. Solid forms	4
2.1.1. Cocrystal's definition and structure.....	6
2.1.2. Regulatory framework	8
2.1.3. Cocrystal's market.....	10
2.2. Cocrystallization methods	11
2.2.1. Cocrystallization from solution.....	14
2.2.2. Slurry cocrystallization	15
2.2.3. Ultrasound-assisted cocrystallization.....	16
2.3. Cocrystal development.....	17
2.3.1. Cocrystal design	17
2.3.2. Cocrystal screening.....	18
2.4. Cocrystals properties	20
2.4.1. Solubility	21
2.5. Cocrystal characterization	23
2.5.1. Vibrational spectroscopy	23

i.	Theory	24
ii.	Instrumentation.....	24
iii.	Near infrared spectroscopy.....	25
iv.	Mid infrared spectroscopy	27
v.	Raman spectroscopy	29
vi.	Vibrational spectroscopy in cocrystal development	30
2.5.2.	Differential scanning calorimetry	32
2.5.3.	Powder X-ray diffraction	32
2.6.	Multivariate data analysis	35
2.6.1.	Pre-processing methods	35
2.6.2.	Principal component analysis	36
2.6.3.	Hierarchical cluster analysis	37
2.7.	Hydrochlorothiazide	38
2.7.1.	Mechanism of action	38
2.7.2.	Hydrochlorothiazide in the treatment of hypertension.....	38
2.7.3.	Absorption, metabolism and excretion.....	39
2.7.4.	Hydrochlorothiazide cocrystals.....	39
3.	Materials and methods	42
3.1.	Materials	42
3.2.	Cocrystallization methods	43
3.2.1.	Screening experiments	43
3.2.2.	Laboratory-scale experiments	45
3.3.	Characterization methods	48
3.3.1.	Mid Infrared spectroscopy	48
3.3.2.	Near Infrared spectroscopy	49
3.3.3.	Raman spectroscopy	49
3.3.4.	Raman microspectroscopy	50
3.3.5.	Differential scanning calorimetry	50
3.3.6.	Powder X-ray diffraction.....	51

3.3.7.	Solubility assays	52
3.4.	Data analysis	54
4.	Results and discussion.....	55
4.1.	Cocrystals screening.....	55
4.1.1.	Cocrystal screening experiments: part I	55
i.	Hydrochlorothiazide: tromethamine (HTZ:Tris)	56
ii.	Hydrochlorothiazide: DL-malic acid (HTZ:Mal).....	62
iii.	Hydrochlorothiazide: citric acid (HTZ:Cit).....	66
iv.	Hydrochlorothiazide: D(-)-mannitol (HTZ:Man).....	70
4.1.2.	Cocrystal screening experiments: part II	74
i.	Hydrochlorothiazide: L(+)-arginine systems (HTZ:Arg)	74
ii.	Hydrochlorothiazide: nicotinamide systems (HTZ:Nic)	76
iii.	Hydrochlorothiazide: <i>p</i> -aminobenzoic acid systems (HTZ:PABA)	79
iv.	Hydrochlorothiazide: citric acid systems (HTZ:Cit)	82
4.1.3.	Screening experiments resume.....	83
4.2.	Laboratory-scale experiments	84
4.2.1.	Hydrochlorothiazide: adenine system (HTZ:Ade)	87
4.2.2.	Hydrochlorothiazide: L(+)-arginine system (HTZ:Arg).....	90
4.2.3.	Hydrochlorothiazide: citric acid system (HTZ:Cit)	93
4.2.4.	Hydrochlorothiazide: D(-)-mannitol systems (HTZ:Man)	96
4.2.5.	Hydrochlorothiazide: nicotinamide systems (HTZ:Nic)	99
4.2.6.	Hydrochlorothiazide: <i>p</i> -aminobenzoic acid systems (HTZ:PABA).....	101
4.2.7.	Hydrochlorothiazide: tromethamine systems (HTZ:Tris)	103
4.3.	Solubility assays.....	106
5.	Conclusion and future perspectives.....	111
6.	References.....	115

LIST OF FIGURES

Figure 1: Structure of the amorphous form and the crystalline forms: salt, polymorphs, solvate and cocrystal (adapted from Schultheiss and Newman ⁽²²⁾).	5
Figure 2: Cocrystallization main products, namely: physical mixture, cocrystal with respective solvate and polymorph, eutectics, single components crystals and component amorphization.	11
Figure 3: Illustrative scheme representing the different stages of cocrystal development (adapted from Duggirala <i>et al.</i> ⁽⁸⁴⁾).	17
Figure 4: Most common chemical groups active in the NIR region, divided in the combination and overtones regions.	26
Figure 5: Most common chemical groups active in the MIR region, divided in the functional group and fingerprint regions.	28
Figure 6: PXRD equipment with the X-ray tubeshield transmitter (a) , the distance ring sample container (b) , detector (c) and the temperature variation chamber (d) .	33
Figure 7: PXRD command module with the detector monitoring and temperature chamber control module (a) and the high voltage generator module (b) .	34
Figure 8: Illustrative scheme DCT as a part of the nephron (left) and of electrolytes transport in a cell of the DCT and representation of the thiazides action on Na ⁺ /Cl ⁻ symporter (right) (adapted from Kester, M. <i>et al.</i> ⁽¹³³⁾).	38
Figure 9: Hydrochlorothiazide structure, with primary sulfonamide group (red circle) and secondary sulfonamide group (blue circle) (Image adapted from PubChem ⁽¹³⁹⁾).	40
Figure 10: Coformers' chemical structure: a) adenine (Ade), b) p-aminobenzoic acid (PABA), c) L-ascorbic acid (Asc), d) L(+)-arginine (Arg), e) caffeine (Caf), f) citric acid (Cit), g) DL-malic acid (Mal), h) D(-)-mannitol (Man), i) nicotinamide (Nic), j) L-tryptophan (Tryp), l) tromethamine (Tris). (Images retrieved from PubChem ⁽¹³⁹⁾).	42
Figure 11: Schematic representation of the 96-well plate with coformers and solvents distribution used in the first cocrystal screening experiment.	44
Figure 12: Schematic representation of the 96-well plate with coformers and solvents distribution used in the second cocrystal screening experiment.	44
Figure 13: Experimental setup of cocrystallization through slurry using a shaker water bath, with horizontal shaking and temperature control (A) ; solvent evaporation method setup using the orbital shaking at room temperature (B) ; solvent evaporation method setup using the orbital shaking and a water bath with temperature control (C) .	46
Figure 14: FT-MIR equipment with ATR accessory (Frontier, PerkinElmer), where samples are directly placed, pressed with a pressure element and measure.	48

- Figure 15:** FT-NIR equipment with sample placed in the accessory of powder measurement (FTLA2000, ABB)..... 49
- Figure 16:** Raman portable spectrometer (right), connected with a computer (left) (Cora 5X00 Raman spectrometer, Anton Paar)..... 50
- Figure 17:** DSC equipment with autosampler accessory (DSC 200 F3 Maia®, Netzsch-Gerätebau GmbH)..... 51
- Figure 18:** Sample assembly process, that start with partial removal of the sample container movable part **(1)**, capillary placement **(2)** and complete SCMP removal for capillary alignment capillary with the help of the apparatus **(3)** constituted by SCMP locking support equipment **(a)** and calibration monocle **(b)**. Alignment is done by observation **(4)** and, finally, sample container movable part is replaced into the sample container fixed part **(5)**. 52
- Figure 19:** Setup of solubility experiments, where is visible the water bath with the heating thermostat and the flask with the solution being stirred. 53
- Figure 20:** Sequential illustration of the steps involved in the work and characterization technique used in each phase. 55
- Figure 21:** Principal components for the system HTZ:Tris 1:1 obtained from a PCA model resorting to **(a)** MIRS spectra; **(b)** NIRS spectra and **(c)** RS spectra. Colors refer to different solvents (dark green: MeOH; pink: EtOH; red: Ace; green: DCM; dark blue: DMSO; blue: EtOAc; yellow: H₂O; dark red: PM). 57
- Figure 22:** **(a)** PCA score plot constructed with the MIRS spectra from the system HTZ:Tris 1:2. Colors refer to different solvents (dark green: MeOH; pink: EtOH; red: Ace; green: DCM; dark blue: DMSO; blue: EtOAc; yellow: H₂O; dark red: PM); **(b)** MIRS spectra of the samples produced with EtOH (blue), DCM (pink) and EtOAc (grey) and from the PM (black)..... 59
- Figure 23:** **(a)** PCA score plot constructed with the NIRS spectra from the system HTZ:Tris 1:2. Colors refer to different solvents (dark green: MeOH; pink: EtOH; red: Ace; green: DCM; dark blue: DMSO; blue: EtOAc; yellow: H₂O; dark red: PM); **(b)** NIRS spectra of the samples produced with EtOH (blue), DCM (pink) and EtOAc (grey) and from the PM (black);..... 60
- Figure 24:** **(a)** PCA score plot constructed with the RS spectra from the system HTZ:Tris 1:2. Colors refer to different solvents (dark green: MeOH; pink: EtOH; red: Ace; green: DCM; dark blue: DMSO; blue: EtOAc; yellow: H₂O; dark red: PM). **(b)** RS spectra of the samples produced with EtOH (blue), DCM (pink) and EtOAc (grey) and from the PM (black)..... 61
- Figure 25:** **(a)** PCA score plot constructed with the MIRS spectra from the system HTZ:Mal 1:2. Colors refer to different solvents (dark green: MeOH; pink: EtOH; red: Ace; green: DCM; dark blue: DMSO; blue: EtOAc; yellow: H₂O; dark red: PM); **(b)** MIRS spectra of the samples produced with DCM (pink) and EtOAc (grey) and from the PM (black). 63
- Figure 26:** **(a)** PCA score plot constructed with the NIRS spectra from the HTZ:Mal 1:2. Colors refer to different solvents (dark green: MeOH; pink: EtOH; red: Ace; green: DCM;

dark blue: DMSO; blue: EtOAc; yellow: H₂O; dark red: PM); **(b)** NIRS spectra of the samples produced with Ace (blue) and EtOAc (grey) and from the PM (black); 64

Figure 27: **(a)** PCA score plot constructed with the RS spectra from the HTZ:Mal 1:2. Colors refer to different solvents (dark green: MeOH; pink: EtOH; red: Ace; green: DCM; dark blue: DMSO; blue: EtOAc; yellow: H₂O; dark red: PM). **(b)** RS spectra of the samples produced with Ace (blue) and EtOAc (grey) and from the PM (black)..... 65

Figure 28: **(a)** PCA score plot constructed with the MIRS spectra from the system HTZ:Cit 1:2. Colors refer to different solvents (dark green: MeOH; pink: EtOH; red: Ace; green: DCM; dark blue: DMSO; blue: EtOAc; yellow: H₂O; dark red: PM); **(b)** MIRS spectra of the samples produced with DMSO (green) and EtOAc (grey) and from the PM (black). 67

Figure 29: **(a)** PCA score plot constructed with the NIRS spectra from the system HTZ:Cit 1:2. Colors refer to different solvents (dark green: MeOH; pink: EtOH; red: Ace; green: DCM; dark blue: DMSO; blue: EtOAc; yellow: H₂O; dark red: PM); **(b)** NIRS spectra of the samples produced with DMSO (green) and EtOAc (grey) and from the PM (black). 68

Figure 30: **(a)** PCA score plot constructed with the RS spectra from the system HTZ:Cit 1:2. Colors refer to different solvents (dark green: MeOH; pink: EtOH; red: Ace; green: DCM; dark blue: DMSO; blue: EtOAc; yellow: H₂O; dark red: PM); **(b)** RS spectra of the samples produced with DMSO (green) and EtOAc (grey) and from the PM (black). 69

Figure 31: **(a)** PCA score plot constructed with the MIRS spectra from the system HTZ:Man 1:2. Colors refer to different solvents (dark green: MeOH; pink: EtOH; red: Ace; green: DCM; dark blue: DMSO; blue: EtOAc; yellow: H₂O; dark red: PM); **(b)** MIRS spectra of the samples produced with MeOH (red) and EtOAc (grey) and from the PM (black). 71

Figure 32: **(a)** PCA score plot constructed with the NIRS spectra from the HTZ:Man 1:2. Colors refer to different solvents (dark green: MeOH; pink: EtOH; red: Ace; green: DCM; dark blue: DMSO; blue: EtOAc; yellow: H₂O; dark red: PM). **(b)** NIRS spectra of the samples produced with MeOH (red) and DCM (pink) and from the PM (black). 72

Figure 33: **(a)** PCA score plot constructed with the RS spectra from the HTZ:Man 1:2. Colors refer to different solvents (dark green: MeOH; pink: EtOH; red: Ace; green: DCM; dark blue: DMSO; blue: EtOAc; yellow: H₂O; dark red: PM). **(b)** RS spectra of the samples produced with MeOH (red) and DCM (pink) and from the PM (black). 73

Figure 34: Dendrogram from the HCA performed with MIR spectra obtained from systems HTZ:Arg 1:2, the PM, arginine and HTZ. 74

Figure 35: MIR **(a)** and RMS **(b)** spectra from the cocrystallization product of HTZ:Arg 1:2 with IPro (brown), PM (black), HTZ (blue) and Arg (red)..... 76

Figure 36: Selected region of MIR spectra from the HTZ:Nic 1:1 IPro (brown dashed), HTZ:Nic 1:2 IPro (brown), pure Nic (red) and pure HTZ (blue). 76

Figure 37: Dendrogram from the HCA performed with the MIR spectra of the systems HTZ:Nic 1:1.....	77
Figure 38: MIR (a) and RMS (b) spectra from the cocrystallization product of HTZ:Nic 1:1 IPro (brown), and respective PM (black) and 1:2 (black).	78
Figure 39: MIR spectra from the cocrystallization product of HTZ:PABA 1:1 Ace (orange dashed), HTZ:PABA 1:2 Ace (orange), pure PABA (red) and pure HTZ (blue).	79
Figure 40: (a) Dendrogram from the HCA made with the MIR spectra of the cocrystallization products of HTZ:PABA systems in both ratios, 1:1 and 1:2. (b) MIR spectra from the cocrystallization product of HTZ:PABA 1:2 Ace (orange), pure PABA (red), pure HTZ (blue) and PM (black).	80
Figure 41: RMS spectra from (a) the products of cocrystallization produced with IPro (brown), ACN (lilac), EtOH (pink), MeOH (green), WS (grey) and the PM (black); (b) the product of cocrystallization produced with Ace (orange).	81
Figure 42: (a) Dendrogram from the HCA made with the MIR spectra of the cocrystallization products of HTZ:Cit 1:2 systems. (b) MIR spectra of HTZ:Cit 1:2 systems with MeOH (green), PM (black), pure citric acid (red) and pure HTZ (blue).	82
Figure 43: MIR (a) and NIR (b) spectra of HTZ:Ade 1:2 cocrystal produced with DMSO (dark yellow) and the respective PM (black).	88
Figure 44: Thermogram of HTZ:Ade 1:2 cocrystal (dark yellow) and the respective PM (black).	89
Figure 45: Diffractogram of HTZ:Ade 1:2 cocrystal (dark yellow) and the respective PM (black).	89
Figure 46: Thermogram of the systems of HTZ:Arg 1:1 (orange) and 1:2 (orange dashed) and PMs of the HTZ:Arg 1:1 (black) and 1:2 (black dashed).	90
Figure 47: (a) MIR spectra of the product of HTZ:Arg 1:2 system (orange dashed), respective PM (black dashed), crystalline arginine (pink) and HTZ (blue); (b) MIR spectrum of amorphous arginine (green).	92
Figure 48: Diffractogram of the HTZ:Arg 1:2 system's product (orange dashed), respective PM (black dashed), pure HTZ (blue) and arginine (pink).	93
Figure 49: MIR (a) and NIR (b) spectra of scale up product of the HTZ:Cit 1:2 system (green), screening product of the same system (green dashed) and respective PM (black).	94
Figure 50: Thermogram of scale up product of the HTZ:Cit 1:2 system (green) and respective PM (black).	95
Figure 51: Diffractogram of scale up product of the HTZ:Cit 1:2 system (green) and respective PM (black).	96

Figure 52: (a) MIRS spectra of the HTZ:Man 1:1 (yellow) cocrystal, PM (black) system, pure D(-)-mannitol (pink) and HTZ (dark blue); **(b)** MIRS spectra of the HTZ:Man 1:2 (light blue) cocrystal, PM (black) system, pure D(-)-mannitol (pink) and HTZ (dark blue). 97

Figure 53: Thermograms of the HTZ:Man 1:1 (yellow) and 1:2 (light blue) cocrystal and PMs of the 1:1 (black) and 1:2 (dashed black) systems..... 98

Figure 54: Diffractogram of the HTZ:Man 1:1 (yellow) and 1:2 (light blue) cocrystal and PMs of the 1:1 (black) and 1:2 (dashed black) systems..... 99

Figure 55: MIR spectrum of HTZ:Nic 1:1 cocrystal produced in scale up (orange), of the same cocrystal produced in screening (brown) and of the PM (black). 100

Figure 56: Thermograms of the cocrystal of HTZ:Nic 1:1 (orange), HTZ:Nic 1:2 (orange dashed), PM 1:1 (black) and PM 1:2 (dark dashed)..... 100

Figure 57: Diffractogram of HTZ:Nic 1:1 cocrystal (orange) and respective PM (black).101

Figure 58: MIR spectra of the HTZ:PABA 1:2 cocrystals produced in scale up (green), produced in the screening (orange) and PM (black). 102

Figure 59: Thermograms of HTZ:PABA 1:2 cocrystal (green) and of the respective PM (black). 102

Figure 60: Diffractogram pattern of the HTZ:PABA 1:2 cocrystal (green) and of the respective PM (black). 103

Figure 61: MIR spectra of the HTZ:Tris 1:2 cocrystal produced in scale up phase (dark yellow), of cocrystal produced in screening phase with DMSO (dark yellow dashed) and with EtOAc (blue) and the PM (black). 104

Figure 62: Thermogram of the HTZ:Tris 1:2 cocrystal (dark yellow) and of the respective PM (black). 105

Figure 63: Diffractogram of the HTZ:Tris 1:2 cocrystal (dark yellow) and of the respective PM (black). 105

Figure 64: Calibration curve made with six solutions of known HTZ concentration, at the wavelength of 320 nm. 106

Figure 65 : (a) Solubility profile of all tested products during 24 hours. **(b)** Solubility profile of HTZ:Tris cocrystal during 48 hours and pure HTZ during 24 hours..... 107

LIST OF TABLES

Table 1: Most usual synthons, formed through hydrogen bonds, divided in homosynthons and heterosynthons. ⁽³²⁾	8
Table 2: Resumed information about FDA and EMA guidelines.....	9
Table 3: Resume of solvent-based cocrystallization methods, including their characteristics, advantages and disadvantages.....	13
Table 4: Resume of solvent-free cocrystallization methods, including their characteristics, advantages and disadvantages.....	14
Table 5: Most used cocrystal characterization techniques and evaluated aspects.	23
Table 6: Hydrochlorothiazide cocrystals described in literature, with resumed information about the cocrystallization method, synthons involved in the cocrystal and properties improved comparing with the API.....	41
Table 7: Systems tested through slurry cocrystallization method and respective solvent used.	45
Table 8: Systems, solvents, volume, and temperature used in the cocrystallization by solvent evaporation.	47
Table 9: Resume of screening results in terms of evidences of cocrystal formation. Preferred ratio (HTZ:coformer) and solvent are also presented.....	83
Table 10: Systems tested in laboratory-scale through solvent evaporation and techniques used for analyze each product.	85
Table 11: Data from DSC analysis with onset temperatures for each endothermic event observed and correspondent enthalpy. In the case of HTZ:Arg 1:1 and 1:2, glass transition temperature (T _g) is presented.	86
Table 12: Maximum apparent solubility values of each tested system, time of the measure and solubility increase fold when compared to HTZ solubility value.....	110

LIST OF ABBREVIATION

A - Absorbance
Ace - Acetone
ACN - Acetonitrile
Ade - Adenine
ANDA - Abbreviated New Drug Application
API - Active Pharmaceutical Ingredient
Arg - L(+)-Arginine
Asc - L-Ascorbic acid
ATR - Attenuated Total Reflectance
BCS - Biopharmaceutic Classification System
Caf - Caffeine
CCD - Charge Couple Devices
Cit - Citric acid
CPP - Critical Process Parameter
CSD - Cambridge Structural Database
DCM - Dichloromethane
DCT - Distal Convoluted Tubules
DMSO - Dimethyl sulfoxide
DPI - Drug Product Intermediate
DSC - Differential Scanning Calorimetry
DTGS - Deuterated Tryglycine Sulphate
EMA - European Medicine Agency
EtOAc - Ethyl acetate
EtOH - Ethanol
EU - European Union
FDA - Food and Drug Administration
FT - Fourier Transform
FT-MIR - Fourier Transform Mid Infrared
FT-NIR - Fourier Transform Near Infrared
GRAS - Generally Referred As Safe
HCA - Hierarchical Cluster Analysis
HSP - Hansen Solubility Parameters
HTS - High Throughput Screening
HTSE - High Throughput Screening Evaporative

HTZ - Hydrochlorothiazide
InGaAs - Indium Gallium Arsenide
IPro - 2-propanol
IR - Infrared
IUPAC - International Union of Pure and Applied Chemistry
LAG - Liquid Assisted Grinding
Mal - DL-Malic acid
Man - D(-)-Mannitol
MeOH - Methanol
MIR - Mid Infrared
MIRS - Mid Infrared Spectroscopy
NAS - New Active Substance
NDA - New Drug Application
Nic - Nicotinamide
NIR - Near Infrared
NIRS - Near Infrared Spectroscopy
PABA - *p*-aminobenzoic acid
PAT - Process Analytical Technology
PC - Principal Component
PCA - Principal Component Analysis
PM - Physical Mixture
PXRD - Powder X-Ray Diffraction
QbD - Quality by Design
R - Reflectance
RH - Relative Humidity
RMS - Raman Microspectroscopy
RS - Raman Spectroscopy
SCFP - Sample Container Fixed Part
SCMP - Sample Container Movable Part
SCXRD - Single Crystal X-Ray Diffraction
SMPT - Solution Mediated Phase Transformation
SNV - Standard Normal Variate
T - Transmittance
T* - Transflectance
THz - Terahertz
Tris - Tromethamine
Tryp - L-Tryptophan

USA - United States of America

UV - Ultraviolet

WHO - World Health Organization

WS - Without Solvent

1. MOTIVATION, OBJECTIVES AND OUTLINE

1.1. Motivation

Cocrystals have been gaining the interest in the academy and industry. This solid form is advantageous to improve physical and/or chemical properties, as solid form manipulation of APIs with low solubility, bioavailability, stability, or others.⁽¹⁻⁷⁾ However, cocrystallization full understanding is still necessary. Cocrystallization process is influenced by several factors, such as coformer choice, solvent, temperature, time, among others, which can impact the final product nature. A deeper comprehension of all of these aspects is of utmost importance.⁽⁸⁻¹⁰⁾

For industrial production of cocrystals, screening phase is essential, helping to become the process faster, more effective and efficient, reducing the quantity of reactants used and associated costs. High-throughput screening methods are capable of analyze a wide range of compounds simultaneously. Typical trial and error approaches are time consuming and usually more expensive, being a disadvantageous option to industrial production. As an answer to industrial necessity of more efficient screening methods, different methods must be developed and optimized.⁽¹¹⁾

Vibrational spectroscopic techniques are fast, non-destructive and non-invasive, do not need pre-treatment of the samples and allow to obtain qualitative and quantitative information. They are useful in cocrystal analysis, once they detect weak interaction as hydrogen bonding, the basis of cocrystal formation. Therefore, its application in cocrystal analysis, together with multivariate analysis, should be studied.^(6, 12-15)

The growing need of cocrystal screening methods for the discovery of new cocrystals with benefic properties and the use of advantageous characteristics of vibrational spectroscopy in these methods led to the following research work.

1.2. Objectives

This dissertation main objective is to develop a high-throughput cocrystal screening method based on vibrational spectroscopy. Screening methods must be efficient and require low quantities of reactants, allowing the analysis of a wide range of API:coformer systems and solvents at the same time. Additionally, the understanding on how the scale increase affect the outcome of the cocrystallization in comparison with the screening experiments.

In a more detailed point-by-point analysis the objectives are:

- To develop cocrystal screening methods that allow a high number of co-formers and solvents to be tested simultaneously.
- To apply different vibrational spectroscopic techniques, e.g., near and mid infrared spectroscopy and Raman spectroscopy to analyze the outcome of the cocrystallization.
- To verify if the vibrational spectroscopic techniques are able to detect cocrystal formation and cocrystal purity.
- To compare the vibrational spectroscopic techniques and to conclude which one is more helpful in the analysis of the products of cocrystallization in terms of information obtained and speed of the procedure.
- To apply multivariate data analysis methods to aid in the analysis of the spectroscopic data.
- To evaluate the effect of the change from screening experiments to laboratory-scale production.
- To produce cocrystal(s) with improved solubility.

It is expected that in the end of this dissertation a deeper knowledge in how vibrational spectroscopy can be helpful in the development of cocrystals from the screening phase until the laboratory-scale up phase.

1.3. Outline

The introduction, chapter 2, provides important information on cocrystals, cocrystallization methods, cocrystals screening methods, cocrystals properties and characterization techniques.

In chapter 3, materials used are identified, cocrystallization methodologies of screening experiments and scale increase experiments are described and all the used techniques for cocrystal characterization are specified.

In chapter 4, results of the experimental work are presented together with their discussion. This chapter is divided in three main sections:

- Section 4.1.: results of cocrystals screening are presented and discussed. This section is subdivided in the two parts. Each API:coformer system is evaluated as an individual case, showing data from vibrational spectroscopic techniques and multivariate analysis, and concluding about the cocrystal formation potentiality;
- Section 4.2.: results of laboratory-scale cocrystals production with a higher scale are presented and discussed. Results from the different characterization techniques are stated and the nature of the formed product is debated.
- Section 4.3.: solubility assays were performed on the selected products and results are showed in this section, discussing the influence of cocrystallization on the solubility of the API.

In chapter 5, conclusions are pinpointed and possible solutions to the questions that this work arise are presented as future perspectives.

The following publications are result of this dissertation work:

- Rodrigues, M., Baptista, B., Lopes, J. A., and Sarraguça, M. C., Pharmaceutical cocrystallization techniques. Advances and challenges, *International Journal of Pharmaceutics*, 2018. 547: p. 404–420;
- Rodrigues, M., Lopes, J., and Sarraguca, M., *Vibrational Spectroscopy for Cocrystals Screening. A Comparative Study*, *Molecules*, 2018. 23(12).
- Submitted to *Pharmaceutics*: Marisa Rodrigues, João Lopes, Jorge Sarraguça, Alexandra Guedes, Mafalda Sarraguça. Considerations regarding cocrystal screening by vibrational spectroscopy. Hydrochlorothiazide cocrystals screening as a case study.
- In preparation: Solid forms of HTZ with improve solubility: synthesis and full characterization.

2. INTRODUCTION

2.1. Solid forms

Generally, drug discovery and development process can be divided into five distinct stages: strategic research, exploratory research, candidate drug selection, exploratory development and full development. During this process, new active pharmaceutical ingredients (APIs) with desirable pharmaceutical activity but unfavorable properties, such as solubility and bioavailability, are a recurrent problem. For example, during candidate drug selection, solubility is a critical factor for the acceptability or not of the candidate drug and many drugs are refused, because of solubility problems. For an oral solid dosage form, a water-soluble, nonhygroscopic, stable, and easily processed crystalline compound is preferred for development purposes.

In order to solve this problem, a full comprehension about solid state forms of an API is necessary. Different solid forms have different physicochemical properties^(12-14, 16), such as solubility^(12, 13), dissolution rate, bioavailability, stability, processability and also different pharmacological activity⁽¹⁷⁾. Therefore, solid forms screening and selection are essential to achieve the most appropriate API's performance.

Solid forms can be crystalline or amorphous, depending on the extent of three-dimensional order and the relative thermodynamic stability hierarchy (Figure 1). Crystalline forms, which are a periodic array of molecules within a three-dimensional framework, are preferred due to inherent stability and facility to purify. However, crystalline forms usually have low solubility. Amorphous forms, which are materials that lack three-dimensional order, generally have higher solubility, but stability problems, since they tend to revert to the most stable form, the crystalline form.⁽¹⁸⁾

Crystalline forms have a structure influenced by intramolecular and intermolecular interactions. Intramolecular interactions are the ones that influence molecular shape and molecular pack in the crystal. Intermolecular interactions are weak forces and they influence the arrangement of molecules within molecular crystals, influencing also the behavior and properties of the material. Therefore, this is the basis of other solid forms formation, such as salts, polymorphs, solvates and cocrystals (Figure 1).⁽¹⁸⁾

Polymorphic compounds exhibit different stacking arrangements and molecular conformations within the crystal lattice, which means they can exist in various crystalline forms, maintaining the same chemical composition.^(19, 20) An API can have different polymorphs with different physicochemical and pharmaceutical properties, such as solubility, bioavailability, stability and hygroscopicity. Thus, polymorphism can affect the

quality, safety, and efficacy of the drug product, consequently, polymorphism control is essential during product life cycle.⁽¹⁹⁻²¹⁾

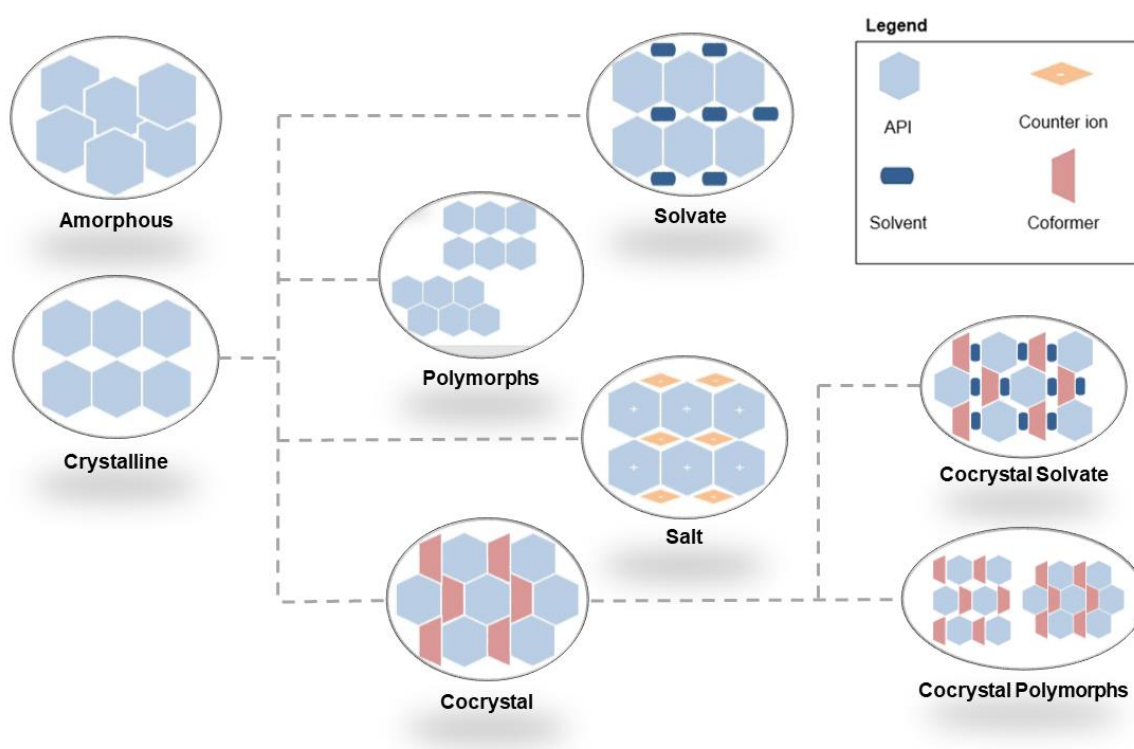


Figure 1: Structure of the amorphous form and the crystalline forms: salt, polymorphs, solvate and cocrystal (adapted from Schultheiss and Newman⁽²²⁾).

Salts are crystalline forms used in pharmaceutical industry to improved drug's properties, such as solubility. They are constituted by cations and anions, arranged in a crystal lattice through ion pairing. Acid-basic reactions are the base of salt formation, which involve complete proton transference.⁽²³⁾ The acidity or basicity of a drug can influence drug's solubility and, consequently, bioavailability. Once salt formation is based in proton transfer, it is restricted to APIs with one or more basic or acidic groups, which is a limitation.⁽²⁴⁾

Solvates are constituted by two or more compounds, one of them a solvent. Frequently, they are products formed during drug's manufacturing process, generally undesired. A hydrate is a type of solvate with water as a solvent.⁽²³⁾ Solvates can also modulate API's properties. However, solvates are not commonly used in pharmaceutical industry due to intrinsic toxicity of solvents used. Solvates are commonly unstable and they can lose the solvent molecule during processing, affecting physicochemical properties. For these reasons, study of solvates' properties and conditions that give origin to them are of highest importance and must be controlled.⁽²⁵⁾

In the last years, cocrystals have emerged as a crystalline form capable of improving API's properties. They have been extensively studied and used to improve API's solubility, stability and other properties. This crystalline form has several advantages in relation to

typical solid forms. Capability of properties manipulation, without limitation to ionizable compounds, generally forming stable products and other benefits can outcome from the use of cocrystals, which will be discussed in the following sections.

2.1.1. Cocrystal's definition and structure

Nomination of this crystalline structure has change along the years. It was called, for example, "molecular complexes", "multi-component molecular crystal" and "cocrystal". Stahly studied the evolution of cocrystals through a review work of the literature prior to the year 2000, where the nomenclature and classification problem can be widely notice.⁽²⁶⁾

Nowadays, according to European Medicine Agency (EMA), cocrystals are "homogenous (single phase) crystalline structures made up of two or more components in a definite stoichiometric ratio where the arrangement in the crystal lattice is not based on ionic bonds (as with salts)".⁽²³⁾

Cocrystal's components are, generally, an API and a cofomer. A cofomer is a compound generally referred as safe (GRAS), meaning that it must be pharmaceutically accepted, in terms of safety and quality. In European Union (EU), if the cofomer was never used before, it may be documented in the same way as for a novel excipient.⁽²³⁾

A cocrystal can also be composed for two APIs, instead of an API and a cofomer. This form is named drug-drug cocrystal and it is a feasible approach if both drugs have a combinatory or synergic effect. It can be an advantage in case of dual drugs therapy. An example is the drug-drug cocrystal composed by telmisartan and atenolol, which had shown improved antihypertensive activity at *in vivo* pharmacodynamics activity test.⁽²⁷⁾

Another possible cocrystal form is the nutraceutical cocrystal that is composed by the API and a nutraceutical molecule, which is considered part of a food with medical or health benefits. One example are nutraceutical cocrystals produced with caffeine and the APIs carbamazepine or pterostilbene.⁽⁷⁾

Cocrystals can have different polymorphs, which happen when the same cocrystal has different stacking arrangements and molecular conformations within the crystal lattice.^(13, 25) It is also possible to form a solvate of a cocrystal, which consist in the integration of a solvent in the crystal lattice of the cocrystal.⁽²⁵⁾

Noncovalent and nonionic interactions between the API and the cofomer are the base of cocrystal's structure, unlike salts, which are based on ion pairing. The interactions involved are intermolecular, such as Van der Waals contact forces, π stacking, hydrogen bonding, electrostatic interaction and halogen bonding, between stoichiometric amounts of the molecules.

The formation of a cocrystal or a salt is dependent of transfer extent of the proton, which is determined by pKa values of the compounds. If there is no complete proton transfer, a cocrystal is formed, and a salt is formed if the transfer is complete. Although, a definitive borderline between the salt formation or cocrystals formation does not exist, according to EMA.⁽²³⁾ Food and Drug Administration (FDA) states that cocrystal or salt formation should be proved by ΔpK_a^1 interpretation. When components have a $\Delta pK_a \geq 1$, a salt will be formed. If $\Delta pK_a < 1$, the complex should be classified as cocrystal. Nevertheless, crystallization environment is important to consider in this decision. For example, if cocrystallization is developed in organic solvents, pKa values can be considerable different than in water. Consequently, if there is a possibility of salt formation, different techniques must be used to clarify this subject, such as single crystal X-ray diffraction, vibrational spectroscopy, and nuclear magnetic resonance spectroscopy, among others.^(28, 29)

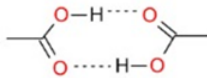
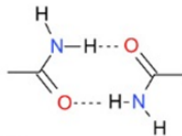
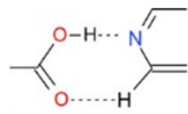
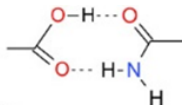
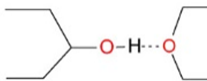
In solids like cocrystals, the single entity created by aggregation of molecules is termed supermolecule. Basic structural units within supermolecules are named supramolecular synthons. Supramolecular synthons are special arrangements of intermolecular interactions, which can be formed by known feasible operations.⁽³⁰⁾ Synthons are divided in two groups: homosynthon, which consist in combinations of similar functional groups; heterosynthon that is composed by different but complementary functional groups (Table 1).^(31, 32)

Crystal engineering works in this field, recognizing and designing synthons, with the goal of cocrystal fast and efficient development, trying to improve API's properties without affecting its intrinsic structure and function. Thus, alterations are made in crystal packing, by changing the internal arrangement of the molecules, breaking and forming noncovalent bonds.^(33, 34)

Etter's work showed the importance of hydrogen bonding in cocrystal formation and proved that supramolecular synthesis in the solid state provides a degree of molecular recognition and a diversity of products matching and even extending those observed in solution methods, demonstrating how grinding would cause hydrogen bonding.⁽³⁵⁾ Desiraju's work was also very relevant, expanding the crystal engineering and supramolecular synthons fields.⁽³⁰⁾ Supramolecular synthons understanding is been considered a requirement for cocrystal design and appropriate cofomers selection.

¹ $\Delta pK_a = pK_a(\text{base}) - pK_a(\text{acid})$

Table 1: Most usual synthons, formed through hydrogen bonds, divided in homosynthons and heterosynthons.⁽³²⁾

Homosynthons	
Carboxylic acid + carboxylic acid	
Amide + Amide	
Heterosynthons	
Carboxylic acid + Pyridine	
Carboxylic acid + Amide	
Ether + Alcohol	

2.1.2. Regulatory framework

The growing interest in cocrystals lead to the establishment of guidelines by the different regulatory agencies. In this thesis, focus is given to EMA and FDA, once they englobe the two main world markets, representing EU and United States of America (USA), respectively. Both agencies agree on the importance of cocrystals as marketable drugs, but their positions are mark by several differences. These differences have become attenuated over time, as can be seen in the most recent guidelines of both agencies. Guidelines from FDA (from 2013 and 2018) and EMA (2015) are resumed in Table 2.

EMA reflection paper (2015) indicate that the cocrystal's compounds can be neutral or ionized, if the association between the coformer and the API is characterized by weaker interactions. Moreover, EMA considers cocrystals with the same approach as solvates, polymorphs, or salts. In this way, cocrystals, as well as solvates, are held together by weak interactions that generally broken upon dissolution, which means that the same API is released and the different forms are bioequivalent. Consequently, cocrystals are considered appropriate for generic applications unless they differ with respect to safety and/or efficacy. Briefly, in the EU, an active substance may be considered as new active substance (NAS), if it exposes the patients to a new therapeutic moiety when compared to the already authorized medicinal products, independent of its solid form.⁽²³⁾

In 2018, FDA release the most recent guideline, where cocrystals are state as distinguishable from salts, once the components interact nonionically, and distinguishable from polymorphs. Instead, the guideline referred that cocrystals are similar to solvates, since they contain more than one component in the lattice, specifically, it indicates cocrystals as a special case of solvates, where the second compound is not a solvent, and it is typically nonvolatile.⁽³⁶⁾

For new drug application (NDA) and abbreviated new drug application (ANDA), appropriate data should be submitted supporting that: both API and cofomer are present in the unit cell; the API and cofomer interact nonionically; and significant dissociation of the API from the cocrystal occurs before reaching the pharmacological activity site. Hereupon, the cocrystal has a regulatory classification like a polymorph of an API, which means that a cocrystal cannot be considered as a new API.⁽³⁶⁾

Both agencies agree in the importance of cocrystals, EMA encourages the use of cocrystals by the industry, claiming cocrystals as viable alternative to salts and a method for achieving a more solid state matter with unique properties.⁽²³⁾ FDA states that cocrystals are presented as new opportunities to engineering solid-state forms, to enhance drug product properties, and to overcome the lack of ionizable functional groups that are a prerequisite for salt formation.⁽³⁶⁾

Table 2: Resumed information about FDA and EMA guidelines.

	FDA (2013) ⁽²⁴⁾	EMA (2015) ⁽²³⁾	FDA (2018) ⁽³⁶⁾
Definition	“Crystalline materials composed of two or more molecules within the same crystal lattice”	“Homogenous (single phase) crystalline structures made up of two or more components in a definite stoichiometric ratio where the arrangement in the crystal lattice is not based on ionic bonds”	“Crystalline materials composed of two or more different molecules within the same crystal lattice that are associated by nonionic and noncovalent bonds”
Classification	Dissociable “API-excipient” molecular complexes	A distinguishable crystalline form, classified as salts, polymorphs and solvates	Special case of solvates in which the second component is nonvolatile
Cofomers	Neutral guest compound, excipient	Non-active components in a pharmaceutical cocrystal, can be neutral, acid or basic	Neutral and nonvolatile
Chemical interactions	Nonionic	Nonionic	Nonionic
Comparable to:	Drug product intermediate (DPI)	Salts	New polymorph
Regulatory	DPI, not a new API	NAS if different with respect to efficacy and/or safety	Depend on bioequivalence, not a new API
Sameness with parent API	Yes	Dependent on sameness on efficacy and/or safety	Depend on bioequivalence
Manufacturing sites	Drug product facilities	API manufacturing facilities	API manufacturing facilities

2.1.3. Cocrystal's market

Cocrystals have gained intellectual importance over the years, which has promoted the cocrystal market worldwide. Several cocrystal and cocrystallization methods have been submitted to patents. In addition, several medicines with cocrystals in their formulations have been approved.

For example, in EU, one of the marketed cocrystals is sold under the brand name Entresto® and it was developed by Novartis. This drug was approved by EMA in 2015. It is composed by a cocrystal complex of the sodium salts of two active components, sacubitril and valsartan, in hydrated form. Sacubitril is a neprilysin inhibitor drug and Valsartan is an angiotensin receptor blocker. Entresto® is indicated to reduce the risk of cardiovascular death and hospitalization for heart failure in patients with chronic heart failure and reduced ejection fraction. In the main study for this drug approval, Entresto® was compared to enalapril, another medicine for the treatment of heart failure, and it was proved to be more effective than enalapril.⁽³⁷⁾

Odomzo® is another medicine developed by Novartis, approved by EMA and FDA in 2015, which involves a cocrystal of sonidegib monophosphate and phosphoric acid. This is a cancer medicine used to treat adults with basal cell carcinoma. Odomzo® was approved by EMA as a new active substance.⁽³⁸⁾

In 2018, Steglatro®, Segluromet® and Steglujan® were approved in EU, as new active substances. These medicines were developed by Merck and they are used to control blood glucose levels in adults with type 2 diabetes mellitus. The active substance is presented in the form of a cocrystal of ertugliflozin with L-pyroglutamic acid in a 1:1 ratio.⁽³⁹⁻⁴¹⁾

2.2. Cocrystallization methods

Cocrystallization is the process that combines two or more molecules (API and coformer(s) or another API) through non-covalent interactions, using crystallization processes. Cocrystallization final product is not necessarily a cocrystal (Figure 2), depending on the process efficiency, which means, a cocrystal is produced when the cocrystallization is successfully performed. If reaction does not take place, the final product of the cocrystallization method is the physical mixture (PM). An eutectic can also be obtained, when a homogeneous mixture of the crystalline components is formed. Single components crystals are produced, when components suffer crystallization separately, a problem of some methods that use solvents. Also, one or both components can suffer amorphization.

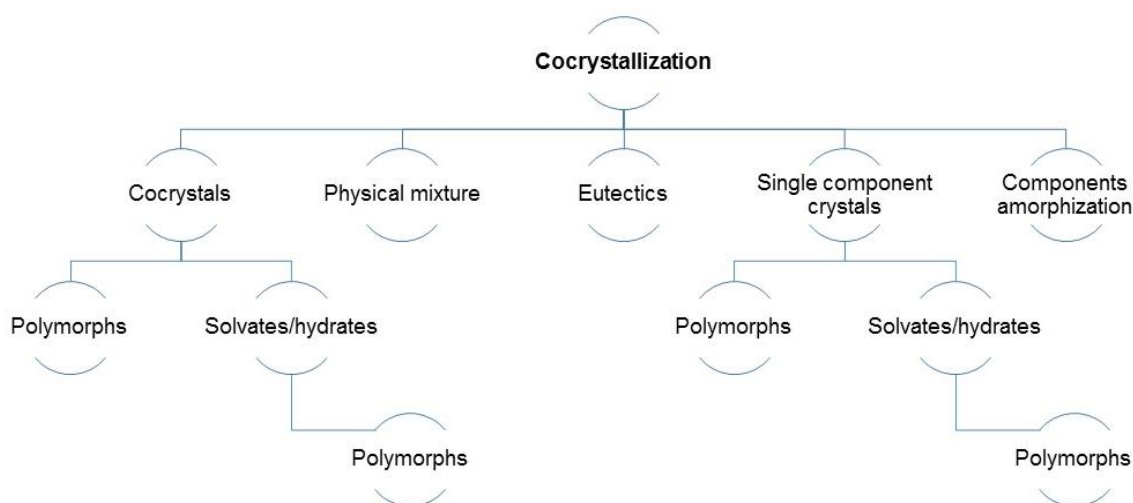


Figure 2: Cocrystallization main products, namely: physical mixture, cocrystal with respective solvate and polymorph, eutectics, single components crystals and component amorphization.

Cocrystals can also form solvates and polymorphs, due to inefficient packing of hydrogen bonds, which influences intermolecular interactions.^(13, 25) Polymorphs can arise from every crystal compound, for example, a solvate can have different polymorphs, due to the different arrangement in the crystal lattice. Polymorphism implies different properties, including solubility and stability of the final product. Since polymorphs and solvates can have different stability and/or efficiency, they are only applicable if the production process is able to control their production.^(23, 25) Thus, it is essential that polymorphs and solvates formation be taken into account, during cocrystal formation.⁽⁶⁾

Cocrystal properties, such as purity, yield, particle size, particle size distribution, and morphology, are influenced by different cocrystallization methods.^(11, 16, 42-44) Consequently, cocrystallization method selection is of utmost importance and its choice must be made considering the requirements of final product. API and coformer's characteristics, such as

solubility, stability and susceptibility to form solvates and polymorphs, must be considered to method selection, since some methods can be incompatible with the nature of the system.

(45, 46)

Eligible methods for screening are not necessarily the same methods suitable for laboratorial scale production or industrial manufacturing. If the propose is a screening, methods characteristics as fastness and capacity to analyze a wide range of compounds simultaneously should be considered. If the objective is laboratorial production, methods with high yield and high purity of final products should be preferred.⁽¹⁶⁾

Cocrystallization methods are usually classified accordingly to the use or not of solvent: solvent-based or solvent-free methods. Solvent-based methods are the most recurrently used, mainly in laboratory (small scale), because of their efficiency, technique and apparatus simplicity, possibility of process monitoring and control of the final product proprieties by, for example, changing the solvent. However, these techniques use hazard solvents, so they are not green techniques. Another problem of some methods that use solvent is the single compounds crystals formation, when compounds have different solubility in the solvent. Main solvent-based methods and their characteristics, advantages and disadvantages are summarized in Table 3.

Cocrystals production has been associated to green chemistry principles. These principles recommend an efficient cocrystal production with less toxicity and byproducts and this means to use safer solvents or, ideally, not to use solvents. Therefore, solvent-free methods are gaining interest in academia and industry due to the fact of being less environmental hazardous.⁽¹⁷⁾ Mechanochemical methods are solvent-free methods or use a very small quantity of solvent and they are applicable to a wide range of compounds, once there are not solubility related problems. They are based on the application of mechanical stress, for example through grinding techniques, which promotes fracture and increase surface area, inducing the reaction by the absorption of the mechanical energy.⁽⁴⁷⁾ In some cases, the use of a small quantity of solvent can accelerate the process.⁽⁴⁸⁾

Solvent-free methods can also use other type of inducing energy besides grinding, such as microwave or heat in thermal methods. A summary of the most used solvent-free methods and their principal advantages and disadvantages is present in Table 4.

Table 3: Resume of solvent-based cocrystallization methods, including their characteristics, advantages and disadvantages.

Solvent-based methods		
Method	Main advantages	Main disadvantages
Solvent evaporation ^(12, 13, 17, 49)	<ul style="list-style-type: none"> • Simple methodology and apparatus; • Efficacy in screening and laboratory scale; 	<ul style="list-style-type: none"> • Single compounds crystals formation; • Environmental hazardous (organic solvents); • Solvates formation; • Difficult to scale-up;
Reaction or precipitation ^(11, 50)	<ul style="list-style-type: none"> • Single compounds crystals prevention; 	<ul style="list-style-type: none"> • Environmental hazardous; • Solvates formation; • Difficult to scale-up;
Cooling ^(4, 51, 52)	<ul style="list-style-type: none"> • Easily scalable; • High control of cocrystal properties (use of different solvents); 	<ul style="list-style-type: none"> • Environmental hazardous (organic solvents); • Several steps;
Antisolvent addition ^(8, 9, 53, 54)	<ul style="list-style-type: none"> • High purity cocrystals; • High control of cocrystal properties (use of different and mixed solvents); • Carried out at ambient temperature; 	<ul style="list-style-type: none"> • Low yields; • Several steps; • Several requirements about solvents (both solvents must be miscible); • Environmental hazardous; • Difficult to scale-up;
Supercritical fluid technology ⁽⁵⁵⁻⁵⁷⁾	<ul style="list-style-type: none"> • Versatility; • Single step process; • Avoids solvates/hydrates formation (using liquid CO₂); 	<ul style="list-style-type: none"> • Environmental hazardous; • Several requirements about solvents (using antisolvent); • Single compounds crystals formation (using supercritical fluid);
Slurry ^(58, 59)	<ul style="list-style-type: none"> • Simple methodology and apparatus; • Single compounds crystals prevention; • Efficacy in screening and laboratory scale; 	<ul style="list-style-type: none"> • Environmentally hazardous (small amounts of solvent); • Difficult to scale-up;
Ultrasound assisted ^(60, 61)	<ul style="list-style-type: none"> • Efficacy in screening and laboratory scale; • High purity cocrystals; 	<ul style="list-style-type: none"> • Environmentally hazardous (small amounts of solvent); • Difficult to scale-up;
Freeze drying ⁽⁶²⁾	<ul style="list-style-type: none"> • Single step process; • Continuous process; • Easily scalable; • Single compounds crystals prevention; 	<ul style="list-style-type: none"> • Environmental hazardous (organic solvents);
Spray drying ^(63, 64)	<ul style="list-style-type: none"> • Single step process; • Continuous process; • Easily scalable; • Single compounds crystals prevention; 	<ul style="list-style-type: none"> • Environmental hazardous (organic solvents);
Vapour-diffusion ⁽⁶⁵⁾	<ul style="list-style-type: none"> • Low energy in-put, compared to mechanochemical methods; 	<ul style="list-style-type: none"> • Environmental hazardous (organic solvents);
High pressure homogenization ⁽⁶⁶⁾	<ul style="list-style-type: none"> • Single step; • Easily scalable; • Avoids solvates formation; 	<ul style="list-style-type: none"> • Environmental hazardous (organic solvents);
High shear granulation ⁽⁶⁷⁾	<ul style="list-style-type: none"> • Facilitates downstream processing; 	<ul style="list-style-type: none"> • Complex process; • Not appropriate to thermal labile drugs; • Solvates formation; • Limited number of studies;

Table 4: Resume of solvent-free cocrystallization methods, including their characteristics, advantages and disadvantages.

Solvent-free methods		
Method	Main advantages	Main disadvantages
Neat grinding ⁽⁶⁸⁻⁷²⁾	<ul style="list-style-type: none"> • Green technique; • Avoid solvates formation; 	<ul style="list-style-type: none"> • Difficult to scale-up; • Efficiency problems (mainly in manual grinding);
Liquid assisted grinding ^(68, 73-75)	<ul style="list-style-type: none"> • Higher efficiency and cocrystal properties control (mainly compared to neat grinding); 	<ul style="list-style-type: none"> • Environmentally hazardous (small amounts of solvent); • Solvates formation; • Difficult to scale-up;
Polymer assisted grinding ^(45, 76)	<ul style="list-style-type: none"> • Avoids solvates formation; • Single step process (only if polymers are biocompatible); 	<ul style="list-style-type: none"> • Impurities (if polymers are not biocompatible);
Hot melt extrusion ^(15, 42, 43, 77)	<ul style="list-style-type: none"> • Green technique; • Single step process; • Continuous process; • Easily scalable; • High purity cocrystals; • Avoids solvates formation; 	<ul style="list-style-type: none"> • Not appropriate to thermal labile drugs; • Complex method (parameters equilibrium must be found);
Matrix-assisted ⁽⁷⁸⁾	<ul style="list-style-type: none"> • Green technique; • Easily scalable; • Cocrystal production and formulation; • Avoids solvates formation; 	<ul style="list-style-type: none"> • Limited number of studies;
Melt and other thermal methods ⁽⁷⁹⁻⁸¹⁾	<ul style="list-style-type: none"> • Green technique; • Avoids solvates formation; 	<ul style="list-style-type: none"> • Not appropriate to thermal labile drugs; • Low mixing;
Spray congealing ⁽⁴⁴⁾	<ul style="list-style-type: none"> • Green technique; • Easily scalable; • Continuous process; • Avoids solvates formation; 	<ul style="list-style-type: none"> • Not appropriate to thermal labile drugs;
Microwave assisted ⁽⁸²⁾	<ul style="list-style-type: none"> • Green technique (without solvents); • Avoids solvates formation; • Do not use shear forces as the usual solvent-free methods; 	<ul style="list-style-type: none"> • Limited number of studies;

2.2.1. Cocrystallization from solution

Cocrystallization from solution generally uses organic solvents with the API and the coformer dissolved in the solution. According to Childs *et al.*, there are two variations of this cocrystallization: the one that uses solvents or solvent mixtures, where both components have similar solubility and where the cocrystal congruently saturates; and other that uses solvents where the components have different solubility, being noncongruently saturating systems. In the last variation, nonequivalent concentrations of the components are generally used, in order to reach the thermodynamically stable solid phase of the cocrystal and avoid single component crystallization. This technique is generally named as reaction or precipitation cocrystallization.⁽¹¹⁾

Solvent evaporation cocrystallization of stoichiometric solutions is based in the first method variation. Stoichiometric amounts of both compounds are dissolved in a solvent and then the solution is left to evaporate. API and coformer have similar solubility in the chosen

solvent, for the congruently saturation of the cocrystal.⁽¹¹⁾ Until now, this process has been successfully used by several authors.^(12, 13, 49)

Solvent selection is extremely important in this method. Solvent can influence the characteristics of cocrystal, such as purity, crystals size and shape and yield. By changing solvent composition is possible to control polymorphism, for example.^(8, 9) Holoň *et al.* had reported the importance of solvent selection in this type of methods. In the cited study, several solvents were initially considered (ethanol, methanol, isopropanol, methylethyl ketone, tetrahydrofuran and acetone) based on API and coformer solubility. Other physical and chemical properties were also evaluated to select the solvent. In the end, methylethyl ketone was the selected solvent.⁽¹⁰⁾ In some situations, solvent selection may require phase diagrams⁽¹⁰⁾, mainly because of the different solubility of the API and coformer, and the use of process analytical tools, to evaluate the process.⁽¹⁴⁾

Sarkar and coworkers tried to increase antiviral drug acyclovir properties, through solvent evaporation. They were able to produce three acyclovir cocrystals with fumaric acid (I), malonic acid (II) and DL-tartaric acid (III) as coformers. Both cocrystals I and II showed remarkable increase stability and all the cocrystals showed higher solubility and faster dissolution. This study also shows that solvent evaporation can be an advantage for systems that cannot form the cocrystal through other techniques. For example, cocrystal I and III were formed through both solvent evaporation and grinding methods, but cocrystal II was only possible using solvent evaporation technique. However, this approach presents limitations, for example, the occurrence of compounds precipitation, which is due to components with lower solubility than their correspondent cocrystals. Also, with this method, undesirable solvates can be formed.⁽¹⁷⁾

Ranjan *et al.* had used a solvent evaporation method to produce three new hydrochlorothiazide cocrystals, with the coformers phenazine (in the stoichiometric ratio 1:1), 4-dimethylaminopyridine (1:2) and picolinamide (1:1). In this work, solvent evaporation method was combined with the liquid assisted grinding, which was the first step of the process, to increase the process kinetics and polymorphic control, followed by mixture dissolution in the solvent with heating and slowly evaporation of the solvent at ambient conditions.⁽²⁾

2.2.2. Slurry cocrystallization

Slurry cocrystallization is another alternative for systems composed of an API and a coformer with different solubility. In this method, a suspension is created and instead of a solution, as in solvent evaporation cocrystallization. Solution mediated phase transformation (SMPT) process is the most plausible explanation for the events of slurry

cocrystallization. Therefore, the process starts with the API and coformer dissolving separately and not completely in the solvent, according to their solubility. During the process, cocrystal nucleation and growth occurs and components concentration in solution decrease, leading to undersaturation. This promotes gradual compounds dissolution and subsequent cocrystallization, until one of the compounds achieve its activity critical value.⁽⁵⁹⁾

Thus, only the cocrystal can precipitate, avoiding single component precipitation, one of the main problems of typical methods of cocrystallization from solution. This is a simple and effective method that allows the achievement of products and requires smaller quantities of solvent when compared to cocrystallization from solution, being less hazardous.⁽⁵⁹⁾ Moreover, water is a possible solvent, as related by Soares *et al.* in the 2017. The work describes the synthesis of a carbamazepine and nicotinamide cocrystal, through a slurry cocrystallization method, using water and different temperatures. This experiment, besides being a greener technique, allows high process control. It shows that purity problems in slurry cocrystallization can be overcome with increase of temperature, once they were able to synthesize highly pure cocrystal at the temperature of 80°C.⁽⁵⁸⁾

2.2.3. Ultrasound-assisted cocrystallization

Ultrasound-assisted cocrystallization is the combination of solution or slurry cocrystallization with ultrasound, with the aim of promoting cocrystal formation. Ultrasound promotes cocrystal formation by ultrasonic waves that create cavitation energy, which reduce the inducing period and the metastable zone, promoting cocrystal nucleation at lower supersaturation levels.⁽⁶⁰⁾

This can be advantageous in solvent evaporation method when the systems represent a non-congruently soluble pair, as in the case of caffeine and maleic acid in methanol. A study presented by Aher *et al.* showed that the use of ultrasound altered supersaturation conditions of the compounds and favoring the cocrystals nuclei. In this study, ultrasound-assisted cocrystallization was compared to slurry and cooling cocrystallization and was selected as the one that allowed obtain pure cocrystals.⁽⁶⁰⁾

Slurry cocrystallization efficiency and final product purity can also be increase with the use of ultrasound, since it provides cocrystallization accelerated conditions. This can be very helpful for noncongruent systems, because ultrasound can help to achieve congruency of systems, having impact on compound's solubility. This is showed through phase diagrams in the work of Apshingekar *et al.*, where this method was used with water for noncongruent cocrystal pair of caffeine and maleic acid. They investigated how ultrasounds affects the different regions of the phase diagram, for example, the stability regions for pure caffeine and maleic acid in water were tighten and the solution region was expanded.⁽⁸³⁾

2.3. Cocrystal development

The development of a marketable pharmaceutical cocrystal involves several stages, as shown in Figure 3. Cocrystal design is the first step before cocrystal screening and it is essential for an efficient screening. The implementation of design and screening phases in cocrystal production allows a more efficient process, with reduced costs associated, mainly compared with typical trial and error approaches. This two phases allow to select the API:coformer systems with the best performance.

Cocrystal with the selected systems in the previously phase must be obtained in a higher scale, but still in laboratory, allowing a complete cocrystal characterization and determination of its properties and pharmacokinetics. This can lead to cocrystal rejection, if it does not achieve pretended characteristics. After cocrystal candidate selection, it must be formulated and an optimization of the entire process is required to become possible the scale up of the process and industrial production of the cocrystal.

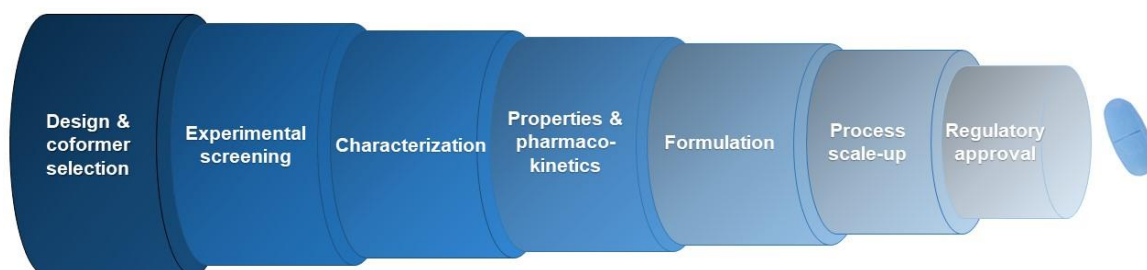


Figure 3: Illustrative scheme representing the different stages of cocrystal development (adapted from Duggirala *et al.*).⁽⁸⁴⁾

2.3.1. Cocrystal design

Cocrystal design involves the understanding of cocrystal formation, intermolecular interactions and other concepts of crystal engineering. There are various techniques used in cocrystal design, that can be used alone or in combination. One of them is a theoretical study of previously reports of cocrystals with similar API. Chemically similar analogues are a huge source for new cocrystals synthesis, being possible to understand the preferred cocrystallization conditions and preferred synthons.^(5, 85)

Since cocrystals are based in supramolecular synthons, design requires the knowledge of available groups to interact through non-covalent interactions, as hydrogen bonds, predicting synthons and cocrystal formation.⁽⁵⁾ Etter *et al.* resumed this prediction in some rules regarded to hydrogen bonds patterns:

- all acidic hydrogen present in a molecule are used in hydrogen bonding in the crystal structure of that compound;

- all good acceptors are used in hydrogen bonding when hydrogen bond donors are available;
- Preferentially hydrogen bonds are formed between the best hydrogen bond donor and the best hydrogen bond acceptor.⁽⁸⁶⁾

Cambridge structural database (CSD) is a repository where high quality molecular crystal structures can be found. CSD can be used to cocrystal design and synthons prediction, leading to a more rational cocrystal system selection.^(85, 87)

There are other techniques that can be used in cocrystal design, including the Hansen Solubility Parameters (HSP), that is a model based on solubility parameters. This model can help to predict materials miscibility and cocrystal formation by indication of cofomers miscibility, since cocrystal's compounds are miscible at molecular level.⁽⁸⁸⁾

Phase diagrams are also helpful tools to determine thermodynamic relationships between cocrystals and the compounds or/and solvent. They can be used not only in screening, assisting cofomer and/or solvent selection, but also can help predict the most adequate cocrystallization method and other parameters. Kun Ma *et al.* demonstrated the importance of phase diagrams, which were constructed to determine the effects of different factors as different solvents, temperatures and API:coformer ratio, on crystallization of single-component, cocrystal formation, cocrystal stability, supersaturation, nucleation, crystal growth and cocrystal yield.⁽⁸⁹⁾

2.3.2. Cocrystal screening

In the pharmaceutical industry, screening phase is used to find the solid form with the best performance at physicochemical and biopharmaceutical level. Cocrystal screening is based on the rational selection of the system that allows to obtain the cocrystal, through the test of several cofomers, API:coformer ratios and solvents (if necessary). Ideally, screening methods must be high-throughput methods, allowing the test of a wide range of cofomers, ratios and solvents simultaneously, in a fast and efficient way and requiring small amounts of reactants.

There are several cocrystal screening methods, so the appropriate method must be selected. High throughput screening (HTS) methods have been gain interest in academy and industry, since they allow testing a wide range of API:coformer systems simultaneously and in a fast and efficient way. They also can be automated and/or miniaturized, which means that low quantity of reactants is used.

Because screening phase can generate large sets of data, multivariate data analysis tools are essentials, as will be discussed further.^(11, 90)

Childs *et al.* compared four different screening methods, using carbamazepine and eighteen carboxylic acids as coformers. The experiments allow the generation of twenty-seven unique solid phases. A mechanochemical method was used, consisting in grinding the compounds with the assistance of a selected solvent.⁽¹¹⁾ The three other methods are solvent based. The first one is called high-throughput screening evaporative (HTSE) and use a 96 well-plate, where selected solvents were put, as well as stoichiometric quantities of API and conformer, with similar solubility in the selected solvent. In the end, the plate was left to slowly evaporate at room temperature. Reaction cocrystallization was other method used. This method requires the addition of pre-saturated solutions of conformer (non-stoichiometric) to the API and stirring of the systems, until transformation take place, which was monitored by automated Raman microscopy. The last method, called SonicSlurry™, involves the preparation of a slurry containing the API and conformer, which is then subject to ultrasonic pulses during a determined period.⁽¹¹⁾

Screening for solid forms by crystallization and cocrystallization using ultrasound is a patented method by Scott Childs, Patricia Mouglin and Barbara Stahly.⁽⁹¹⁾ Slurry methods involve a suspension, with a partial dissolution of the compounds in the solvent, where nucleation and cocrystal growths occur. This technique does not need the careful attention on solvent selection due to solvent differences, being less limited than solvent evaporation techniques.⁽⁵⁹⁾ Slurry experiments are usually combined with ultrasound to promote cocrystallization.⁽¹¹⁾ Slurry method combined with ultrasound performed in a 96 well-plate was described as an effective method that allows an efficient cocrystals screening, testing an wide range of coformers and solvents simultaneous.⁽⁹²⁾

Thermal methods are one of the most common screening methods. Differential scanning calorimetry (DSC) technique is a thermal method and implies the study of the components phase behavior. The use of DSC as screening tool is based on the analysis of the physical mixture, composed with the two potential cocrystal components, heated beyond eutectic point. When the result consists in an endothermic peak associated with the eutectic melting, instantly followed by an exothermic peak, cocrystallization is considered possible. Following, another endothermic peak should be observed, corresponding to the cocrystal melting point.^(93, 94) Karki and coworkers used a procedure for cocrystal screening from the melting and compared it with other screening techniques. The melting stage to achieve cocrystals involves cyclic heating and cooling the mixtures in a DSC aluminium pan. In this study, this screening technique was compared with neat grinding, liquid assisted grinding (LAG) and cocrystallization from solution, and it was concluded that the screening through cocrystallization from melting was more efficient than through cocrystallization from solution, but less efficient when compared with LAG and neat grinding techniques.⁽³³⁾

2.4. Cocrystals properties

Improving physicochemical properties of APIs is the foremost goal of cocrystal production. There are several reports of cocrystals with improved properties, such as, solubility⁽¹⁻³⁾, dissolution⁽¹⁾, bioavailability⁽⁴⁾, permeability⁽⁹⁵⁾ and physical and chemical stability^(3, 5). Besides properties improvement, adding a cofomer can introduce additional nutritional and health benefits to the API.^(6, 7)

Biopharmaceutical Classification System (BCS) classify drug substances, accordingly to its aqueous solubility and intestinal permeability, as:

- Class I: high solubility, high permeability;
- Class II: low solubility, high permeability;
- Class III: high solubility, low permeability;
- Class IV: low solubility, low permeability.⁽⁹⁶⁾

BCS class II and IV drugs are the main target of crystal engineering, due to their low solubility, which can lead to low bioavailability.

Bioavailability tests are necessary to bioequivalence demonstration, once EMA admit the possibility to considered cocrystals as “generic medicinal product”, if cocrystal and the initial API are considered bioequivalent; or new active substances, if they are not bioequivalent compounds. Bioequivalence is demonstrated if two medicines are pharmaceutically equivalent or pharmaceutical alternatives and their bioavailability, both rate and extent, after administration in the same molar dose lie within acceptable predefined limits. Therefore, a cocrystal is treated as a generic product if, through a 90% confidence interval statistical study, its pharmacokinetic parameters area under the curve and relative mean maximum concentration are 80-125% similar to those approved for the brand drug.⁽⁹⁷⁾

Crystal engineering by cocrystallization can also improve mechanical properties, which is of utmost importance in drug development. Compactness, comprehensibility and flowability are properties that influence tableting behavior and they can be improved through cocrystals production. This is possible through cocrystal size and morphology control, by cofomer selection or cocrystals synthesis method.^[47]

Physical and chemical stability can be positively change through cocrystallization, affecting the release form, shelf life, handling and transportation of formulations. Stability studies are usually made at accelerated conditions, exposing the final product to different conditions, of temperature and/or relative humidity.^[7, 40, 55, 72, 100] Hygroscopicity is an important parameter that can be controlled, avoiding hydrate formation and increasing the storage life time, resistance to high relative humidity (RH) conditions and, thus, drug's quality. This parameter can be evaluated through RH stress, using powder X-ray diffraction to visualize the solid state transformations under different RH conditions.^[32, 55] Hydrate

formation depends on the interactions between the API and the solvent and through cocrystallization is possible modify these interactions, reducing the possibility of hydrogen bonds formation.^[7, 40] In a 2015 work, three cocrystals forms were identified with the API acyclovir and the cofomers fumaric acid, malonic acid and tartaric. Two of them were considered more stable than the original drug molecule. It was concluded that cofomer acidity affect the cocrystal stability, as well as the fact of dicarboxylic acids introduction probably prevent the absorption of water, by supramolecular synthon formation through hydrogen bonding.^[7]

Physical stability, when in solution or slurry, is one of the drawbacks of cocrystals, which have a great tendency to convert to individual cocrystal components. Solutions and slurries are essential formulations for toxicology studies, so adequate stability is required, in order to cocrystals can be submitted to this phase. Cocrystal can be physically instable when in solution and stable when in solid state. For example, McNamara *et al.* reported a nonhygroscopic cocrystal form that sorbs less than 0.08% water at high humidity (95% RH), but when it was exposed to water in a dissolution bath at 37°C for 24h, the cocrystal was completely converted to the original form.^[40]

2.4.1. Solubility

Solubility is defined by International Union of Pure and Applied Chemistry (IUPAC) as the analytical composition of a saturated solution, expressed in terms of the solute's proportion in a solvent (concentration, molality, mole ratio, etc).⁽⁹⁸⁾

Solubility is an important property that have a significant impact on the bioavailability of drugs. In early phases of drug development, solubility measurement helps to predict the bioavailability of a drug. It is expected that a drug with low solubility will have low bioavailability, which means that will be absorbed in a low rate or extent, having difficulties in becoming available at the site of action. Drug's solubility is dependent on properties such as temperature, pH⁽⁹⁹⁾ and melting point^(7, 100).

Solubility testes are done to confirm the potential pharmaceutical interest, the manufacturability, the performance, the efficacy and safety. A solubility study can involve, for example^(4, 17, 63, 101, 102):

- Equilibrium/ apparent solubility test;
- Phase solubility studies;
- pH-dependent solubility studies;
- Dynamic solubility studies.

Intrinsic solubility is the true solubility of a fully unionized drug compound. Apparent solubility is the experimental solubility with un-ionized or ionized forms. Solubility can also

be thermodynamic, being measured equilibrium solubility values, or kinetic, corresponding to values associated with metastable condition.⁽⁹⁰⁾

Shake-flask method is a widely used solubility measurement method. This method determines thermodynamic solubility. It is based in preparation of a saturated solution, with excess amount of drug. When the saturated solution achieves the equilibrium (generally within 24 hours, but dissolution profile of the drug must be investigated), it is necessary to separate phases, through centrifugation or filtration. Then, saturated solution is measure trough the appropriate method.⁽¹⁰³⁾

Solubility can be related to the melting point of the cocrystal, one of the physical properties that can be modified through cocrystallization. Cocrystal melting point can be determined through DSC.⁽¹³⁾ There are indication of an inverse correlation between the solubility and the cocrystal melting point. This is confirmed by thermodynamics, which state that the portion of the energy required for the solubility process of the solid state structure is directly related to the energy required for the transition from solid to liquid state.⁽¹⁰²⁾ In general, the cocrystal melting point is in-between the one of the API and the cofomer or lower than both indicating a cocrystal with higher solubility than the API.^(7, 100) Therefore, cofomers with low melting points should be preferred. However, the comprehension on how the cofomer affects the melting point and solubility is still limited, so a great effort is necessary to clarify these attempts to correlate these properties.

Solubility and, consequently, bioavailability improvements are the main advantages and probably one of the key reasons for cocrystal application and growing interest. There are several studies that confirm solubility increase of the cocrystal in comparison with the pure API.^(4, 17, 55, 102, 104)

2.5. Cocrystal characterization

Cocrystal characterization is performed using several techniques, which allows to verify phase transformation, cocrystal structure, synthons involved, molar ratio, purity, etc. Table 5 presents a resume of the most used characterization techniques and properties evaluated through these techniques.

Table 5: Most used cocrystal characterization techniques and evaluated aspects.

Technique	Evaluated properties
Differential scanning calorimetry ^(12, 13, 105)	Melting point, crystallinity, purity
High performance liquid chromatography ⁽²⁾	Identification, dosing, purity
Laser diffraction ⁽⁴²⁾	Particle size distribution
Microscopy ⁽⁴⁶⁾	Morphology
Solid-state nuclear magnetic resonance spectroscopy ⁽¹⁰⁶⁾	Proton transference (salt determination)
Powder X-ray diffraction ^(12, 13)	New phase formation, crystallinity, purity
Single crystal X-ray diffraction ⁽²⁾	Crystal structure
Vibrational spectroscopy ^(6, 12-14, 54)	Molecular bonds, polymorphism, purity

2.5.1. Vibrational spectroscopy

Vibrational spectroscopy is based on atoms' vibration in molecules. It englobes near infrared (NIR), mid infrared (MIR), Raman and Terahertz (THz) spectroscopy, encompassing the spectral range between 14000 cm⁻¹ and 3 cm⁻¹. These techniques have been used as tools to chemical elucidation and identification of unknown compounds. They have a wide range of applicability on several scientific and industrial fields, since product quality control, process monitoring, compounds characterization, between others. They provide qualitative and quantitative information.

In pharmaceutical industry, vibrational spectroscopy has been widely used, mainly in conjugation with multivariate analysis. These techniques can be used over pharmaceutical production cycle, from raw materials to final products. They can be advantageous in raw materials for determination of water content, impurities, quantification and/or identification of polymorphism and identification of API and excipients. Operations such as granulation, drying, blending, compaction, coating can also be monitored using vibrational spectroscopic techniques.

i. Theory

Vibrational spectroscopy is based on vibration of atoms in molecules and on the radiation absorption by the molecule, when the frequency of the specific vibration is equal to the frequency of the radiation directed on the molecule.

Briefly, each atom has three degrees of freedom and, consequently, a polyatomic molecule of n atoms has $3n$ total degrees of freedom. 3 of these degrees are required to describe translation and other 3 or 2 degrees describe the rotation of the entire molecule, for nonlinear and linear molecules, respectively. Therefore, $3n - 6$ or $3n - 5$ degrees of freedom correspond to fundamental vibrations for nonlinear and linear molecules. These fundamental vibrations are known as normal modes of vibration. Infrared activity is the result of fundamental vibrations that produce a change in the dipole moment and Raman activity is the result of the ones that produce polarizability changes. This way, Raman spectroscopy and infrared spectroscopy are complementary, in the way that there are Raman active vibrations and others infrared (IR) active, according to the molecule symmetry or lack of it, respectively.^(107, 108)

Between the three different vibration transitions (fundamental, combination and overtones), fundamental vibrations, which are the ones involving a unit change in quantum number, are the basis of mid infrared absorption bands. In the case of NIR spectroscopy, bands are the result of combination and overtones. Overtones are transitions between vibrational energy states where the change in quantum number is ± 2 , ± 3 , etc. Combination bands are the result of the interaction between two or more vibration modes in polyatomic molecules, in a way that it causes simultaneous energy changes.^(107, 108)

ii. Instrumentation

Equipment of vibrational spectroscopy can be from two types: dispersive or Fourier transform (FT) spectrometers.

Basic configuration of dispersive spectrometer consists in a light source, a light dispersing element (grating), a sample and a detector. Sample excitation can happen before or after light dispersion. These spectrometers have a double-beam design, one for the sample and another one for the reference. Generally, the source produces continuous radiation that is sent through the sample and a reference, passing through a chopper, which moderate the energy. Then, the energy is direct to a dispersing element, where light is separate into its wavelengths in the spectral range. Each wavelength is directed to a slit and to the detector, being measured one at time. When the beams reach the detector, an electrical signal is created, that give origin to a recorder response.⁽¹⁰⁷⁻¹⁰⁹⁾

FT spectrometers are based in an interferometer. They are composed by radiation source, a beamsplitter, two mirrors (a moving and a fixed mirror), a laser and detector. Generally, the radiation is directed from the source to the beamsplitter, which is a semireflecting device, splitting the beam into two parts. One part is transmitted to the moving mirror and another part is reflected to the fixed mirror. The moving mirror have a constant velocity movement, which originate different paths between the beams. Mirror movement's velocity is timed according to the laser wavelength, which also have a function of internal wavelength calibration. Both beams are reflected from the mirrors to the beamsplitter where the two beams are combined and an interference pattern is created to produce an interferogram. The interferogram is directed through the sample, where energy is absorbed and transmitted. Finally, the transmitted energy reaches the detector. In opposition to diffuse equipment, here the detector reads information about every wavelength at the same time.⁽¹⁰⁷⁻¹⁰⁹⁾ The interferogram is a function of the light measure by the detector and the moving mirror position. The mathematical technique called Fourier transformation is applied by the instrument software to obtain a typical spectrum.

Generally, dispersive spectrometers have several disadvantages, such as, low signal to noise ratio, sensitivity and resolution. However, these spectrometers are sometimes preferred depending on the application and on the spectroscopy type, which will be discussed further.

FT spectrometers have three main advantages over dispersive spectrometers:

- The multiplex or Fellgett's advantage: Due to the measurement of the wavelengths simultaneously, a higher signal-to-noise ratio is obtained.
- The throughput or Jacquinot's advantage: Due to the lack of slits, a higher amount of energy reaches the detector resulting in a signal-to-noise ratio, sensitivity and resolution.
- The wavelength accuracy or Connes' advantage: Due to the internal laser that controls the velocity of the moving mirror and serves as internal calibration, the internal precision and high accuracy is maintained.⁽¹⁰⁹⁾

iii. Near infrared spectroscopy

Near infrared spectroscopy (NIRS) englobes the spectral range between 14000 cm^{-1} and 4000 cm^{-1} . It has been widely used to obtain physical and chemical information about the sample, for example, particle size through scattering and compound's chemical groups, respectively. It can be used for qualitative and quantitative analysis. The technique does not need sample preparation or pre-treatments and it is a non-destructive technique, allowing the reuse of the sample. It is very fast, taking few seconds to obtain a spectrum.⁽¹¹⁰⁾ It is extensively applied in pharmaceutical industry due to its advantageous characteristics

to analyze raw materials, in quality control and in process monitoring. Using fiber optical probes, the technique is a viable possibility for in- and on-line monitoring.⁽¹⁰⁷⁻¹⁰⁹⁾

Spectrum's complexity is a disadvantage, mainly in the case of complex matrix that provokes the overlapping of absorption bands, becoming its analysis difficult. It is also necessary the use of chemometrics methods to obtain relevant information. Also, the technique does not detect trace amounts, because it has a high detection limit.⁽¹⁰⁹⁾

NIR spectrum is composed by overtones and combination absorption bands. Combinations are more complex, once there are a high number of possible combinations from a group of fundamental absorptions, comparing to the number of possible overtones. Hydrogens atoms are very important in NIR spectroscopy, once they are very active in this technique (see Figure 4), so groups as OH, CH and NH are easily detected.⁽¹⁰⁹⁾

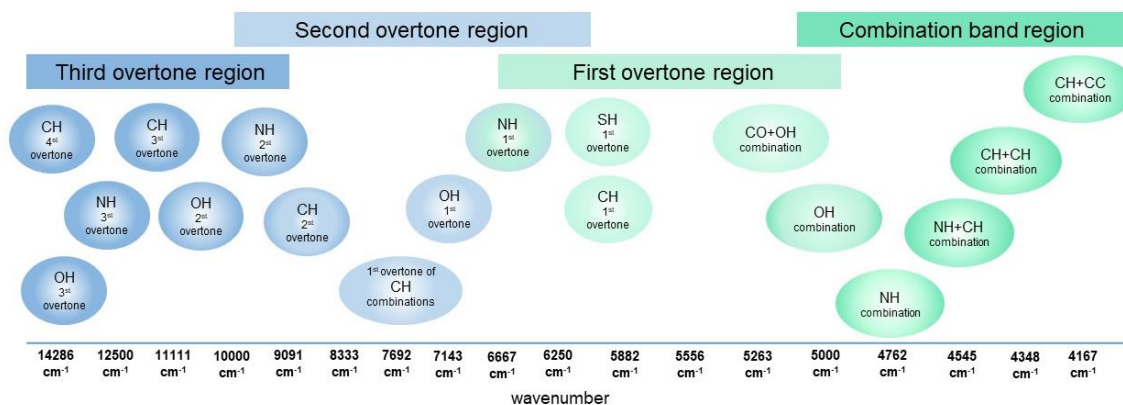


Figure 4: Most common chemical groups active in the NIR region, divided in the combination and overtones regions.

Instrumentation for NIR spectroscopy can be from one of the two types explained in section 2.5.1.(ii), dispersive or Fourier transform near infrared (FT-NIR) spectrometers. Dispersive spectrometers were the firsts being used. They can have different types of light dispersing elements, for example scanning grating monochromators or, more recently, acousto-optical tunable filters.⁽¹⁰⁹⁾

Despite of disperse instruments general disadvantages, these ones are preferred in process control activities, namely, in on-line and in-line measurements. There are also portable spectrometers that can be useful for *in situ* measurements. FT-NIR spectrometers are preferred to laboratory analysis, in off- and at-line measurements, once reliability and high signal-to-noise ratio are essentials.⁽¹⁰⁹⁾

Tungsten-halogen light source is the most applied for NIRS and it produces a broadband, pseudo-blackbody emission spectrum. It is inexpensive but, if operated in appropriate conditions, it has a long-time life.⁽¹⁰⁷⁻¹⁰⁹⁾

Detector can be one from main two classes: thermal detectors, which use IR radiation heating effect; and quantum mechanical (photonic) detectors that uses the IR radiation as light and result in a more sensitive detector with faster response time. Thermal

detectors are mainly used in FT-NIR and they are composed by a ferroelectric material, as deuterated tryglycine sulphate (DTGS), capable of operating from the NIR to the MIR wavelength. Photonic detectors can be photoconductive or photodiode. Photoconductive detectors have a slab of a semiconductor material. Photodiode detectors have a doped semiconductor material, such as indium gallium arsenide (InGaAs). InGaAs is the most expensive detector, however, is the one that have high speed, appealing size and wavelength range from 10000 cm^{-1} to 4000 cm^{-1} .⁽¹⁰⁷⁻¹⁰⁹⁾

NIR measurement modes can be from three types:

- Reflectance (R) mode measures the light reflected by the sample. It contains a specular component, which have little information about composition, and diffuse reflectance, used in NIR measurements, and that provides a measure of the ratio between the light intensity that is reflected from the sample and the one that is reflected from the background. This mode is used in solids and turbid liquids. Absorbance (A) values can be obtained through the negative of $\text{Log}_{10}(\text{R})$;
- Transmittance (T) mode measures the decrease of radiation intensity caused by radiation absorption in the sample. This mode is mostly applied to liquids and suspensions with a transparent medium. Absorbance values can be obtained through the negative of $\text{Log}_{10}(\text{T})$;
- Transflectance (T^*) mode is a combination of reflectance and transmittance modes. The light transmitted through the sample is reflected in a mirror or a diffuse reflectance surface and is directed back to the sample before reaching the detector. This mode is applied to liquid and semi-solid samples. Absorbance values can be obtained through the negative of $\text{Log}_{10}(\text{T}^*)$.

iv. Mid infrared spectroscopy

Mid infrared spectroscopy (MIRS) covers the wavelength range between 4000 to 400 cm^{-1} , where fundamental vibrations of the most common chemical groups are located. This spectroscopy is widely applied in pharmaceutical industry. It can be used to identify functional groups or to elucidate compounds structures, applied to drugs, excipients and in quality control. It is useful as tool to characterize solid state forms, as salts, polymorphs or hydrates.

This technique was one of the first types of vibrational spectroscopy used. MIR spectra can be obtained from samples as liquids or solids and sample preparation can be required and it have a high influence on spectra quality (except using attenuated total reflectance). It is also a fast technique, once a spectrum can be collected in minutes.⁽¹⁰⁷⁻¹⁰⁹⁾

MIR spectrum is divided in two regions: a functional group and a fingerprint region (Figure 5). Functional group region is easier to interpretation and to bands association to

characteristic functional groups. In this region, fundamental absorptions arising from functional groups and corresponding mainly to stretching vibrations are seen. Fingerprint is more complex, but very specific for each compound, being an important region for compounds identification. Here bands associated to fundamental absorptions from molecular skeleton, such as C-C and C=C bonds, are visible, as well as groups containing heavier atoms, as C-Cl or C-N. Predominant type of vibrations are bending, but other types, such as scissoring, rocking, wagging and twisting vibrations are visible in this region.⁽¹⁰⁷⁻¹⁰⁹⁾

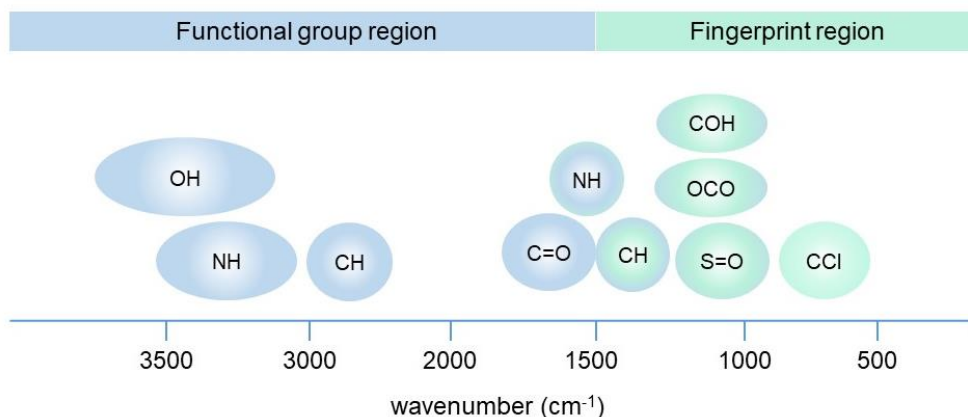


Figure 5: Most common chemical groups active in the MIR region, divided in the functional group and fingerprint regions.

FT spectrometers are the most used in MIR spectroscopy (FTIR). FTIR sources have low power out-put and MIR detectors have low specific detectivity, so the Jacquinot and Fellgett advantages can be fully realized.⁽¹⁰⁷⁻¹⁰⁹⁾

Light sources for MIRS are mainly thermal sources, producing a blackbody or near blackbody emission spectrum. There are two types of elements used in thermal sources, the open source element and the closed source element. The open source element, which is a variant of a light bulb with an enclosed electrically heated element within a standard package, is the used for MIRS, once is less energetic and adequate to MIR wavelength.⁽¹⁰⁷⁻¹⁰⁹⁾

As in the NIR case, there are two types of detectors: thermal and photonic detectors. Thermal detectors, namely the DTGS detectors, are the mostly used, once they cover a wide wavelength range, they are able to work at room temperature, they have higher sensibility, but they are expensive and they are not very fast. For faster analysis, mercury cadmium telluride detectors are more used.⁽¹⁰⁷⁻¹⁰⁹⁾

Relatively to measurement modes, transmittance was the most used. However, this technique requires pre-treatment of the samples, for example, solids must be mix with potassium bromide and the mixture is then pressed to form a pellet, which is insert into a holder in the spectrometer.⁽¹⁰⁷⁻¹⁰⁹⁾

Nowadays, the use of the attenuated total reflectance (ATR) accessory allows to obtain a good quality and reproducible spectrum without the complex and timely sample preparation. This constitute a big advantage, making the technique faster and non-destructive (or almost). With the ATR accessory the sample must be press against the crystal using mechanical force to improve signal-to-noise ratio and reproducibility. ATR is based in the internal reflection of light by a transmission medium. Sample is placed directly in the element of internal reflection, which is a material (crystal of e.g. zinc selenide or diamond) with high refractive index. The IR beam is directed to ATR element by several mirrors, it is reflected through the crystal and then it is directed to the detector by a set of mirrors. ATR measure the changes that occur in a totally internally reflected IR beam when it is in contact with the sample.^(107, 111)

v. Raman spectroscopy

Raman spectroscopy is based on inelastic scattering of light by matter. When an incident light achieves a molecular system that has two vibrational energy levels, a ground state and an excited state, it induces transition to virtual levels. Then, it returns to the initial state through three different ways, giving origin to the basic transitions involved in the spontaneous Raman scattering, the Rayleigh scattering (elastic), Stokes and anti-Stokes scattering (inelastic). Rayleigh scattering is based in a transition that begins and finishes at the same vibrational energy level. Stokes Raman scattering involves a transition that finishes at a higher vibrational energy level than the ground state vibrational energy level. Anti-Stokes Raman scattering arise from a transition that begins in a higher and ends in a lower vibration energy level. This way, anti-Stokes scattering is less probable to happen and, consequently, less intense than Stokes scattering, once most part of molecules are in the ground state energy level at ambient temperatures.^(109, 111)

Therefore, Raman effect is based in a change in electric dipole-electric dipole polarizability, being the intensity of the Raman scattering proportional to polarizability change. The Raman spectrum is given by scattering intensity as a function of the frequency shifts.^(109, 111)

Raman spectroscopy provide information on chemical structure and identity of a compound, phase and polymorphism, contamination and impurities. It is useful in pharmaceutical industry, for example, analyzing APIs with aromatic conjugate systems, which have strong Raman signal. Another characteristic is that water does not have a strong Raman signal, once is not Raman active.⁽¹¹²⁾

Raman spectroscopy is a fast technique, only requiring a few seconds to record a spectrum. It is a non-destructive technique and does not need sample preparation. In relation to instrumentation, FT and dispersive spectrometers are also used in Raman

spectroscopy. Instrument selection depends on the application. Dispersive Raman spectrometers have laser sources with wavelength in the ultraviolet, visible or NIR region. Laser choice have a large impact on experimental performance. Sensitivity is influenced by laser wavelength, once lasers with higher wavelength result in lower scattering intensity. It also depends on samples nature. Ultraviolet (UV) lasers have higher sensibilities and they are useful in bio-molecules analysis, but also, as a factor of the higher energy, it can cause samples degradation. NIR lasers are required to fluorescence suppression, but they have lower sensitivity. Multichannel detectors are the mainly used in this technique, such as charge couple devices (CCD). CCD are very sensitive photodetectors, with low noise, allowing the simultaneously measurement of a particular spectral region, which is a similar advantage of FT instruments (multiplex advantage).^(109, 111)

FT Raman spectrometers have only NIR lasers, 1064 nm or 780 nm. This can be a disadvantage, if higher sensibility is required. This technique can be useful in systems that present fluorescence problems.⁽¹¹¹⁾ FT Raman detectors are usually InGaAs.^(109, 111)

There are three ways of measurement. Backscattering is the most used one and involves collection of the scatter radiation on the same side of the sample. Spatially offset collects scatter radiation from a different part of the sample from the point of illumination. In transmission, the laser beam is directed to one side of the sample and the light is collected on the opposite side.⁽¹¹³⁾

Raman microspectroscopy (RMS) combines a Raman spectrometer with an optical microscope. The laser beam is focused through the microscope to generate a micro-spot, the Raman signal from the sample is created in a similar area and passes through the microscope until the spectrometer. Raman microscopy has the advantage of a Raman spectroscopy analysis with microscopic spatial resolution. This technique allows the analysis of individual particles with small dimensions. It is also possible the location and identification of samples contamination or specific parts in heterogeneous samples.⁽¹¹⁴⁾

vi. Vibrational spectroscopy in cocrystal development

Vibrational spectroscopy had been widely used for cocrystal characterization. These techniques have several advantages that justify the increase use of them in cocrystals analysis. In general, they require small quantity of samples, they are fast, non-destructive, do not need sample pre-treatment or require minimum preparation and they very sensitive to hydrogen bonding, which are the basis of cocrystallization. These techniques can provide information about cocrystals formation⁽¹³⁾, synthons involved⁽¹³⁾ and cocrystal purity⁽¹⁴⁾.

These techniques are reliable tools to detect cocrystal formation and also to discriminate between different solids forms as salts⁽¹¹⁵⁾, polymorphs^(6, 116) or solvates⁽¹¹⁷⁾.

They can be applied in screening procedures, once they are fast and efficient techniques to verify cocrystal formation.⁽⁶⁾ They can also be used in cocrystal characterization, once they provide reliable chemical and physical information. In pharmaceutical industry, they can be useful tools in quality control and quality assurance.

Vibrational spectroscopy can be used in process monitoring, which is based in quantitative and qualitative measurement of changes during cocrystal formation, using process analytical technology (PAT)⁽¹²⁾, in batch⁽¹³⁾ or continuous manufacturing⁽¹⁵⁾. In real-time process monitoring are efficient techniques achieve the intended quality of cocrystals.⁽¹⁴⁾

NIR spectroscopy has a great potential as a process monitoring method, using fiber optical probes.^(12, 14) Sarraguça *et al.* reported a study on a strategy for the implementation of NIRS as a PAT tool for the on-line monitoring of cocrystallization by solvent evaporation processes. The cocrystallization of furosemide with adenine using methanol as solvent was monitored on-line with NIRS resorting to a fiber optic diffuse reflectance probe. It was concluding that a chemometric assisted NIR spectral analysis resorting to PCA is an efficient method to report main cocrystallization events, namely, the nucleation and solvent evaporation, control cocrystallization process and allow process optimization.⁽¹²⁾ Raman spectroscopy, as NIR spectroscopy, can also be applied to *in situ* measurements and process monitoring.^(54, 58)

Nowadays, the concept of quality control of the pharmaceutical final product is overcome by the necessity of built in the quality of the products, through design strategies. Quality-by-Design (QbD) appears as a systematic and more flexible regulatory approach, capable of continuous improvement and based on optimization and understanding of how design of a product and its manufacturing process may affect product quality.⁽¹¹⁸⁾ PAT is consistent with this system, being recommended by FDA and EMA. The use of PAT tools, namely vibration spectroscopy techniques within this context is encouraged, reducing risks to quality and regulatory concerns while improving efficiency. It was defined by the FDA as a system for the design, analysis and control of manufacturing processes through timely measurements of critical quality and performance attributes of raw and in-process materials and processes, with the goal of ensuring final product quality.^(119, 120)

Moradiya *et al.* reported several studies using NIR spectroscopy as PAT for in-line and off-line measurements. Those studies use QbD approach in continuous and scalable cocrystallization manufacturing processes, using hot melt extrusion cocrystallization method. A NIR probe was used for in-line control. The study proved that NIRS is a viable technique to in-line and in real-time process monitoring, to support the establishment of critical processing parameters (CPP) and to method's optimization.^(15, 42, 43)

2.5.2. Differential scanning calorimetry

DSC is a thermal analysis technique that allows to study the influence of the temperature in the heat capacity of the compounds. It involves the heating or cooling of a sample with a known mass, which suffers changes in its heat capacity that is traced in changes of the heat flow. DSC allows the detection of melting points, glass transitions and phase changes. It is widely used in pharmaceutical industry to verify phase changes or polymorphs⁽¹⁰⁵⁾ and to obtain information on sample's purity. Therefore, this technique is commonly used in analytical laboratories, process control and quality assurance.⁽⁹⁰⁾

DSC equipment can be from two main types: heat flux and heat flow. Heat flux DSC is composed by a furnace with one block for both sample and reference. Sample is placed in a pan (aluminum, stainless or platinum pans) and the reference is an empty pan. In the sample holder, sample and the reference are connected by a low-resistance heat flow path. The temperature difference between sample and reference is measure. Sensors used are generally thermal sensors, as thermocouples. In heat flow DSC have the heat that enters and leave the sample is directly measure. The calorimeter uses a feedback loop to keep the temperature within the material constant and measures the required power to do this against known standards.⁽⁹⁰⁾

DSC curves or thermograms represent heat flow as function of temperature. Usually, there are two types of events occurring in thermograms: endothermic and exothermic. Endothermic events can represent melting, sublimation, solid-solid transitions, desolvation or chemical reactions. Exothermic events can be crystallizations, soli-solid transitions, decomposition or chemical reactions. In the event of a glass transition only a baseline shift is seen corresponding to a change in the heat capacity of the sample.⁽⁹⁰⁾

DSC can be used as a screening technique, as described in section 2.3.2.. As a characterization technique, it allows to determine cocrystal melting point, which is, in the most part of the cases, different from the melting point of components. In this case, cocrystal's thermogram has one endothermic peak. It can also provide information about sample's purity, analyzing the number of peaks that the thermogram presents.^(101, 105, 121)

2.5.3. Powder X-ray diffraction

Diffraction techniques that use X-rays are used to obtain structural information of the compounds, once wavelengths used are between the range of 0.5 and 2.5 Å, being the same order than the shorter interatomic interactions. When sample is irradiated with an X-ray beam, a diffraction pattern is produced and this process is based in Bragg's law. An X-ray can be partially scattered by crystal's surface and the part that is not scattered passes

through the next layer of atoms and the process happens repeatedly in the next layers, producing a characteristic diffraction pattern.⁽¹²²⁾

Only crystalline samples provoke diffraction of the X-ray and the spacing between layers must be similar to beam's wavelength. Diffracted beams can be in phase, producing a constructive interference and the diffraction pattern shows a peak, or out of phase, which promotes a destructive interference and no peak is seen.⁽¹²²⁾

Powder X-ray diffraction (PXRD) and single crystal X-ray diffraction (SCXRD) are both diffraction techniques. A powder is used in PXRD, while in SCXRD, an individual crystal is required. PXRD is generally easier and convenient, once it does not require individual crystals, which sometimes does not represent the entire sample, and it can be performed with bulk materials of crystalline solids.⁽¹²²⁾

A diffraction pattern plot represents intensity as a function of detector's angle (2θ).

The powder X-ray diffractometer is constituted by four parts: the chamber, the command center, the computer system and the refrigeration system. Chamber is divided into three parts: the X-ray source (X-ray tubeshield transmitter), the sample stage (distance ring sample container), a detector (curved position sensitive detector) and a way to vary de angle θ (Figure 6). The distance ring sample container is placed between the transmitter and the detector. It is constituted for a sample container fixed part (SCFP), in the lower part, and a sample container movable part (SCMP), in the upper part.

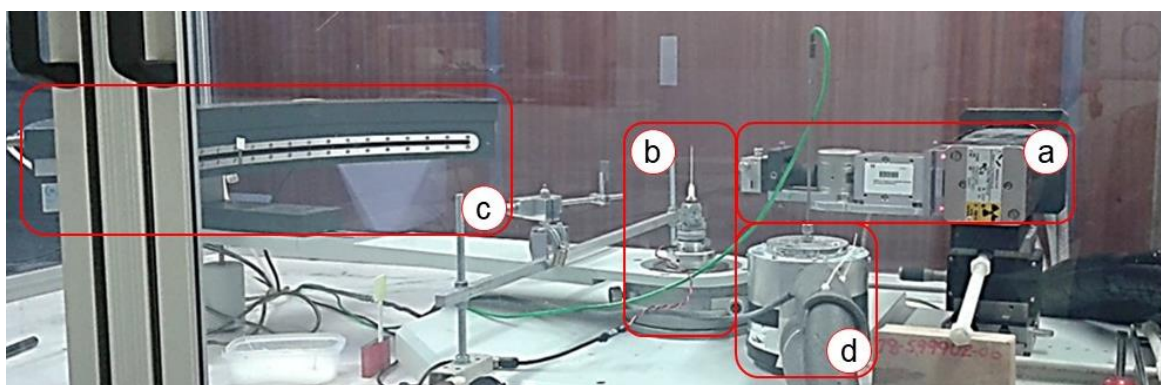


Figure 6: PXRD equipment with the X-ray tubeshield transmitter (a), the distance ring sample container (b), detector (c) and the temperature variation chamber (d).

The command module, which is placed outside the chamber, is divided into the module of the detector monitoring and chamber's temperature control and the module of high voltage generator and X-ray glass-tube control (Figure 7). The computer system allows data acquisition, analysis control and monitoring and results treatment and interpretation. Sample preparation generally involve capillaries or mark-tubes made of glass, which are fill with the sample and placed on the SCMP to proceed to the analysis.

PXRD is a preferred technique to cocrystal's characterization, once it can detect changes in crystal lattice. It is also widely used in pharmaceuticals to the study of

polymorphs and salts. However, this technique has some drawbacks, such as long measurement time, intensity concerning isostructural crystals and problems with preferred orientation effects.⁽¹²³⁾ Quantitative analysis is also possible, being possible to obtain information about cocrystal's purity. Padrela *et al.* developed a PXRD method for cocrystal's purity quantification. The method was developed for the system indomethacin-saccharin and characteristic diffraction peak of the system was used to construct the calibration curve.⁽¹²⁴⁾

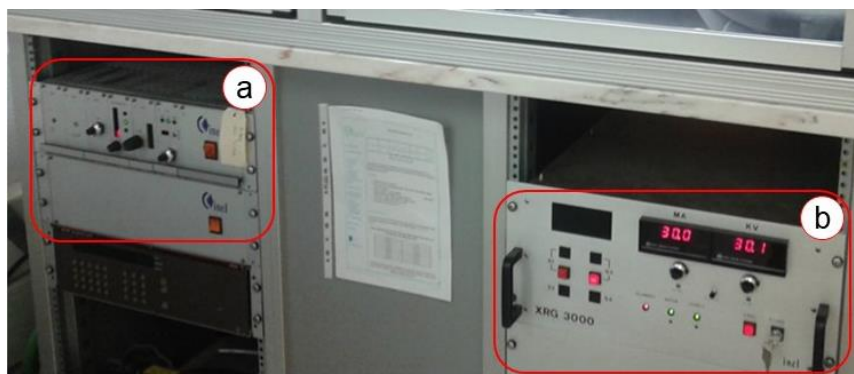


Figure 7: PXRD command module with the detector monitoring and temperature chamber control module **(a)** and the high voltage generator module **(b)**.

2.6. Multivariate data analysis

Vibrational spectroscopy generates large data sets, so appropriated data treatment tools are needed. The information obtained from vibrational spectroscopy is multivariate, due to non-selective nature of the techniques. Therefore, multivariate analysis is necessary, allowing the simplification of the large data sets, providing essential knowledge of processes and qualitative and quantitative information.⁽¹²⁵⁾

Before performing the multivariate analysis, a spectral pre-treatment can be required. This is based in mathematical corrections that allow removing interfering spectral parameters, such as light scattering, pathlength variations and random noise. Methods as standard normal variate (SNV) are used. To improve resolution and remove base line offsets, derivatives are useful techniques. However, derivatives amplifies the noise, so smoothing algorithms, such as Savitzky-Golay are used.⁽¹²⁶⁾

Principal component analysis (PCA) is a method of data deduction or data compression. This method is useful to describe a large portion of the variability in highly multivariate data with a low number of new variables.

Hierarchical cluster analysis (HCA) is a cluster method that joins similar objects (samples) in a group (cluster); in this way, objects in the same group have similar properties and are in some way different from objects from another group.⁽¹²⁶⁾

2.6.1. Pre-processing methods

SNV pre-processing is used for signal and offset correction, being important for reducing effects as light scatter correction on data. This method is particular important in diffuse reflectance spectroscopy, since light meets a particle and it is reflected when the refractive index changes. Light's scattering will depend on particles' size/shape and on differences in refractive indices. For example, small particles scatter more light than larger ones. In NIR spectroscopy, the analysis of powders by diffuse reflectance is highly affected by the physical properties of the samples, therefore if only the chemical composition of the sample is of interest, the physical information need to be reduce applying normalization methods such as SNV.⁽¹²⁶⁾

SNV method centers and scales individual spectra, allowing the elimination of variation between spectra. This way, spectrum becomes centered on zero, in vertical scale, and varies from -2 to +2. SNV's transformed value is

$$x_{ik}^* = (x_{ik} - m_i) / s_i \quad (\text{Eq.1})$$

where x_{ik} is the spectral measurement at the k th wavelength for the i th sample, m_i is the mean of the k spectral measurements for sample i and s_i is the standard deviation of the same k measurements.⁽¹²⁶⁾

There are other methods to achieve the similar results. The main difference is that SNV standardizes each spectrum using only data from the spectrum and not using the mean spectrum of any set.⁽¹²⁶⁾ Methods choice is a matter of taste and software availability, aiming to modulate the acquired spectra for a better identification of spectra differences.

Mean center is a method based on centering data around zero. This is performed by subtracting a mean value of each column to the variable. Autoscale is another scaling method that performs a mean center and then scale each variable to unit standard deviation. Both methods can be employed before, for example PCA, since this type of method requires normalization of the initial data.⁽¹²⁶⁾

2.6.2. Principal component analysis

The wavenumbers obtained in vibrational spectra are a large number of correlated variables, which can be reduced using PCA. PCA is a method of data reduction, which is useful to reduce the dimensionality of a data set with a high quantity of correlated variables, in a low number of new variables called principal components (PC). This is accomplished by converting the original variables into the PC, that are uncorrelated and ordered so that the first few PC retain most of the variation present in all of the original variables.^(109, 126, 127) This can be helpful in data understanding and interpretation, once it enables a simple comprehensive visualization of the whole data.

PCA is based on an eigenvector decomposition of the covariance or correlation matrix of the original variables. For a given data matrix \mathbf{X} with m rows, each one being a sample, and n columns, each one being a variable, the covariance matrix of \mathbf{X} is

$$\text{cov}(\mathbf{X}) = \frac{\mathbf{X}^T \mathbf{X}}{m-1} \quad (\text{Eq. 2})$$

where \mathbf{X}^T is the transpose of the matrix \mathbf{X} . If the columns have been autoscaled equation 2 gives the correlation matrix of \mathbf{X} . PCA decomposes the data matrix \mathbf{X} as the sum of the outer product of vectors \mathbf{t}_i (scores) and \mathbf{p}_i (loadings) plus a residual matrix \mathbf{E} . this decomposition is given by

$$\mathbf{X} = \mathbf{t}_1 \mathbf{p}_1^T + \mathbf{t}_2 \mathbf{p}_2^T + \dots + \mathbf{t}_A \mathbf{p}_A^T + \mathbf{E} \quad (\text{Eq.3})$$

where A is the number of principal components and have to be less or equal to the smallest dimension of \mathbf{X} . The scores contain information about how the samples relate to each other and the loadings contain information on how the variables relate to each other. The PCA model can be described in matrix notation as

$$\mathbf{X} = \mathbf{TP}^T + \mathbf{E} \quad (\text{Eq. 4})$$

where \mathbf{T} is the matrix scores and \mathbf{P} is the loading matrix. \mathbf{E} contains the residuals, containing information about noise or irrelevant variability in \mathbf{X} . The scores \mathbf{T} are linear combination of the originals variables of \mathbf{X} . Loading \mathbf{P} are estimated by regressing \mathbf{X} onto \mathbf{T} . Residual matrix \mathbf{E} is calculate by subtracting the estimates of \mathbf{TP}^T from \mathbf{X} .⁽¹²⁸⁾

2.6.3. Hierarchical cluster analysis

HCA is a clustering method which explore the association of samples in groups and among groups showing a hierarchy. The result of HCA is typically presented in a dendrogram, a plot that shows the organization of samples and its relationships in tree form.^(126, 129)

HCA can be divided in agglomerative and divisive methods. In agglomerative methods, search for clusters is started by treating each sample as a separate group and in the end all samples are in the same large group. Divisive methods start with all samples in one group and hierarchically divide the group into clusters. Focusing on the agglomerative methods, a measure of dissimilarity between sets of observations is require, in order to decided which clusters should be combined. Generally, this is accomplished firstly by choose an appropriate metric, which means a measure of distance between pairs of observations. Secondly, defining a linkage criterion to specify the dissimilarity of sets as a function of the pairwise distances of observation in sets.⁽¹²⁶⁾

Ward's method, or minimum variance method, is a variant of linkage criterions based in optimal value of a target function. As others clustering methods, Ward's method begins with n clusters, each one containing a single object. These clusters are combined to make one cluster containing all objects, step by step. In each step, a new cluster that minimizes variance is produced, measured by an index called E or sum of squares index.⁽¹³⁰⁾

2.7. Hydrochlorothiazide

Hydrochlorothiazide (HTZ) is a diuretic thiazide. Thiazides were discovered in 1957 and became one of the most used antihypertensive drugs, once they are generally effective and inexpensive. HTZ promotes the increase of water and electrolytes excretion, such as sodium, potassium, chloride and magnesium, by reducing the reabsorption of electrolytes from the renal tubules. HTZ is used in the treatment of several disorders, namely, hypertension, edema, diabetes insipidus and hypoparathyroidism.⁽¹³¹⁾

2.7.1. Mechanism of action

HTZ block the Na^+/Cl^- symporter in the distal convoluted tubules (DCT), a nephron segment, which prevents the water reabsorption. In a normal situation, this symporter transports sodium and chloride ions from the lumen into the epithelial cell of the DCT.^(131, 132) This transport depends of the sodium gradient provided by Na^+/K^+ ATPases, which are located in the basolateral membrane. When sodium is inside the cell, the Na^+/K^+ ATPase transports it out into the interstitium (Figure 8). The transport promotes an osmolarity increase, creating an osmotic gradient for water reabsorption. HTZ inhibit the Na^+/Cl^- symporter, decreasing Na^+ transport and, thus, reduces the osmotic gradient and water reabsorption.⁽¹³¹⁾

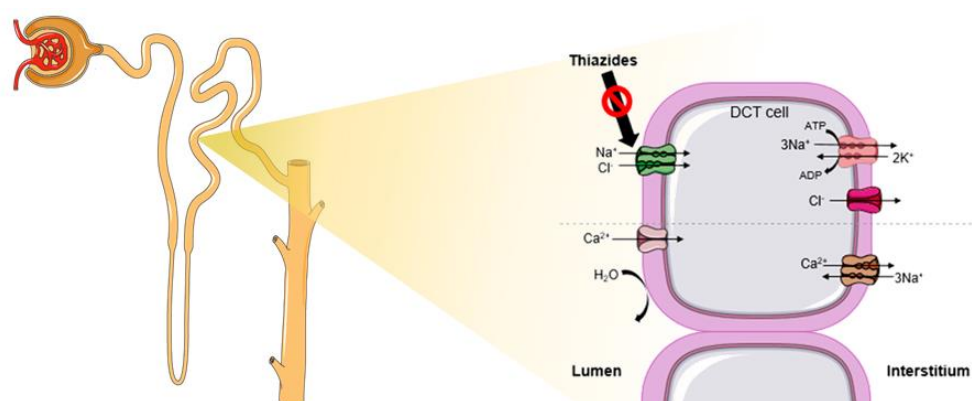


Figure 8: Illustrative scheme DCT as a part of the nephron (left) and of electrolytes transport in a cell of the DCT and representation of the thiazides action on Na^+/Cl^- symporter (right) (adapted from Kester, M. *et al.* ⁽¹³³⁾).

2.7.2. Hydrochlorothiazide in the treatment of hypertension

Hypertension, or high or raised blood pressure is considered a public global health issue by the World Health Organization (WHO). It affects 1,13 billion people worldwide and it is one of the major risk factors for global mortality. Hypertension is characterized by a persistent raised pressure in blood vessels and it is a major risk for coronary heart disease, ischemic and hemorrhagic stroke, heart failure, peripheral vascular disease, renal injury, retinal hemorrhage and visual damage.⁽¹³⁴⁾

HTZ is used alone or in combination with other antihypertension agents for the treatment of hypertension, preventing morbidity and mortality related to this disorder. HTZ mechanism to prevent hypertension is not fully understood. Indirectly, promotes the decrease of blood pressure, by decreasing sodium reabsorption in DCT cells. This way, water reabsorption is decreased, which results in increased fluid loss to urine and decreased plasma volume. This volume loss fallout in reduced venous return, reduced cardiac output and, consequently, decreased blood pressure. This effect leads to renin release and activation of renin-angiotensin system, which ends in vasoconstriction to restore blood pressure.⁽¹³⁵⁾

HTZ action at long term has not necessarily due to diuretic function. Thiazides have an activating effect in calcium-activated potassium channels in vascular smooth muscles and an inhibitory effect in several carbonic anhydrases in vascular tissue. These effects promote directly vasodilation.^(131, 136)

2.7.3. Absorption, metabolism and excretion

HTZ belongs to class IV of BCS, which means that it has low solubility and low permeability. Water solubility of HTZ is $722 \text{ mg}\cdot\text{L}^{-1}$, at 25°C .⁽¹³⁷⁾ HTZ is orally administrate and between 50 and 60% of the therapeutic level dose of HTZ is available in the blood stream. Its absorption takes place mainly in duodenum and upper jejunum. Around 40% of the absorbed hydrochlorothiazide binds to plasma proteins and the drug accumulates in erythrocytes. Peak plasma levels are reached between 2 and 3 hours after dosing. Half-life of HTZ is 5.6 and 14.8 hours. Hydrochlorothiazide is not metabolized and it is eliminated rapidly by the kidney.^(131, 138)

2.7.4. Hydrochlorothiazide cocrystals

HTZ's solubility problems have been the main focus for the solid manipulation of this API through cocrystallization. There are several hydrochlorothiazide cocrystals described in literature (Table 6).

Palash Sanphui and Lalit Rajput were one of the firsts reporting HTZ cocrystals and their single crystal structures, with the aim of solubility improvement. The cofomers used were nicotinic acid, nicotinamide, succinamide, *p*-aminobenzoic acid, resorcinol and pyrogallol. The cocrystallization method was liquid-assisted grinding. They found out that the N-H \cdots O sulfonamide catemer synthons found in the stable polymorph of pure HTZ are replaced in the co-crystals by drug-coformer heterosynthons. Solubility and stability experiments were performed in water, with neutral pH, at room temperature and the cocrystal with *p*-aminobenzoic acid was selected as the best solid form in terms of solubility

and stability. They also stated that there are an inverse correlation between the melting points of cocrystals and their solubility.⁽³⁾

Analyzing the already reported cocrystals, HTZ seems prefer to bind to hetero atoms of the coformer. N-H...O synthon is the most common, namely, in cocrystals with coformers as nicotinamide^(3, 95), nicotinic acid^(3, 95), succinamide^(3, 95), *p*-aminobenzoic acid^(3, 95), 4-dimethylaminopyridine⁽²⁾, picolinamide⁽²⁾, malonamide⁽¹⁾, isonicotinic acid⁽¹⁾, pyrazinamide⁽⁸⁷⁾ and 4,4'-bipyridine⁽⁸⁷⁾. N-H...H synthon is also common. Primary and secondary sulfonamides are HTZ groups frequently involved in cocrystal formation (see Figure 9).

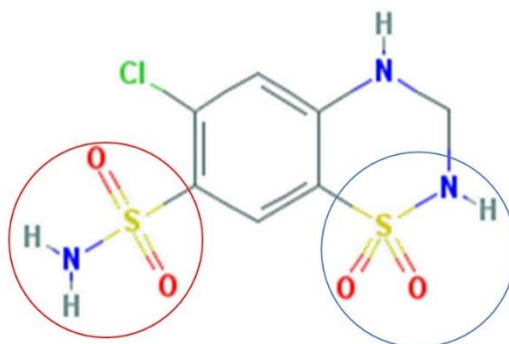


Figure 9: Hydrochlorothiazide structure, with primary sulfonamide group (red circle) and secondary sulfonamide group (blue circle) (Image adapted from PubChem⁽¹³⁹⁾).

Several cocrystallization methods are also reported, being the liquid assisted grinding the one mostly used.^(1, 3, 95, 140) A prolonged neat grinding was used in the case of the coformer isonicotinic acid, because of the long induction period before cocrystal formation.⁽¹⁾ Solution cocrystallization⁽²⁾ and reaction cocrystallization⁽⁸⁷⁾ are also described.

Solubility is the property that is frequently studied and improved with cocrystal formation. Cocrystals with nicotinamide^(3, 95), *p*-aminobenzoic acid^(3, 95), resorcinol^(3, 95), pyrogallol^(3, 95), phenazine⁽²⁾, 4-dimethylaminopyridine⁽²⁾, are some examples of described cocrystals with improved solubility comparing to the API. There are also cases where cocrystal formation enhanced properties as dissolution⁽⁸⁷⁾ and permeability^(3, 95). Despite of the several studies about cocrystal's properties, studies conditions are different, so an absolute comparison is not possible.

Cocrystal with HTZ and sucralose as the coformer is an interesting case, where dissolution profile was improved and the coformer allowed masking the taste, an important characteristic for the development of oral disintegrating tablets.⁽¹⁴¹⁾

Table 6: Hydrochlorothiazide cocrystals described in literature, with resumed information about the cocrystallization method, synthons involved in the cocrystal and properties improved comparing with the API.

Coformer	Cocrystallization method	Synthons involved	Properties improvement
Nicotinic acid ^(3, 95)	Liquid assisted grinding	N-H···O	Improved permeability
Nicotinamide ^(3, 95)	Liquid assisted grinding	N-H···O	Improved solubility and permeability
Succinamide ^(3, 95)	Liquid assisted grinding	N-H···O	Improved permeability
<i>p</i> -aminobenzoic acid ^(3, 95, 142)	Liquid assisted grinding	N-H···O	Improved solubility and permeability
Resorcinol ^(3, 95)	Liquid assisted grinding	-	Improved solubility and permeability
Pyrogallol ^(3, 95)	Liquid assisted grinding	-	Improved solubility and permeability
Phenazine ⁽²⁾	Solution crystallization	N-H···H O-H···N	Improved solubility
4-dimethylaminopyridine ⁽²⁾	Solution crystallization	N-H···O C-H···O	Improved solubility
Picolinamide ⁽²⁾	Solution crystallization	N-H···O N-H···N	Without significant differences
Aerosil ⁽¹⁴⁰⁾	Liquid assisted grinding	N-H···O	Improved solubility
Piperazine ⁽¹⁾	Liquid assisted grinding	N-H···N	Improved solubility and better diffusion behavior
Tetramethylpyrazine ⁽¹⁾	Liquid assisted grinding	N-H···N	Without significant differences
Picolinamide ⁽¹⁾	Liquid assisted grinding	N-H···O	Improved solubility and better diffusion behavior
Isoniazid ⁽¹⁾	Liquid assisted grinding	N-H···N	Without significant differences
Malonamide ⁽¹⁾	Liquid assisted grinding	N-H···O	Without significant differences
Isonicotinic acid ⁽¹⁾	Prolonged neat grinding	N-H···O	Without significant differences
Pyrazinamide ⁽⁸⁷⁾	Reaction crystallization	N-H···O	Improved solubility and dissolution
4,4'-bipyridine (cocrystal hydrate) ⁽⁸⁷⁾	Reaction crystallization	N-H···O O-H···N	Improved solubility and dissolution
1,2-bis(4-pyridyl)ethane ⁽⁸⁷⁾	Reaction crystallization	N-H···N	Improved solubility and dissolution
trans-1,2-bis(4-pyridyl)ethylene ⁽⁸⁷⁾	Reaction crystallization	N-H···N	Improved solubility and dissolution
Sucralose ⁽¹⁴¹⁾	Solvent evaporation	-	Improved dissolution
Isonicotinamide (cocrystal hydrate) ⁽¹⁴³⁾	Slow solvent evaporation	N-H···O O-H···N	High thermal stability

3. MATERIALS AND METHODS

3.1. Materials

Hydrochlorothiazide crystalline ($\geq 99.0\%$ purity), adenine ($>99.0\%$ purity), L-ascorbic acid ($>99.0\%$ purity), caffeine ($>99.0\%$ purity), citric acid ($\geq 99,5\%$ purity), nicotinamide ($\geq 99,5\%$ purity), *p*-aminobenzoic acid ($>99.0\%$ purity) and tromethamine ($>99.0\%$ purity) were acquired from Sigma-Aldrich (St. Louis, USA). DL-malic acid ($>99.5\%$ purity) was acquired from Merck (Darmstadt, Germany) and D-mannitol ($>99.0\%$ purity) from Riedel-de-Haën (Seelze, Germany). L(+)-arginine ($\geq 98\%$ purity) was purchase from Acros Organics (New Jersey, USA) and L-tryptophan (99%) from Alfa Aesar (Kandel, Germany). Cofomers structure can be seen in Figure 10. Sodium phosphate dibasic dihydrate ($\text{HNa}_2\text{O}_4\text{P}\cdot 2\text{H}_2\text{O}$) and sodium phosphate monobasic monohydrate ($\text{NaH}_2\text{O}_4\text{P}\cdot \text{H}_2\text{O}$) were acquired from Sigma-Aldrich (St. Louis, USA).

All the solvents were analytical grade. Methanol (MeOH) and acetone (Ace) were acquired from VWR Chemicals (Fontenay-sous-Bois, France). Dichloromethane (DCM), 2-propanol (IPro) and ethyl acetate (EtOAc) were acquired from Sigma-Aldrich (St. Louis, USA). Ethanol (EtOH) was acquired from Chem-Lab NV (Zedelgem, Belgium) and dimethyl sulfoxide (DMSO) from Riedel-de-Haën (Seelze, Germany). Acetonitrile (ACN) was purchase from Fisher Scientific (Loughborough, UK).

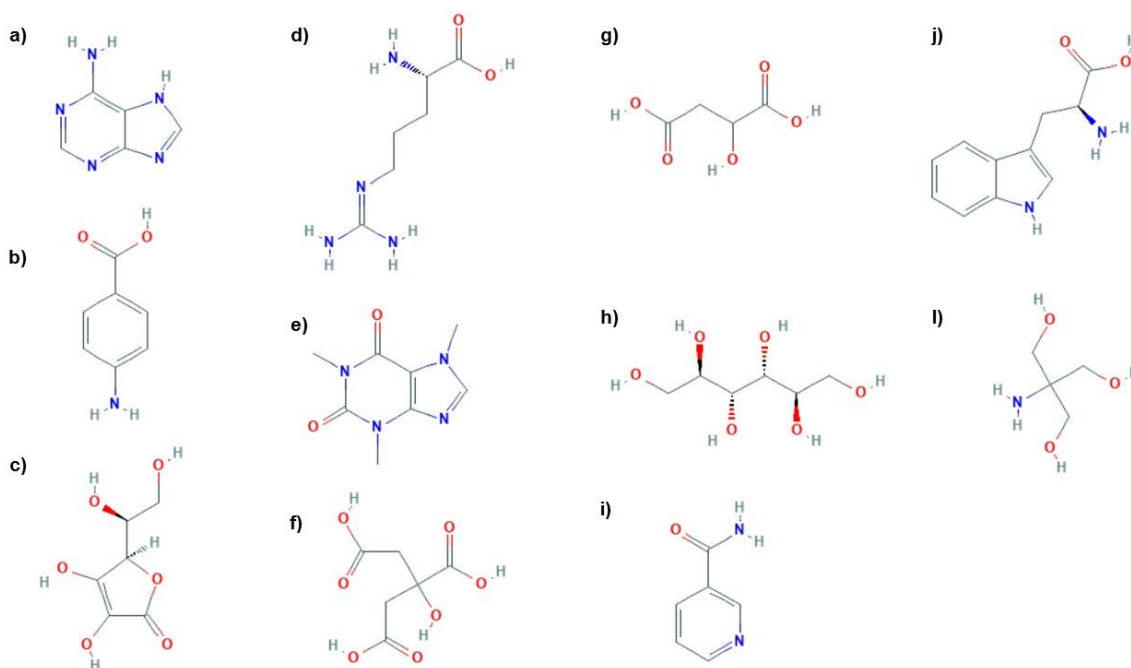


Figure 10: Cofomers' chemical structure: **a)** adenine (Ade), **b)** *p*-aminobenzoic acid (PABA), **c)** L-ascorbic acid (Asc), **d)** L(+)-arginine (Arg), **e)** caffeine (Caf), **f)** citric acid (Cit), **g)** DL-malic acid (Mal), **h)** D(-)-mannitol (Man), **i)** nicotinamide (Nic), **j)** L-tryptophan (Tryp), **l)** tromethamine (Tris). (Images retrieved from PubChem⁽¹³⁹⁾)

3.2. Cocrystallization methods

3.2.1. Screening experiments

Two cocrystal screening experiments were performed, based in a slurry ultrasound-assisted method. 96-well plates (Orange Scientific, Braine-l'Alleud, Belgium) were used and the API and coformers were distributed in the wells, accordingly to Figure 11 and Figure 12. Seven solvents and six different coformers were selected based on literature review and theoretical studies on the functional groups of HTZ frequently involved in cocrystal formation and synthons. For the same reason, the molar ratios of HTZ:coformer 1:1 and 1:2 were chosen.

In the first cocrystal screening experiments, HTZ and the six coformers were weighted and transferred to the 96-well plate. The quantity of HTZ dispensed was 25 mg (0.084 mmol) on each well. The coformers were added posteriorly in the pre-defined ratio. The last line of the plate (line H) corresponds to reference samples, the physic mixtures. An amount of 30 μ L of the selected solvent was added to each well, except in the line containing the physical mixtures. In the end, the 96-well plate was sealed with parafilm and subjected to ultrasounds, in an ultrasound bath, for 2 hours. Afterwards, the plate was unsealed and left to evaporate overnight in a fume hood.

After the solvent evaporated, the final product of each well was characterized by NIRS, MIRS and RS. During the period that the plate was not being used, it was sealed with parafilm and placed on a desiccator, to avoid product alteration.

In the second cocrystal screening experiments, for each column of the 96-well plate, a mixture of HTZ and the correspondent coformer in the defined ratio were prepared. Each mixture was composed for 300 mg of HTZ and the correspondent quantity of coformer in the defined ratio. Approximately 35 mg of each mixture was distributed in the respective well. An amount of 100 μ L of the selected solvent was added to each well, except in the line H containing the physical mixtures. Comparing with the first plate, an increased amount of solvent was used in this plate as a tentative to increase samples homogeneity. The 96-well plate was sealed with a cover and parafilm and subjected to ultrasounds, in an ultrasound bath, for 4 hours, in a controlled temperature of 40°C. An enlarged time of ultrasound was applied, as well as a controlled temperature, to improve method's performance.

Finally, the plate was unsealed and left to evaporate overnight in a fume hood. After solvent evaporation, the final product was immediately characterized by MIR and RMS. During the period that the plate was not being used, it was sealed with the cover and parafilm and placed on a desiccator, to avoid product alteration.

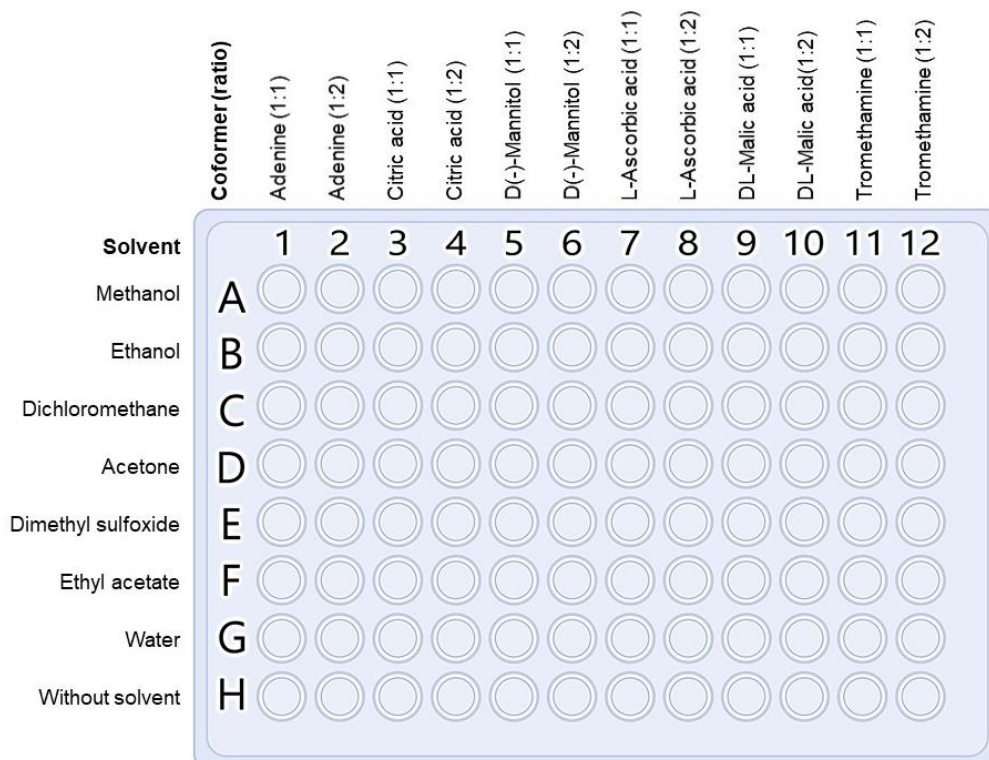


Figure 11: Schematic representation of the 96-well plate with cofomers and solvents distribution used in the first cocrystal screening experiment.

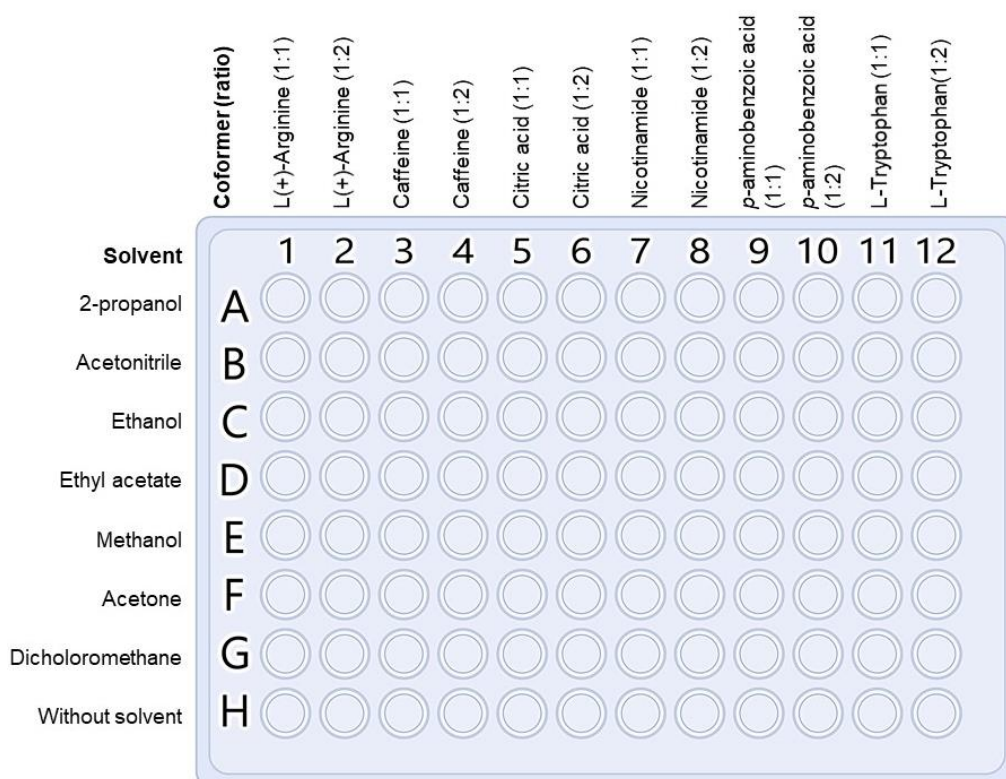


Figure 12: Schematic representation of the 96-well plate with cofomers and solvents distribution used in the second cocrystal screening experiment.

3.2.2. Laboratory-scale experiments

After analysis of screening procedure, all systems were submitted to laboratory-scale experiments, in order to verify screening results, analyzing the influence of scale increase on cocrystallization outcome and to produce a reasonable quantity of product to be characterized by NIRS, MIRS, DSC and PXRD, and to do solubility assays.

Laboratory-scale experiments were performed firstly through slurry cocrystallization method. In Table 7, the systems submitted to slurry cocrystallization are presented, with selected solvents. Slurry experiments were performed by adding 500 mg of HTZ and the equivalent molar amount of the coformer and 1.5 mL of the selected solvent into a borosilicate flask. The flask was closed and placed in a horizontal shaking bath (NE5-10D Shaking Water Baths, Clifton Range®, Nickel-Electro Ltd., Weston-super-Mare, United Kingdom) at 200 rpm and 40°C during 8h (Figure 13 (A)). Then, the solvent was left to evaporate at room temperature in a fume hood. Products were immediately characterized and, in the periods that they were not being used, they were kept in closed tubes.

Table 7: Systems tested through slurry cocrystallization method and respective solvent used.

System (ratio)	Solvent	System (ratio)	Solvent
HTZ:Ade (1:1)	DMSO	HTZ:Man (1:1)	DMSO
HTZ:Ade (1:2)	DMSO	HTZ:Man (1:2)	EtOH EtOAc
HTZ:Arg (1:1)	IPro	HTZ:Nic (1:1)	Ace IPro
HTZ:Arg (1:2)	IPro	HTZ:Nic (1:2)	MeOH
HTZ:Caf (1:1)	MeOH	HTZ:PABA (1:1)	EtOH
HTZ:Caf (1:2)	MeOH	HTZ:PABA (1:2)	MeOH EtOH
HTZ:Cit (1:1)	DMSO	HTZ:Tris (1:1)	DMSO
HTZ:Cit (1:2)	DMSO	HTZ:Tris (1:2)	DCM EtOAc
HTZ:Mal (1:1)	DCM EtOAc	HTZ:Tryp (1:1)	MeOH
HTZ:Mal (1:2)	DCM EtOAc	HTZ:Tryp (1:2)	MeOH

After analysis by MIRS and NIRS, it was found that the purity of these systems was not satisfactory. Therefore, a solvent evaporation method was used to improve purity.⁽⁶⁰⁾ All the systems were submitted to solvent evaporation method with a rationally selected solvent, based on compounds solubility. Some ratios were not tested, since slurry

experiments results demonstrate a preference for one of the ratios. Tested systems and method's conditions are presented in Table 8.

For the solvent evaporation method, 500 mg of HTZ and the equivalent amount of coformer were completely dissolved in the selected solvent or mixture of solvents⁽¹⁴⁴⁾. If need, heating was used to help the complete dissolution.

After complete dissolution, solvent was left to evaporate at room temperature in an orbital shaker at 200 rpm (3005, GFL, Burgwedel, Germany) until complete solvent evaporation (Figure 13 (B)). This method was applied with some variations, depending on systems:

- When DCM was used the crystallizer was covered with parafilm and small orifices were made. This was performed to decrease solvent evaporation rate, once this solvent has high volatility;
- Since DMSO is a low volatile solvent, the solutions were heated at 50 °C in a water bath with a thermostat (microprocessor control MPC, Huber Kältemaschinenbau AG, Germany) without agitation, to promote solvent evaporation;
- Some systems that continued with homogeneity problems were performed in the water bath at 10 °C, to increase cocrystallization time. Bath's temperature was controlled with the thermostat and with a cooler (Haake EK20, Thermo Scientific™, Karlsruhe, Germany) (Figure 13 (C)).

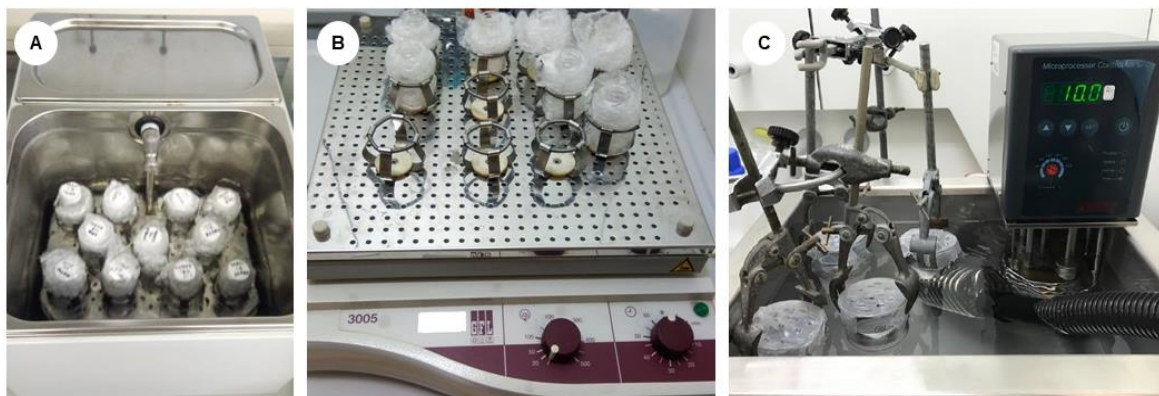


Figure 13: Experimental setup of cocrystallization through slurry using a shaker water bath, with horizontal shaking and temperature control (A); solvent evaporation method setup using the orbital shaking at room temperature (B); solvent evaporation method setup using the orbital shaking and a water bath with temperature control (C).

Table 8: Systems, solvents, volume, and temperature used in the cocrystallization by solvent evaporation.^a performed in a water bath with temperature control.^b Performed with the crystallizer cover with parafilm with small orifices.

System	Solvent	Volume (mL)	Dissolution temperature (°C)	Evaporation temperature (°C)
HTZ:Ade (1:1)	DMSO	20	25	50 ^a
HTZ:Ade (1:2)	DMSO	20	25	50 ^a
HTZ:Arg (1:1)	EtOH/H ₂ O	280/30	40	25
HTZ:Arg (1:2)	EtOH/H ₂ O	230/40	40	25
HTZ:Caf (1:1)	Ace	50	40	25
HTZ:Cit (1:1)	DMSO	20	25	50 ^a
HTZ:Cit (1:2)	DMSO	20	25	50 ^a
	DCM	20	25	25 ^b
	MeOH	50	40	25
	MeOH	50	40	10 ^a
HTZ:Mal (1:1)	Ace	20	25	25
	DCM	20	25	25 ^b
HTZ:Mal (1:2)	DCM	20	25	25 ^b
	EtOAc	20	25	25
	EtOH	20	25	25
HTZ:Man (1:1)	DMSO	20	25	50 ^a
HTZ:Man (1:2)	EtOH/H ₂ O	50/20	40	10 ^a
HTZ:Nic (1:1)	Ace	50	40	25
HTZ:Nic (1:2)	Ace	50	40	25
HTZ:PABA (1:2)	MeOH	50	40	25
HTZ:Tris (1:1)	DMSO	20	25	50 ^a
	MeOH	50	25	10 ^a
HTZ:Tris (1:2)	DCM	20	25	25 ^b
	DMSO	20	25	50 ^a
	MeOH	50	25	10 ^a
	EtOH/H ₂ O	280/30	40	25

3.3. Characterization methods

Characterization methods used were near and mid infrared spectroscopy, Raman spectroscopy, Raman microspectroscopy, differential scanning calorimetry and powder X-ray diffraction. In the screening phase of the work, the final product of the first screening experiment was characterized through NIRS, MIRS and RS. In the second screening experiment, MIRS and RMS were used. Final products of laboratory-scale experiments were characterized with MIRS and NIRS, DSC and PXRD.

3.3.1. Mid Infrared spectroscopy

Mid infrared spectra between 4000 cm^{-1} and 600 cm^{-1} were acquired using a Fourier transform mid infrared (FTIR) spectrometer (Frontier, PerkinElmer, Beaconsfield, UK) equipped with an attenuated total reflectance (ATR) accessory (PerkinElmer, Beaconsfield, UK), which can be seen in Figure 14. The resolution was set to 4 cm^{-1} and each stored spectrum is the average of 32 co-added scans. The spectrophotometer has a deuterated triglycine sulphate (DTGS) detector and a mid-infrared light source. To allow optimal contact between the sample and the crystal as well as sample-to-sample reproducibility, the ATR accessory is equipped with a pressure arm with the indication of force. Samples were directly applied on the ATR crystal and the same force was applied in each measurement. The instrument is controlled via the Spectrum software (PerkinElmer, Beaconsfield, UK). A background was made with the ATR accessory empty. For each sample, three replicas were taken.



Figure 14: FT-MIR equipment with ATR accessory (Frontier, PerkinElmer), where samples are directly placed, pressed with a pressure element and measure.

3.3.2. Near Infrared spectroscopy

Near infrared spectra in the range 10000 to 4000 cm^{-1} were acquired using Fourier-transform near infrared analyzer (FTLA2000, ABB, Québec, Canada) that can be seen in Figure 15. The spectrophotometer is equipped with an indium-gallium-arsenide (InGaAs) detector and powder sampling accessory (ACC101, ABB, Québec, Canada) with a 2 cm diameter window enabling measurements on a 0.28 cm^2 illumination area. The resolution was set to 8 cm^{-1} and each stored spectrum was an average of 64 co-added scans. The instrument is controlled via the Grams LT software (version 7, ABB, Québec, Canada). The background was taken with a certified material of 100% reflectance, (polytetrafluoroethylene, PTFE, SKG8613G, ABB, Québec, Canada). For each sample, three spectral replicates were made.



Figure 15: FT-NIR equipment with sample placed in the accessory of powder measurement (FTLA2000, ABB).

3.3.3. Raman spectroscopy

In the first screening analysis, spectra were acquired using a Raman CORA5700 (Cora 5X00 Raman spectrometer, Anton Paar, USA) equipped with a 785 nm laser, which is demonstrated in Figure 16. Spectra's range was from 98 to 1800 cm^{-1} and laser power was setting to 450 mW. Sample's exposure time was 20 seconds and, for each sample, two spectral replicates were made by placing the powder into a glass support that was inserted inside the spectrometer align with the laser.



Figure 16: Raman portable spectrometer (right), connected with a computer (left) (Cora 5X00 Raman spectrometer, Anton Paar).

3.3.4. Raman microspectroscopy

For the second screening analysis, Raman microspectroscopy (RMS) was applied and each sample was analyzed inside the well, directly in the 96-well plate (*in situ* analysis). Raman spectra were obtained using two Raman spectrometers. A Raman LabRAM HORIBA Jobin Yvon Spex spectrometer interfaced to an Olympus microscope with 100x objective lens, diffraction gratings with $1800 \text{ lines mm}^{-1}$ and equipped with a 632.8 nm emission line of a HeNe laser at a power of 20 mW. For the samples containing L-tryptophan, an Horiba Jobin-Yvon LabRam Microscope XploRATM with 100x objective lens, equipped with a excitation wavelength of 532 nm from a Nd:YAG laser at a power of 25 mW and with a range of diffraction gratings with 600, 1200, 1800 and $2400 \text{ lines mm}^{-1}$ available was used.

For both, the incident beam perpendicular to the plane of the sample is focused through the microscope lens, which also collects the Raman scattered radiation in back-scattering geometry. A highly sensitive CCD camera was used to collect the Raman spectra. Extended scans were performed on the spectral range 300 to 4000 cm^{-1} . The time of acquisition and the number of accumulations varied in order to obtain an optimized spectrum for each analyzed sample.

3.3.5. Differential scanning calorimetry

The DSC measurements were carried out on two equipment. The first one was a thermal analyzer (DSC 200 F3 Maia®, Netzsch-Gerätebau GmbH, Wittelsbacherstraße, Germany) under nitrogen atmosphere, which can be seen in Figure 17. The heating ramp was between 25°C and 300°C at a heating rate of $10^\circ\text{C}\cdot\text{min}^{-1}$. Approximately 1–2 mg of the sample was placed in aluminum-sealed pans. Obtained thermograms were analyzed using Proteus® software (Netzsch-Gerätebau GmbH, Wittelsbacherstraße, Germany) to determination of onset temperature, maximum temperature and enthalpy.

A differential scanning calorimeter (TA instruments, Q200, New Castle, USA) was also used, with sample purged flow at 50 mL.min⁻¹ with nitrogen. Heating ramp was defined with the rate of 10 °C.min⁻¹ from 20 °C to 300 °C. Approximately 3-4 mg of sample was weighted to aluminum hermetic crucibles for analysis. Obtained thermograms were analyzed using TA Universal Analysis software (TA, New Castle, USA) to determination of onset temperature, maximum temperature and enthalpy.



Figure 17: DSC equipment with autosampler accessory (DSC 200 F3 Maia®, Netzsch-Gerätebau GmbH).

3.3.6. Powder X-ray diffraction

Powder X-ray diffractometer used was an Equinox 3000 PXRD (Inel Inc[®], Stratham, USA) equipped with a high voltage generator (XRG 3000, Inel[®]), an X-ray monochromatized Cu K α 1 radiation ($\lambda=1.54056$ Å) glass-tube (PANanalytical, Netherlands) and a curved position sensitive detector (CPS 120, Inel[®]).

Sample preparation involved fill the capillaries or mark-tubes made of glass no. 14 (Hilgenberg, length=80mm; outside $\varnothing=1,0$ mm; wall thickness=0,01mm) with a certain amount of powder. The amount of powder was approximately 4 cm of mark-tube length. After powder filling, upper part of capillary was cut and closed with a lighter. Capillary was inserted in the orifice at the surface of sample container movable part (SCMP) and fixed with silicone paste. An apparatus for capillary alignment was used, where the SCMP was placed horizontally and the adjustment was done by observation and comparison with a reference line. Finally, the SCMP with the sample were replaced into the sample container fixed part (SCFP) (see Figure 18).

For PXRD analysis, a calibration file concerning the system at hand was produced and applied to the SYMPHONIX software (Inel[®] France). Data were collected by initiating the analysis and, for each sample, data collection was made until the achievement of a satisfactory noise-to-signal diffractogram (20 minutes). Data treatment, interpretation and exporting process was held in Peacock (Inel[®] France), where “x” axis of diffractograms was switched to “2-theta” and files must be exported as a text files (.txt) for latter analysis.

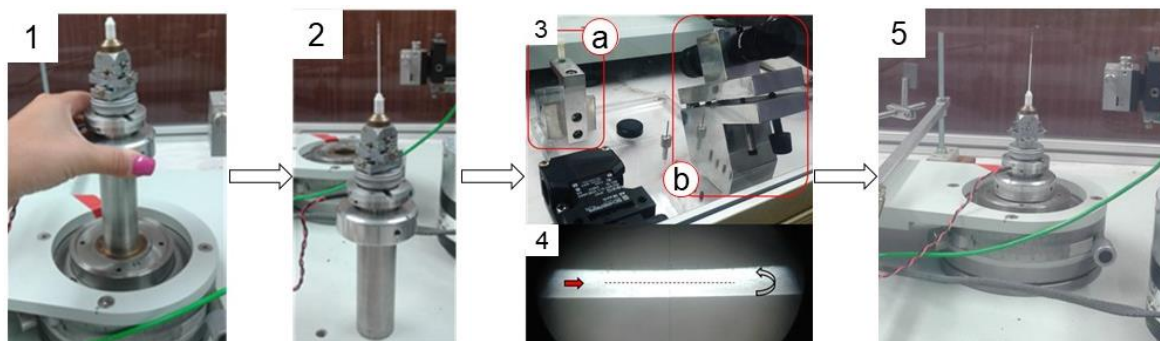


Figure 18: Sample assembly process, that start with partial removal of the sample container movable part (1), capillary placement (2) and complete SCMP removal for capillary alignment capillary with the help of the apparatus (3) constituted by SCMP locking support equipment (a) and calibration monacle (b). Alignment is done by observation (4) and, finally, sample container movable part is replaced into the sample container fixed part (5).

3.3.7. Solubility assays

Selected cocrystallization products were submitted to solubility assays. To mimic physiologic pH, a phosphate buffer (pH 7.4) was used. To prepare the phosphate buffer, 405.0 mL of a 0.2 M solution of sodium phosphate dibasic dihydrate and approximately 90.5 mL of a 0.2 M solution of sodium phosphate monobasic monohydrate were used. On a pH meter, $\text{NaH}_2\text{O}_4\text{P}\cdot\text{H}_2\text{O}$ solution was added to $\text{HNa}_2\text{O}_4\text{P}\cdot 2\text{H}_2\text{O}$ solution until pH 7.40 was achieved. Solution was added up to 1 L with distilled water. Phosphate buffer was used as solvent in all solutions.

Preliminary tests were executed with HTZ and all cofomers to select the most suitable wavelength. Solutions of a known concentration were prepared and spectra measurement was performed in a UV-Vis spectrophotometer (V-660 spectrophotometer, JASCO, Pfungstadt, Germany). A wavelength of 320 nm was chosen corresponding to a region where HTZ had the highest absorbance without cofomers interference.

Calibration curve was done with six solutions of HTZ with concentrations of 10, 25, 50, 75, 90 and 100 $\mu\text{g}/\text{mL}$. Absorbance measurements were performed at 320 nm with the temperature set at 37°C. Measurements were made in triplicate and the mean used to construct the calibration curve (absorbance vs HTZ's concentration). A linear regression was made and its equation was determined, as well as the correlation coefficient.

To determine solubility profile of HTZ and each cocrystal, 50-30 mL of a saturated solution was prepared in an Erlenmeyer flask. Closed flasks were placed in a water bath at 37°C under stirring (see Figure 19).

Aliquots of 1 mL were taken with syringes (B. Braun, Melsungen, Germany) and filtered with 0.45 μm filters (Filter-Bio, Nantong, Jiangsu P.R China). Samples were diluted in a ratio of 1:20 with phosphate buffer. Absorbance measurements were performed at 320 nm with the temperature set at 37°C. In total 13 aliquots were taken in a period of 24 hours.

The first aliquot was taken after 10 seconds of dissolution and, during the first hour, aliquots were taken and measured every fifteen minutes. After, aliquots were taken every hour for three hours and every two hours, until 12 hours of dissolution. The last aliquot taken after 24 hours. Another two aliquots at 36 and 48 hours were taken in the case of cocrystals with Tris.

Concentration value of HTZ was obtained through interpolation in the calibration line. A solubility curve (concentration vs time) was made for each cocrystal and for pure HTZ.

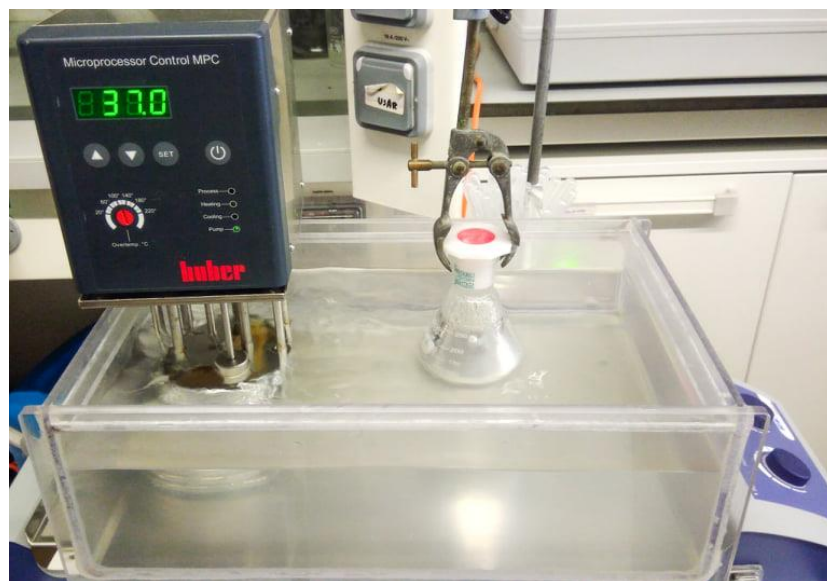


Figure 19: Setup of solubility experiments, where is visible the water bath with the heating thermostat and the flask with the solution being stirred.

3.4. Data analysis

For the first screening procedure, the MIR, NIR and RS spectra was analyzed by PCA to determine cocrystal formation and purity. Before the PCA the NIR and MIR spectra were pre-processed with SNV. In the case of the NIR spectra, the SNV was used to remove physical interferences due to differences in particle size. For the analysis of the MIR spectra, SNV was applied to remove spectral differences due to variations in spectral intensity provoked by small differences in the force applied between the samples and the ATR accessory. Mean center was used in all cases before PCA analysis.

For the second screening procedure, HCA using the Ward's method was used to see similarities between the MIR spectra of the cocrystallization products. For the HCA analysis the MIR spectra were pre-processed with autoscale. For the HTZ:PABA and HTZ:Cit systems, SNV was applied before the autoscale.

Matlab version 8.3 (MathWorks, Natick, MA, USA) and the PLS Toolbox version 7.5 (Eigenvector Research Inc., Wenatchee, WA, USA) were used for this analysis.

4. RESULTS AND DISCUSSION

The work is divided in cocrystal screening and cocrystal laboratory-scale production. After rational coformer selection based in literature, groups available to interaction and synthons prediction, screening experiments were performed. In these experiments, several coformers, ratios and solvents were tested, using techniques of vibrational spectroscopy and multivariate analysis of data, in order to select the most promising results in terms of cocrystal formation.

The laboratory-scale experiments involved the production of cocrystals in a higher scale to subsequent products characterization through several techniques. In Figure 20, a scheme of the sequence of the experimental work is presented.

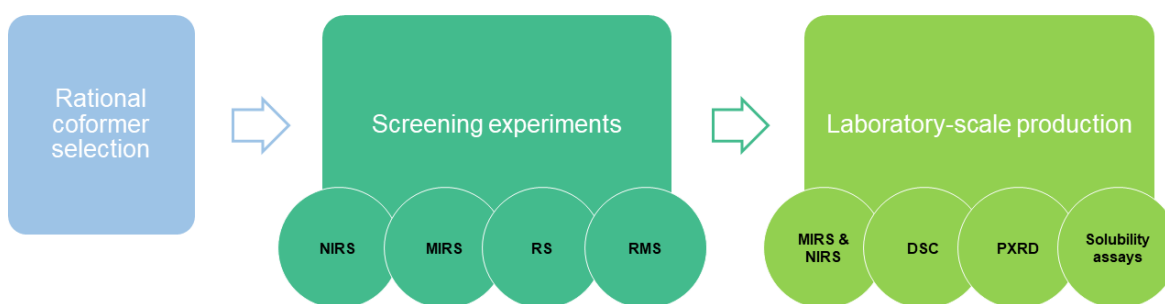


Figure 20: Sequential illustration of the steps involved in the work and characterization technique used in each phase.

4.1. Cocrystals screening

Cocrystals screening experiments involved two 96-well plates, where a total of eleven coformers, two API:Coformer ratios (1:1 and 1:2) and nine solvents were tested. Three vibrational spectroscopy techniques applied to screening experiments were study, analyzing advantages and disadvantages of each one.

4.1.1. Cocrystal screening experiments: part I

The cocrystallization products were analyzed with MIRS, NIRS and RS. Cocrystal formation was assessed through a comparison between the spectrum of the cocrystallization products with the one of physical mixture (mixture composed by the API and coformer). This process was repeated for all potential coformers. Additionally, spectra were analyzed by PCA to evaluate the similarity between products obtained with different solvents and PM.

After the completion of the cocrystal screening procedure, the wells containing ascorbic acid showed an apparently degraded product. Therefore, the results from these systems were not considered.

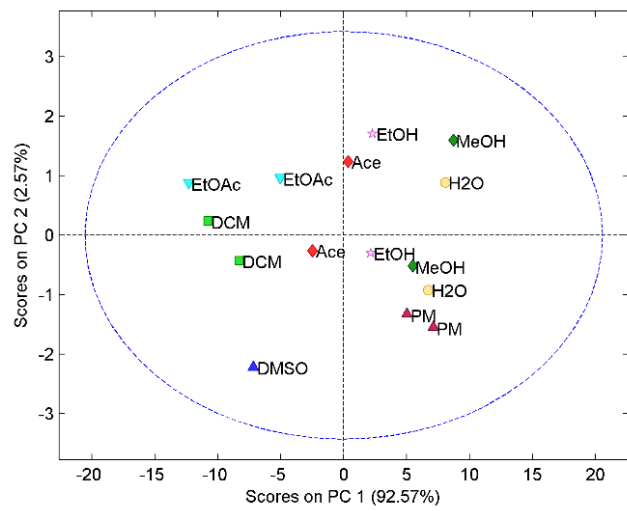
The analysis of the systems containing adenine showed that there were no differences between the spectra of the cocrystallization products and the PM. All vibrational spectroscopy techniques were consistent. It can be concluded that no cocrystal was obtained between HTZ and adenine.

Analysis of remaining systems showed spectral differences between cocrystallization product and PM. Therefore, results from the systems with the cofomers tromethamine, DL-malic acid, citric acid and D(-)-mannitol will be presented separately.

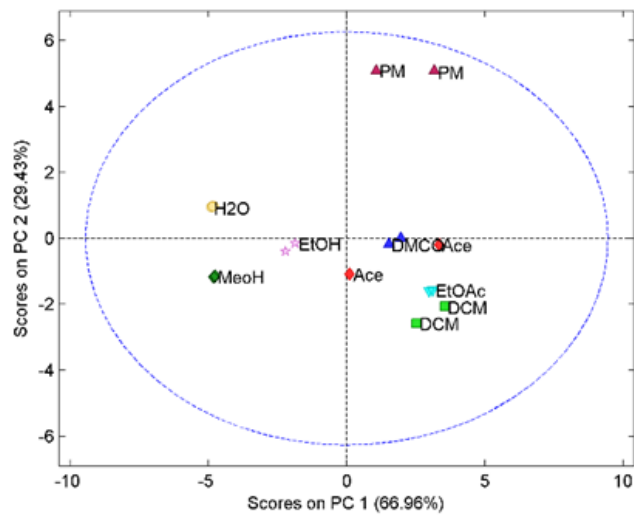
i. Hydrochlorothiazide: tromethamine (HTZ:Tris)

HTZ:Tris 1:1 systems present a score plot of the first two components from the PCA model constructed with the vibrational spectra that can be seen in Figure 21. The score plot of MIRS results (Figure 21 (a)) shows that the samples produced with DCM and EtOAc are the ones more distant of the PM in the first component, meaning that these samples present more spectral differences when compared with the PM. The visual analysis of the spectra revealed that the MIRS show differences consistent with cocrystal formation. The score plot for NIRS (Figure 21 (b)) shows a similar trend in the second component. In the case of NIRS, the first component appears to reflect differences related with physical properties, such as particle size. Visual analysis of NIR spectra also revealed differences between spectra. RS confirms the above results, both with PC analysis (Figure 21 (c)) and visual spectra analysis. Systems yielding a more promising cocrystal were obtained with DCM and EtOAc. The spectra of the 1:1 ratio systems were compared with the spectra of the 1:2 ratio systems and it was verified that the samples obtained with the two ratios show similar spectra. In fact, it can be seen that the changes in the spectra are the same. Nevertheless, the 1:2 ratio systems seem to present more differences in relation with the PM. Therefore, it can be inferred that the 1:2 ratio systems formed a purer cocrystal.

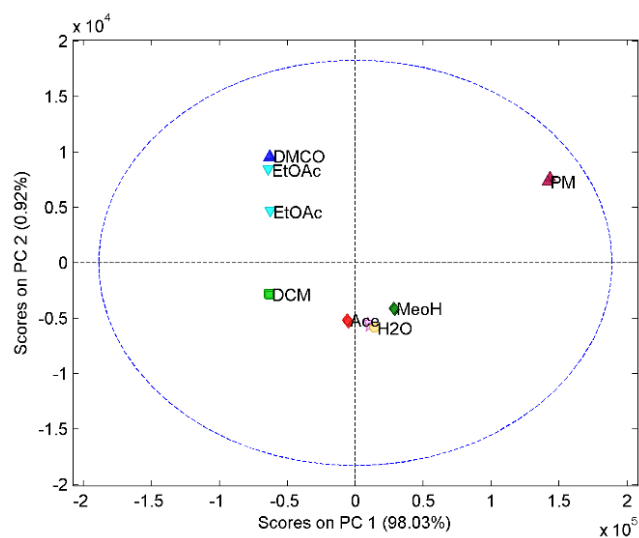
In relation to HTZ:Tris 1:2, the score plot of the PCA constructed with the MIRS spectra (Figure 22 (a)) show a trend in the first component associated with the purity of the samples. Samples further away from the PM in the first component are the ones with a purer cocrystal. This conclusion was supported by the analysis of the spectra. Differences in the purity of the samples can be seen in the example given in Figure 22 (b). The samples produced with DCM and EtOAc, the ones that are farther away in PC1 from the PM present spectra with significant differences compared with the PM. The main differences can be seen in three regions. In the amine region between 3400 cm^{-1} and 3000 cm^{-1} , there are shifts in two bands corresponding to amine groups of HTZ and Tris.



(a)



(b)



(c)

Figure 21: Principal components for the system HTZ:Tris 1:1 obtained from a PCA model resourcing to (a) MIRS spectra; (b) NIRS spectra and (c) RS spectra. Colors refer to different solvents (dark green: MeOH; pink: EtOH; red: Ace; green: DCM; dark blue: DMSO; blue: EtOAc; yellow: H₂O; dark red: PM).

In the second region, around 1600 cm^{-1} , the band corresponding to the vibration of the heterocyclic ring system (C=C stretching) of HTZ and to the vibration of the amine group in Tris shifted from 1600 cm^{-1} to 1585 cm^{-1} . The third region, between 1200 cm^{-1} and 800 cm^{-1} , presents several differences associated with the symmetric stretching of SO_2 groups of HTZ.

The spectra from the sample produced with EtOH, which in the PCA score plot is in between the PM and the EtOAc samples, have bands characteristic of the PM and of the cocrystal (for example, the bands at 3350 cm^{-1} and 1600 cm^{-1}), indicating that the sample is impure.

The analysis of the NIRS spectra by PCA confirms that a cocrystal was in fact produced. However, the samples are not pure (Figure 23 (a)). Again, the differences are seen in the second component. The analysis of the spectra (Figure 23 (b)) show differences, when compared with the PM, mainly in the region between 5000 cm^{-1} and 4100 cm^{-1} . This spectral region encloses the first overtone region of the amine group.

The PCA score plot obtained with the RS spectra shows differences in the purity of the cocrystal reflected on the first component (Figure 24 (a)). The region of the symmetric and asymmetric stretch of the S=O group of HTZ (between 1400 cm^{-1} and 1300 cm^{-1}) is the one with a large number of differences associated with cocrystal formation (Figure 24 (b)).

The three techniques showed the formation of a cocrystal between HTZ and Tris. The PCA applied to the spectra also revealed that the extension of the cocrystal formation was dependent of the solvent used. In this case, the samples produced with DCM and EtOAc were the ones that produced a purer cocrystal. Also, 1:2 ratio seems to be the preferred ratio. The groups involved in the formation of the cocrystal are the sulfonamide group of HTZ and the amine group of Tris.

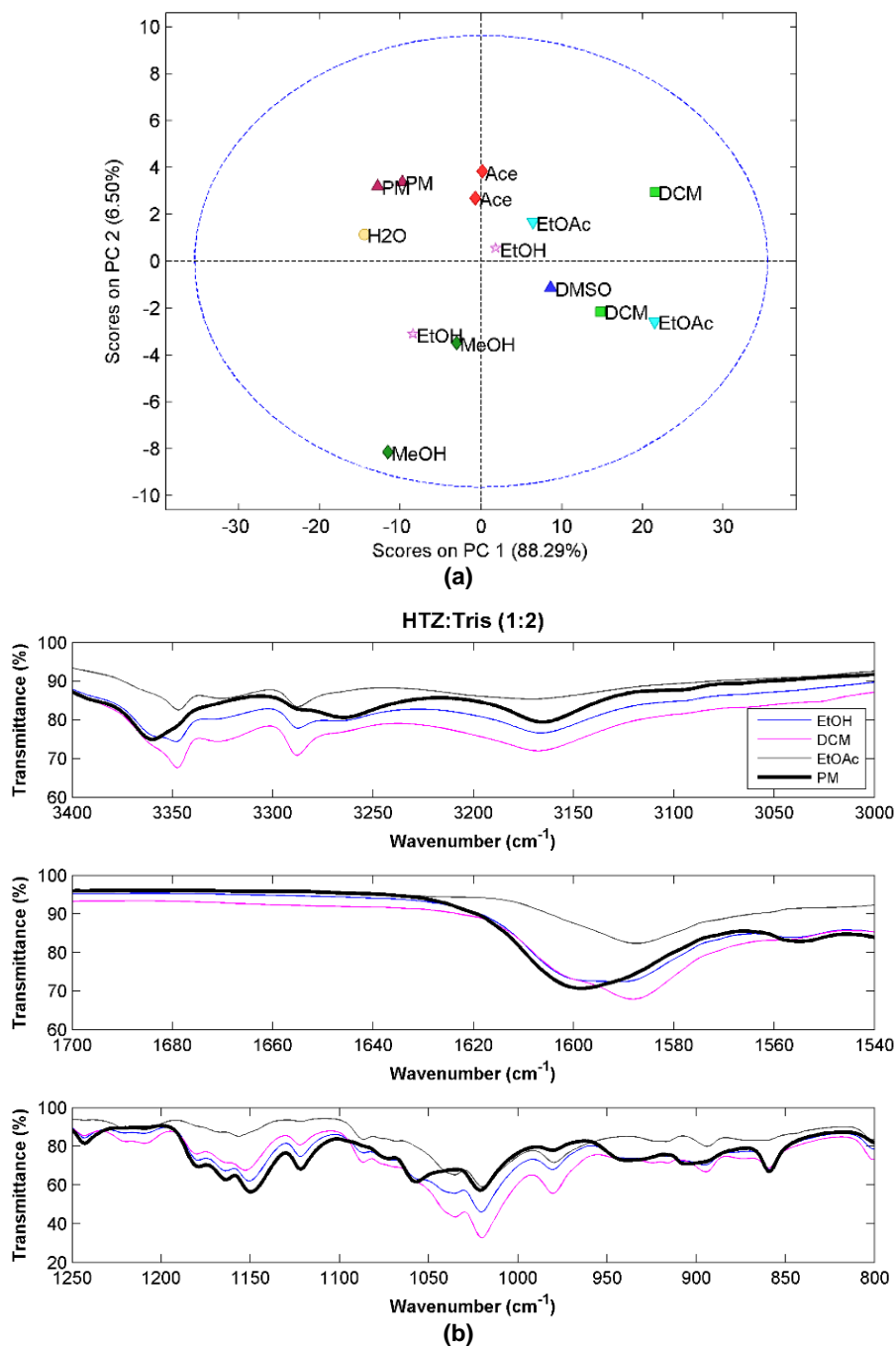
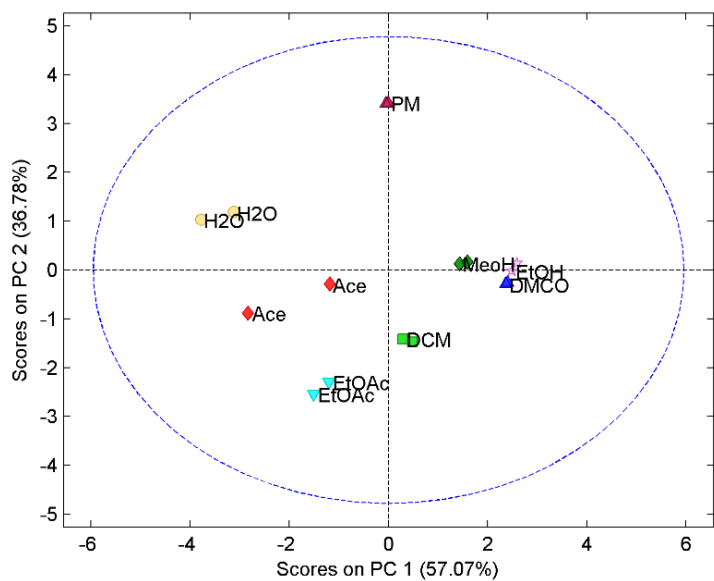
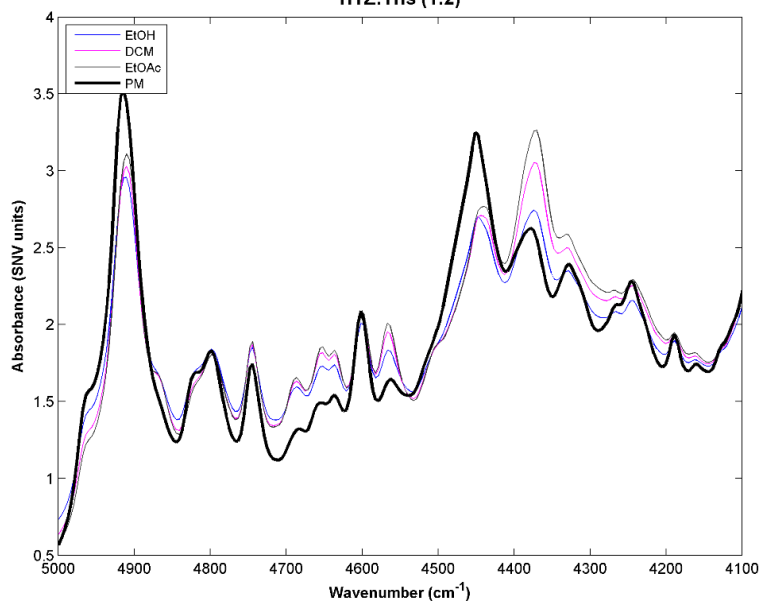


Figure 22: (a) PCA score plot constructed with the MIRS spectra from the system HTZ:Tris 1:2. Colors refer to different solvents (dark green: MeOH; pink: EtOH; red: Ace; green: DCM; dark blue: DMSO; blue: EtOAc; yellow: H₂O; dark red: PM); (b) MIRS spectra of the samples produced with EtOH (blue), DCM (pink) and EtOAc (grey) and from the PM (black).



(a)

HTZ:Tris (1:2)



(b)

Figure 23: (a) PCA score plot constructed with the NIRS spectra from the system HTZ:Tris 1:2. Colors refer to different solvents (dark green: MeOH; pink: EtOH; red: Ace; green: DCM; dark blue: DMSO; blue: EtOAc; yellow: H₂O; dark red: PM); (b) NIRS spectra of the samples produced with EtOH (blue), DCM (pink) and EtOAc (grey) and from the PM (black);

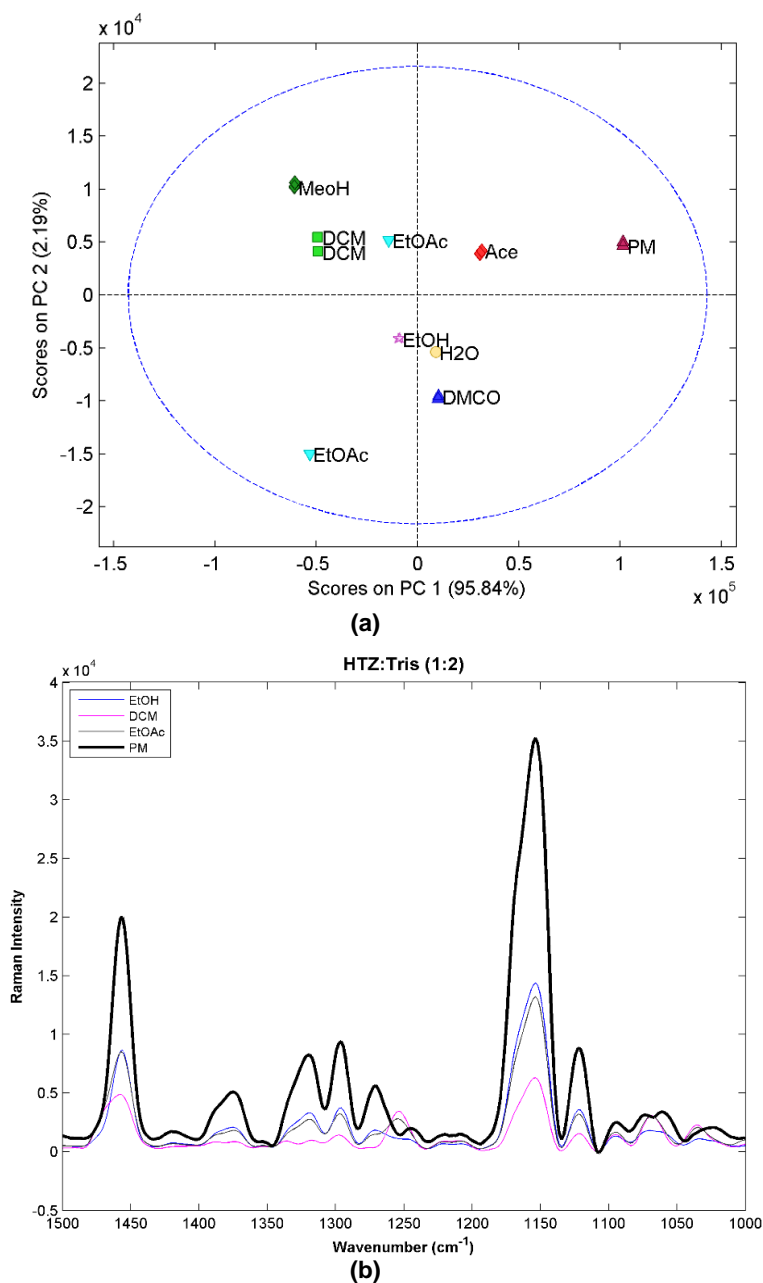


Figure 24: (a) PCA score plot constructed with the RS spectra from the system HTZ:Tris 1:2. Colors refer to different solvents (dark green: MeOH; pink: EtOH; red: Ace; green: DCM; dark blue: DMSO; blue: EtOAc; yellow: H₂O; dark red: PM). (b) RS spectra of the samples produced with EtOH (blue), DCM (pink) and EtOAc (grey) and from the PM (black).

ii. Hydrochlorothiazide: DL-malic acid (HTZ:Mal)

The three vibrational spectroscopic techniques were coherent regarding the HTZ:Mal 1:1 systems. Samples processed with DCM, Ace, EtOAc and DMSO seems to had produce cocrystals. However, the spectral analysis indicated incomplete cocrystal formation. The comparison between the 1:1 and 1:2 ratios showed that, despite similarity between spectra, the 1:2 ratio evidenced a superior cocrystal yield. Therefore, a more detailed analysis will be performed for the 1:2 ratio systems.

All HTZ:Mal 1:2 experiments have evidence of cocrystal formation. This can be confirmed by the score plots for the three techniques showing a similar pattern, as shown in Figure 25 (a), Figure 26 (a) and Figure 27 (a). The first principal component seems to be related with cocrystal purity. The score plot of MIRS (Figure 25 (b)) shows that the samples presenting superior differences in relation to the PM were produced with EtOAc and DCM. The NIRS (Figure 26 (b)) and RS (Figure 27 (b)) results seem to confirm this result.

Comparing the spectra obtained from the cocrystallization product and the PM, the MIRS spectra is, again, the technique providing more detailed information regarding the groups involved in the cocrystal formation (Figure 25 (b)). Several new bands and band shifts can be observed. The differences verified between 3500 cm^{-1} and 3400 cm^{-1} are related to the stretching vibration of the OH group from the DL-malic acid. The carbonyl group stretching vibrations region, at 1700 cm^{-1} , also shows differences in the cocrystallization product spectra. Emerging bands and band shifts are seen in the region of the asymmetric and symmetric stretching of the SO_2 groups of HTZ (between 1350 cm^{-1} and 1100 cm^{-1}).

In the NIRS region, the main spectral differences between the cocrystallization product and the PM (Figure 26 (b)) are seen on the second overtone of the vibration of the alcohol group from malic acid ($\sim 6900\text{ cm}^{-1}$) and on the region between 4600 cm^{-1} and 4550 cm^{-1} , corresponding to combination bands of alcohol, amine and amide groups.

On the RS spectra (Figure 27 (b)), the bands corresponding to C=O vibrations (1635 and 1675 cm^{-1}) from DL-malic acid, to the S=O vibrations ($\sim 1300\text{ cm}^{-1}$) and to SN stretching plus NH deformation of HTZ (between 980 cm^{-1} and 920 cm^{-1}) are the major differences between the cocrystal and the PM spectrum.

Evidences of cocrystal formation were detected by the three techniques, as well as differences in purity. The ratio preferred for HTZ:Mal cocrystals seems to be 1:2. The NIRS method provides less information regarding the groups involved in the cocrystal formation. The sulfonamide group of HTZ and the acid group of DL-malic acid were identified as the groups involved in the formation of the cocrystal. Solvents as EtOAc and DCM produced higher purity in final product.

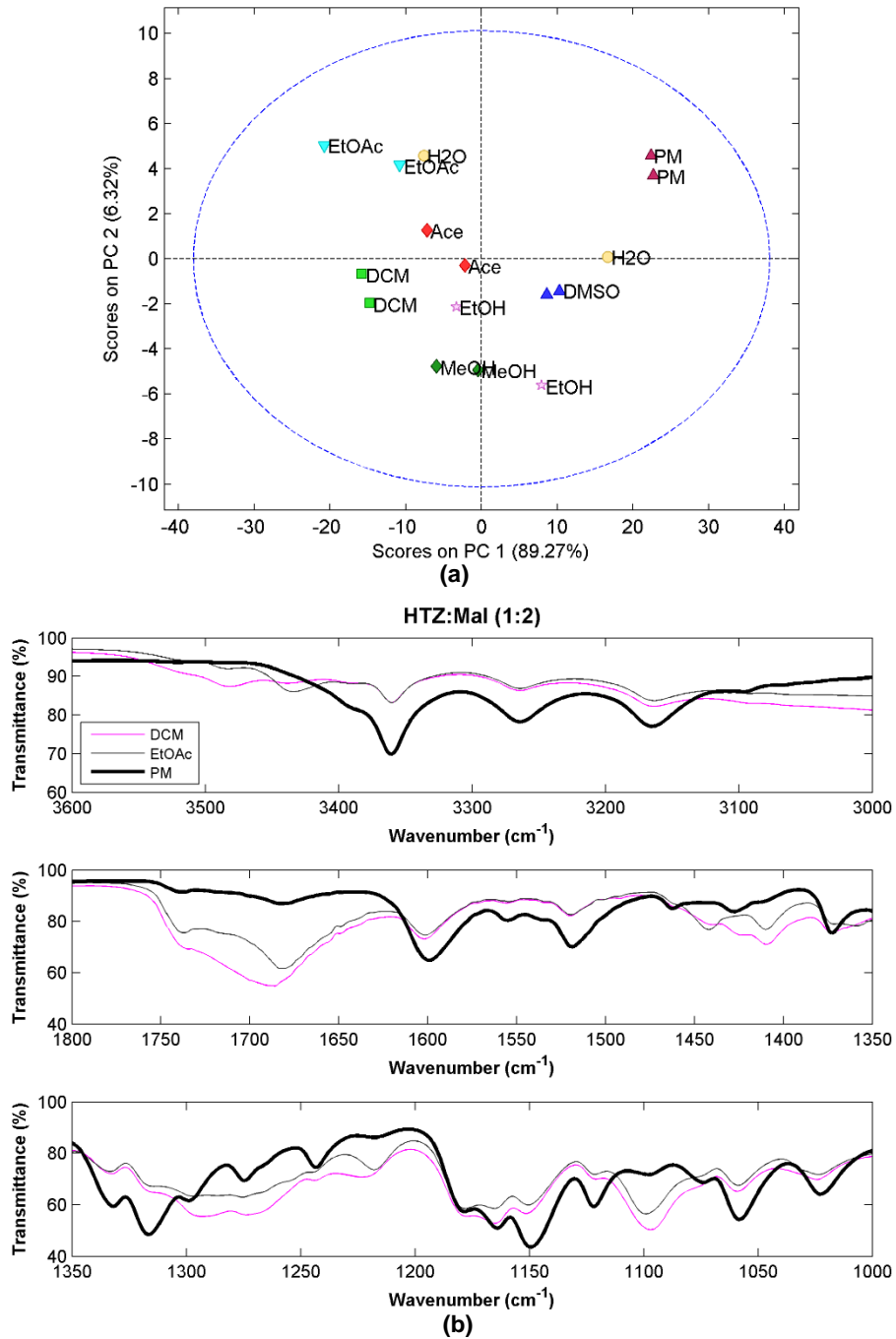


Figure 25: (a) PCA score plot constructed with the MIRS spectra from the system HTZ:Mal 1:2. Colors refer to different solvents (dark green: MeOH; pink: EtOH; red: Ace; green: DCM; dark blue: DMSO; blue: EtOAc; yellow: H₂O; dark red: PM); (b) MIRS spectra of the samples produced with DCM (pink) and EtOAc (grey) and from the PM (black).

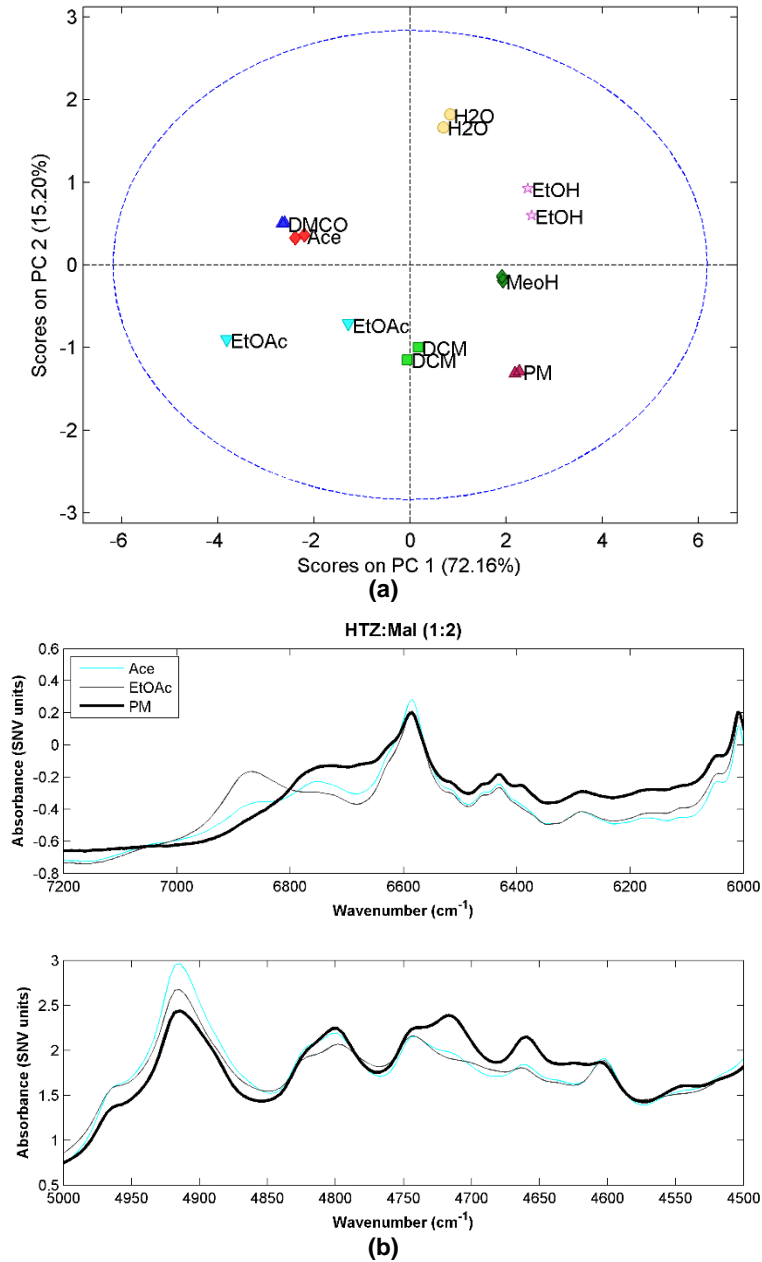


Figure 26: (a) PCA score plot constructed with the NIRS spectra from the HTZ:Mal 1:2. Colors refer to different solvents (dark green: MeOH; pink: EtOH; red: Ace; green: DCM; dark blue: DMSO; blue: EtOAc; yellow: H₂O; dark red: PM); (b) NIRS spectra of the samples produced with Ace (blue) and EtOAc (grey) and from the PM (black);

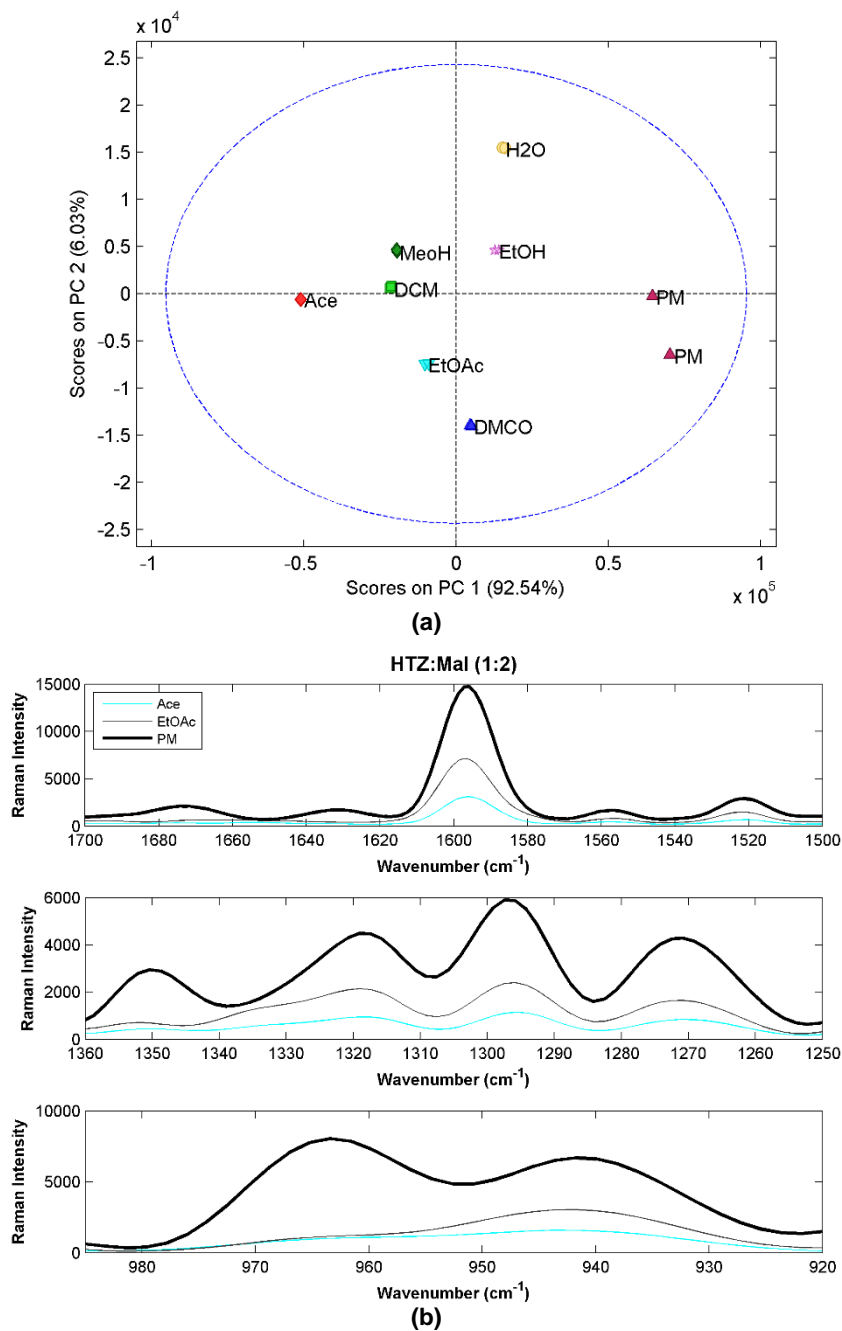


Figure 27: (a) PCA score plot constructed with the RS spectra from the HTZ:Mal 1:2. Colors refer to different solvents (dark green: MeOH; pink: EtOH; red: Ace; green: DCM; dark blue: DMSO; blue: EtOAc; yellow: H₂O; dark red: PM). (b) RS spectra of the samples produced with Ace (blue) and EtOAc (grey) and from the PM (black).

iii. Hydrochlorothiazide: citric acid (HTZ:Cit)

Systems of HTZ:Cit 1:1 produced a low purity cocrystal, as in the case of DL-malic acid and tromethamine. For the HTZ:Cit 1:2 systems, all spectra of the cocrystallization products present significant differences to the PM spectrum, indicating cocrystal formation, which is clear after the PCA analysis (Figure 28 (a), Figure 29 (a), Figure 30 (a)). For RS, the difference is perceived in the score plot of the second against the third component (Figure 30 (b)). Additionally, there is a visible separation between the samples produced with DCM and other solvents. A more detailed analysis of the RS spectra of these samples shows incongruences in the spectra when compared with the other cocrystallization products. Since none of the other two techniques showed this trend, it was considered that these two spectra were outliers.

The PCA results show that the cocrystals produced with DMSO and EtOAc are the purest (Figure 28 (a)). The MIRS spectra of these samples (Figure 28 (b)) present alterations in bands associated to NH_2 and $\text{S}=\text{O}$ groups of HTZ, from 3300 cm^{-1} to 3100 cm^{-1} and from 1400 cm^{-1} to 1100 cm^{-1} , respectively. The region associated with the $\text{C}=\text{O}$ group stretching vibration from citric acid ($\sim 1700\text{ cm}^{-1}$ and 1750 cm^{-1}) clearly changed.

In the NIR spectra, the region of the first and second overtone corresponding to the vibration of OH group of citric acid ($\sim 5200\text{ cm}^{-1}$ and $\sim 4700\text{ cm}^{-1}$) and in the first overtone of the amine group of HTZ ($\sim 4550\text{ cm}^{-1}$) (Figure 29 (b)) are seen the main differences between the PM and cocrystal spectra. The changes on the RS spectra (Figure 30 (b)) are related with the $\text{C}=\text{O}$ group of citric acid and the $\text{S}=\text{O}$ group of HTZ.

As in the previous systems, the vibrational spectroscopic techniques were able to detect the cocrystal formation and differences in their purity, allowing to select 1:2 ratio as the preferred one, as well as the solvents DMSO and EtOAc. The groups involved in the cocrystallization are the carboxyl group of the citric acid and the sulfonamide group of HTZ.

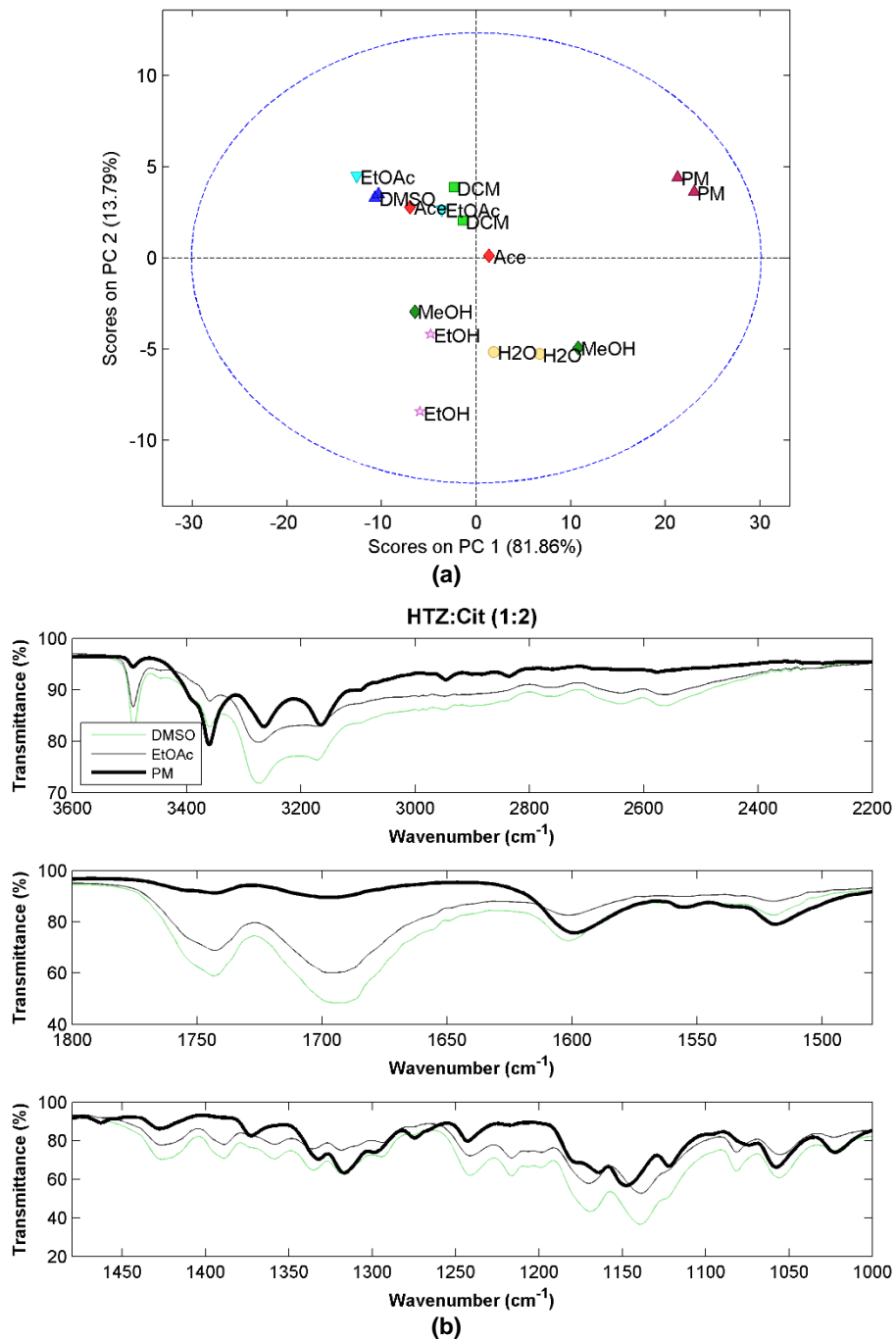


Figure 28: (a) PCA score plot constructed with the MIRS spectra from the system HTZ:Cit 1:2. Colors refer to different solvents (dark green: MeOH; pink: EtOH; red: Ace; green: DCM; dark blue: DMSO; blue: EtOAc; yellow: H₂O; dark red: PM); (b) MIRS spectra of the samples produced with DMSO (green) and EtOAc (grey) and from the PM (black).

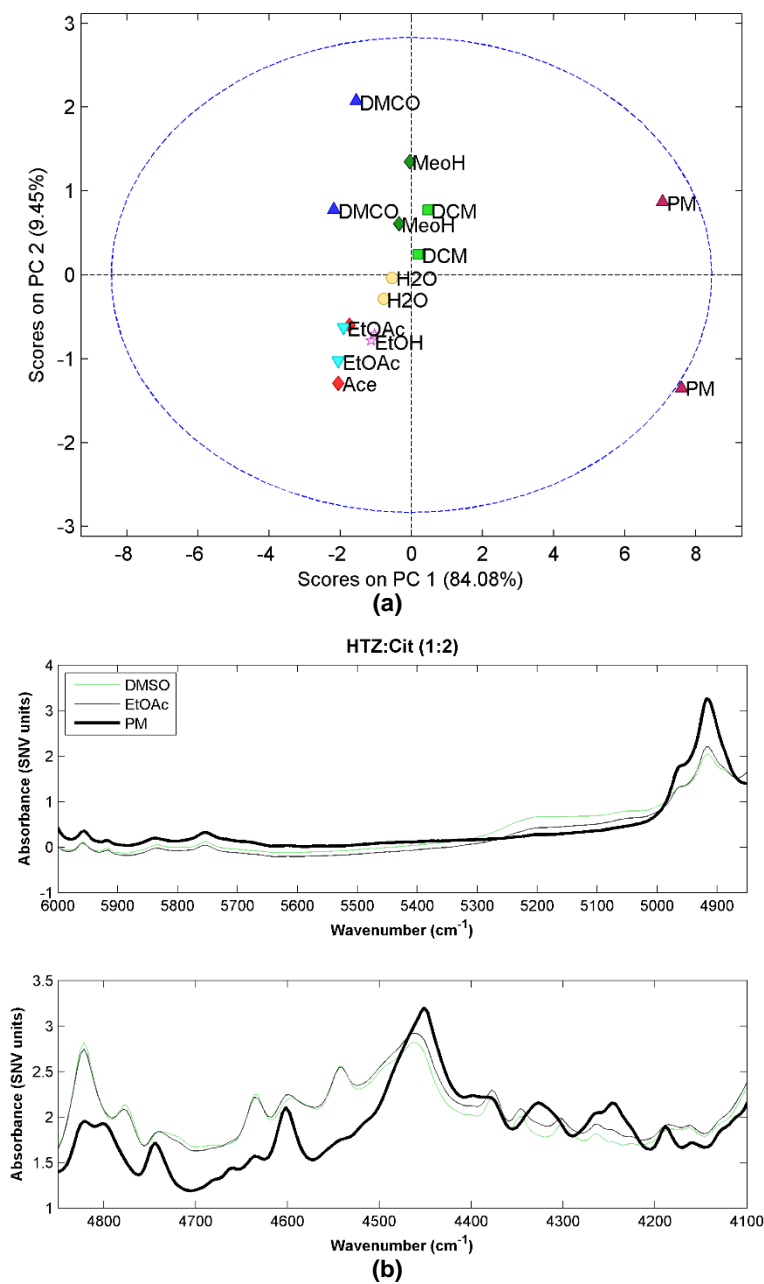


Figure 29: (a) PCA score plot constructed with the NIRS spectra from the system HTZ:Cit 1:2. Colors refer to different solvents (dark green: MeOH; pink: EtOH; red: Ace; green: DCM; dark blue: DMSO; blue: EtOAc; yellow: H₂O; dark red: PM); (b) NIRS spectra of the samples produced with DMSO (green) and EtOAc (grey) and from the PM (black).

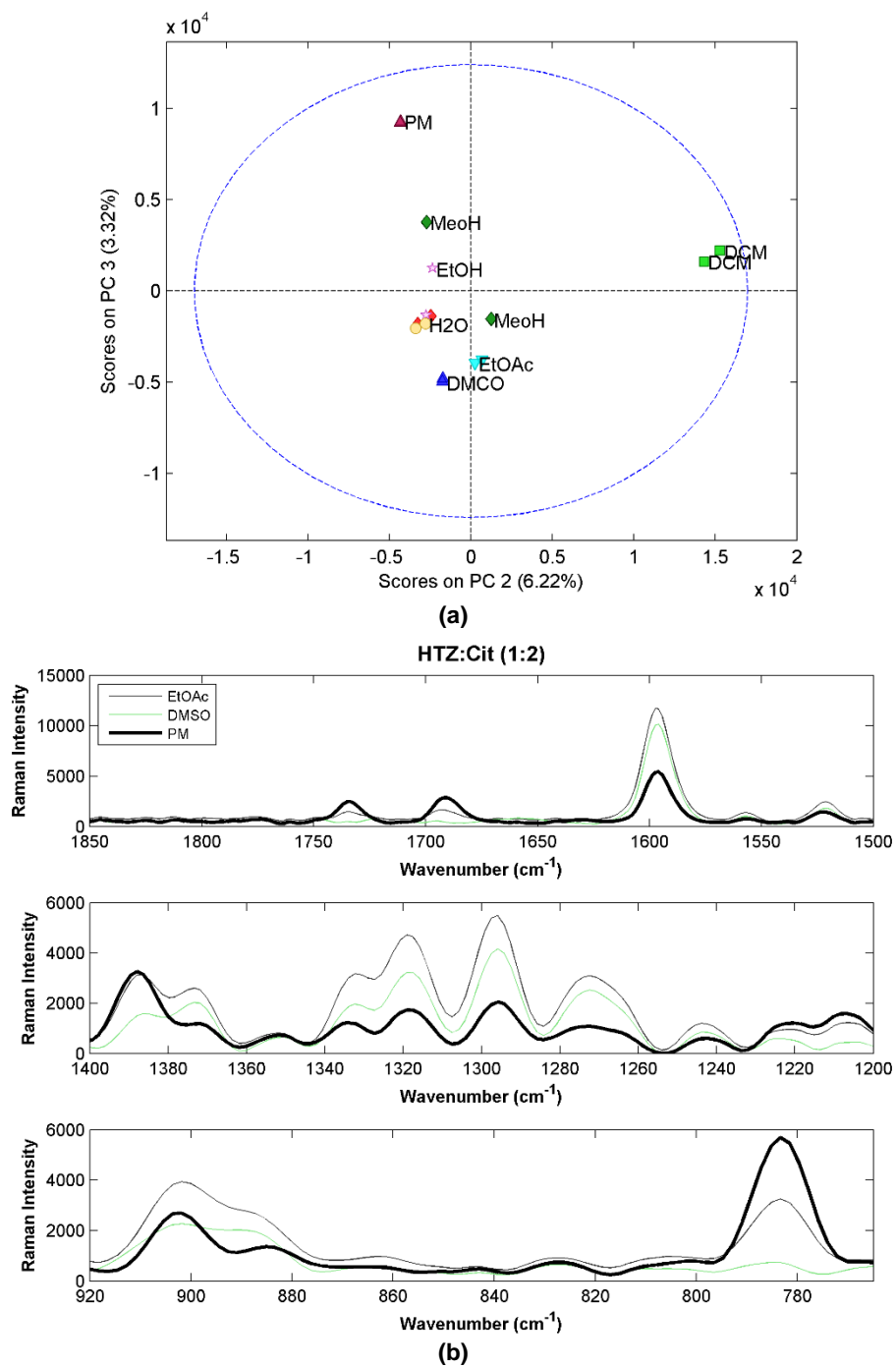


Figure 30: (a) PCA score plot constructed with the RS spectra from the system HTZ:Cit 1:2. Colors refer to different solvents (dark green: MeOH; pink: EtOH; red: Ace; green: DCM; dark blue: DMSO; blue: EtOAc; yellow: H₂O; dark red: PM); (b) RS spectra of the samples produced with DMSO (green) and EtOAc (grey) and from the PM (black).

iv. Hydrochlorothiazide: D(-)-mannitol (HTZ:Man)

As for the previously analyzed systems, the 1:1 ratio also gave cocrystals with lower purity. Therefore, only the results for the 1:2 ratio systems will be discussed.

Figure 31, Figure 32 and Figure 33 show the score plots of the PCA model constructed and the respective spectra of the HTZ:Man 1:2 systems (only spectral regions with more differences between spectra). In the first component of PCA model (Figure 31 (a), Figure 32 (a) and Figure 33 (a)), all the techniques display the same trend. In the case of MIRS, the sample obtained with EtOAc shows the major differences in relation to the PM, indicating the possibility of cocrystal formation. Additionally, in the second component, the samples produced with MeOH are separated from the remaining, also indicating that a cocrystal was obtained, but with a spectral signature different from the one of the samples produced with the other solvents (Figure 31 (a)).

MIRS spectra (namely the one corresponding to EtOAc) analysis shows differences at regions typical of NH_2 vibrations of HTZ (3360 and 3170 cm^{-1}), OH stretching vibrations of D(-)-mannitol (3360 cm^{-1}) and bending vibrations of the same group (1400 - 1425 and 1375 cm^{-1}), asymmetric and symmetric stretching vibrations of SO_2 group of HTZ (1325 , 1150 and 1060 - 1040 cm^{-1}). This suggest that groups appearing to be involved in the cocrystal formation are the alcohol group of D(-)-mannitol and the sulfonamide groups of HTZ (Figure 31 (b)). Additionally, clearly the cocrystals are not pure, even the ones obtained with EtOAc (first component of Figure 31 (a)).

In the NIRS and RS case, PCA shows that samples produced with DCM presents the major differences in relation to the PM, as Figure 32 (a) and Figure 33 (a) show. Spectral analysis proves that the same groups appear to be involved in the cocrystal formation, as in the MIRS situation (Figure 32 (b) and Figure 33 (b)). Also, PCAs of NIRS and RS show that the samples produced with MeOH are separated from the PM and the remaining samples as it is seen in the MIRS case, signifying spectral differences.

The existence of two different cocrystal polymorphs can be a possible explanation for the observed differences. D(-)-mannitol has three different polymorphs.⁽¹⁴⁵⁾ Therefore, it can be possible that a different polymorph of the cofomer may lead to a different cocrystal polymorph. This system's results show that vibrational spectroscopy can be very helpful not only in determining the formation and purity of the cocrystal but also in the recognition of different polymorphs.

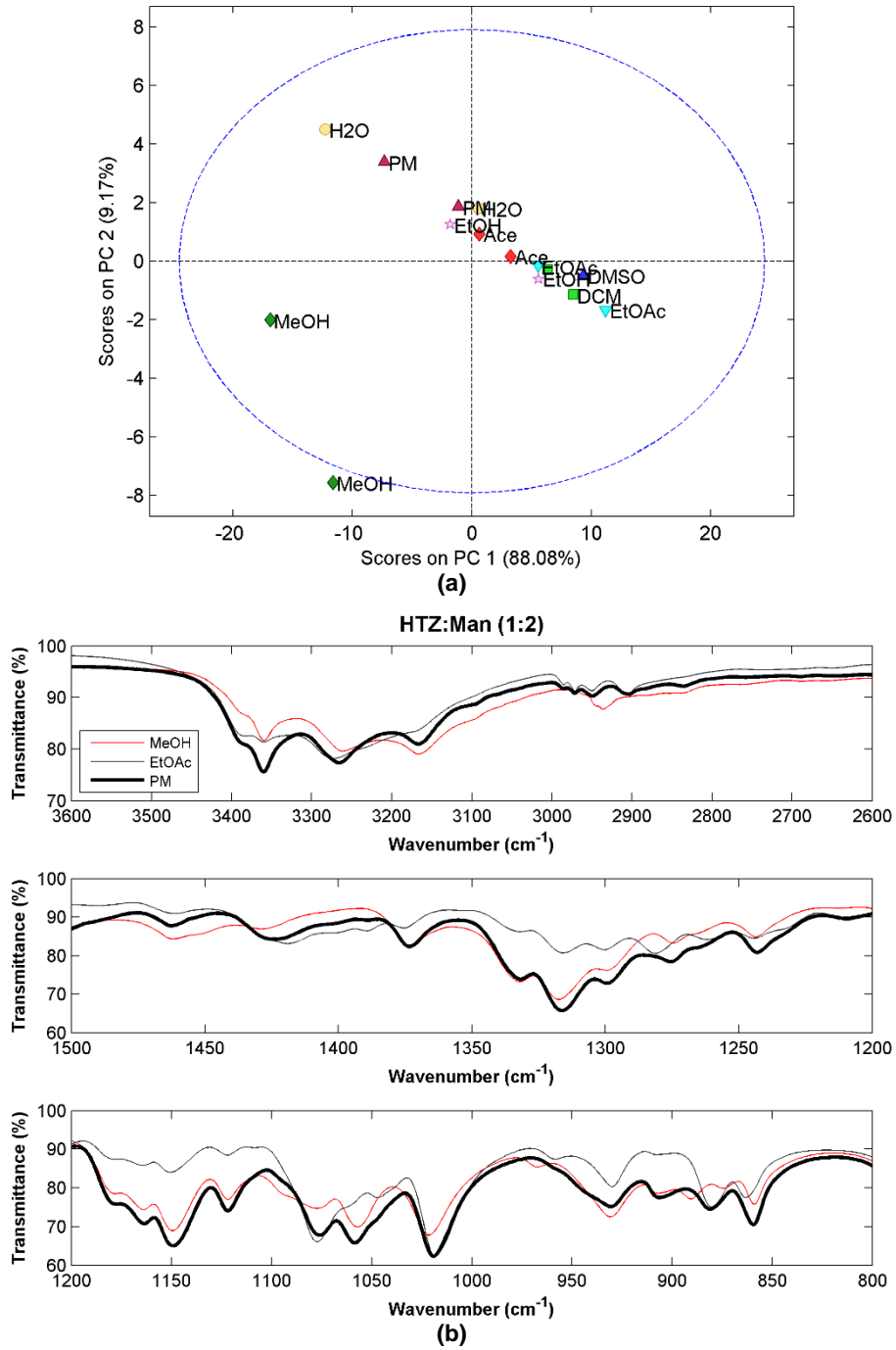


Figure 31: (a) PCA score plot constructed with the MIRS spectra from the system HTZ:Man 1:2. Colors refer to different solvents (dark green: MeOH; pink: EtOH; red: Ace; green: DCM; dark blue: DMSO; blue: EtOAc; yellow: H₂O; dark red: PM); (b) MIRS spectra of the samples produced with MeOH (red) and EtOAc (grey) and from the PM (black).

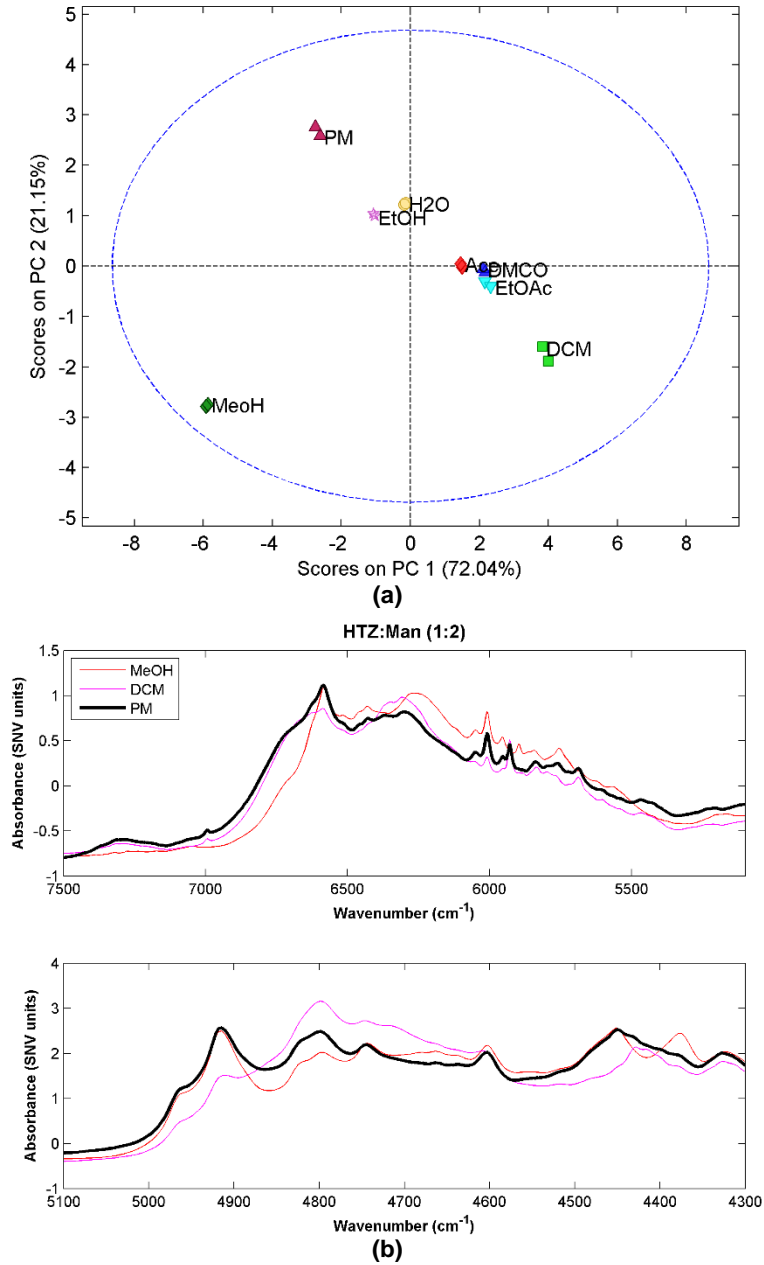


Figure 32: (a) PCA score plot constructed with the NIRS spectra from the HTZ:Man 1:2. Colors refer to different solvents (dark green: MeOH; pink: EtOH; red: Ace; green: DCM; dark blue: DMSO; blue: EtOAc; yellow: H₂O; dark red: PM). (b) NIRS spectra of the samples produced with MeOH (red) and DCM (pink) and from the PM (black).

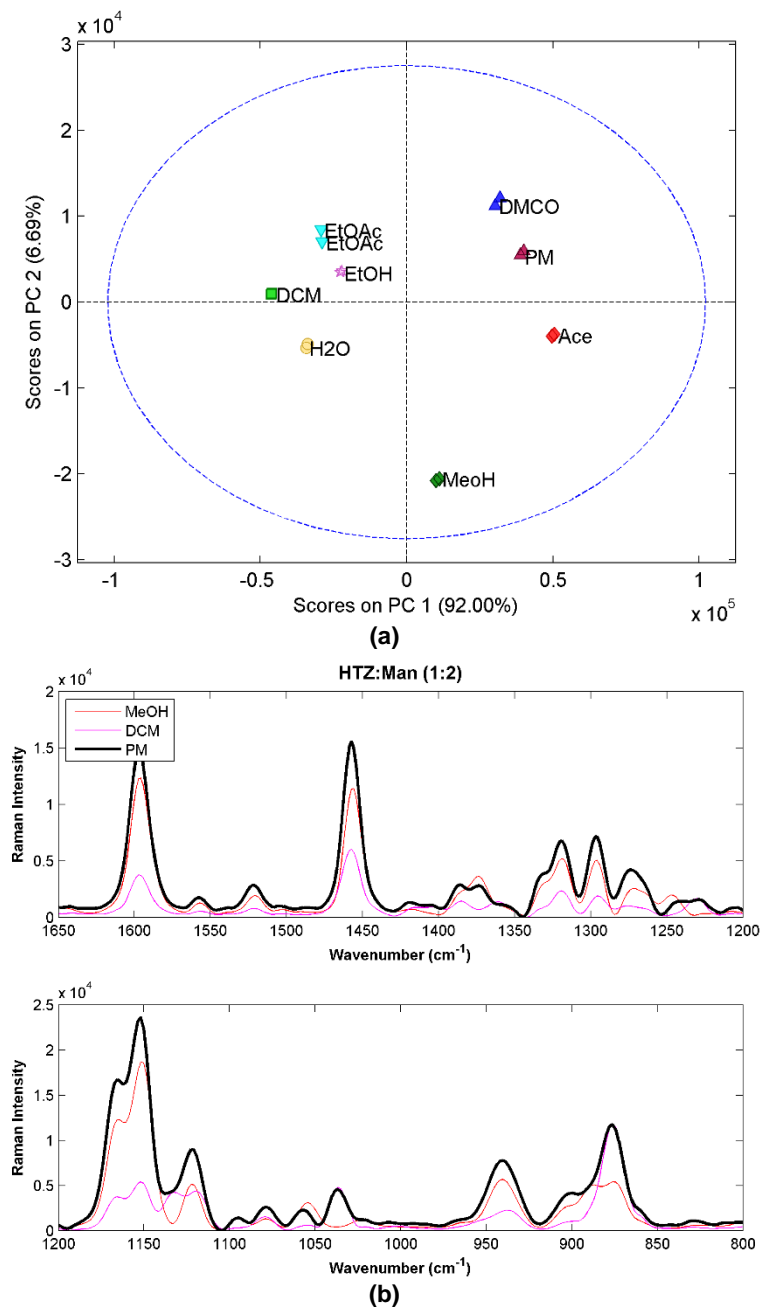


Figure 33: (a) PCA score plot constructed with the RS spectra from the HTZ:Man 1:2. Colors refer to different solvents (dark green: MeOH; pink: EtOH; red: Ace; green: DCM; dark blue: DMSO; blue: EtOAc; yellow: H₂O; dark red: PM). (b) RS spectra of the samples produced with MeOH (red) and DCM (pink) and from the PM (black).

4.1.2. Cocrystal screening experiments: part II

In the second part of the screening experiments, six coformers and solvents were tested. The cocrystallization products were analyzed by MIRS and RMS. As in the first plate, cocrystal formation was assessed through comparison between the spectrum of the cocrystallization products with the PM. HCA was used to evaluate the similarity between products obtained with different solvents and PM.

Citric acid was again used as coformer, in order to test more solvents for the same system. Between the tested coformers, L(+)-arginine, nicotinamide, *p*-aminobenzoic acid and citric acid show spectral differences. However, system with L(+)-arginine present spectral differences that were not conclusive about cocrystal formation. Regarding caffeine and L-tryptophan, no spectral changes were observed between the PM and cocrystallization products spectra by either spectroscopic technique, indicating that no new form was obtained. Samples with solvents EtOAc and DCM were not considered due to a plate degradation resulting in samples contamination.

i. Hydrochlorothiazide: L(+)-arginine systems (HTZ:Arg)

Both spectroscopic techniques showed differences between the spectra of some cocrystallization products when compared with the respective PM for both ratios, but more evident for the 1:2 ratio. In the case of 1:2 ratio, the dendrogram from the HCA using the MIR spectra (Figure 34) allowed to ranking solvents accordingly to the distance from the product to the PM, being samples produced with IPro the more distant from the PM, so the ones with more spectral differences, following by ACN and EtOH, MeOH and Ace.

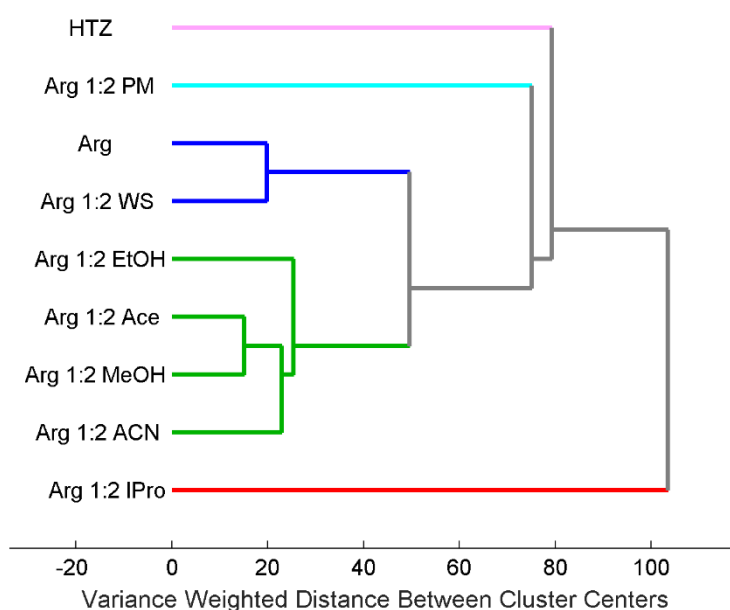
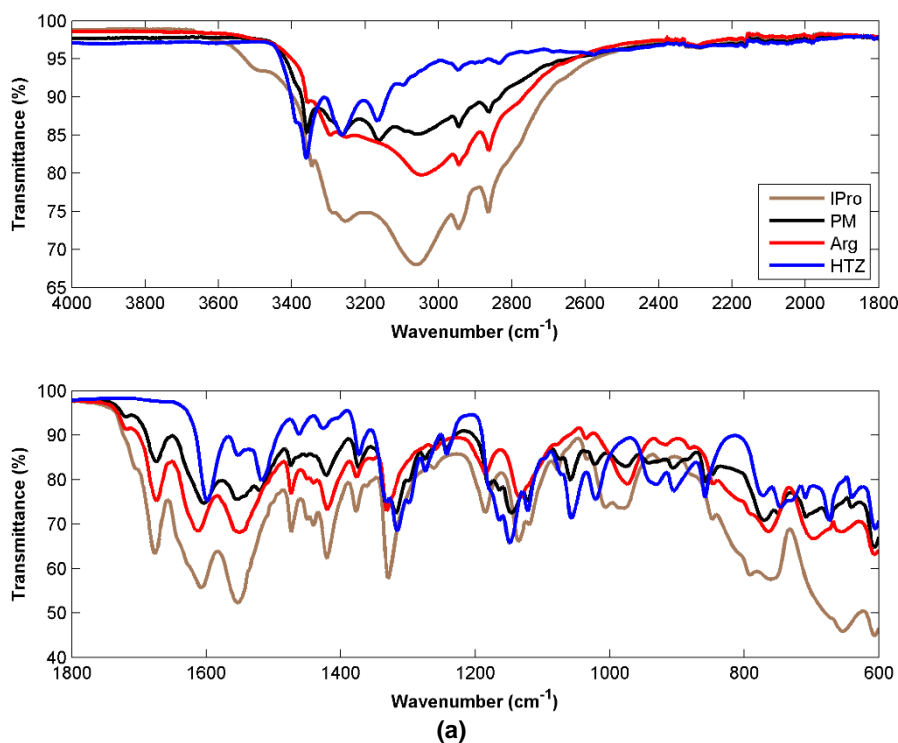


Figure 34: Dendrogram from the HCA performed with MIR spectra obtained from systems HTZ:Arg 1:2, the PM, arginine and HTZ.

A more detailed analysis of the MIR spectra showed similarity between the spectra from product obtained with IPro and the spectrum of L(+)-arginine, but less defined in some regions (Figure 35 (a)). Also, non or almost non spectral evidence of HTZ was found. Analyzing the Raman spectra of the system HTZ:Arg 1:2 produced with IPro (Figure 35 (b)) the same conclusion was reached, the product spectrum has only spectral characteristics of Arg. Probably, this systems suffer a phase separation in the well, becoming the samples heterogeneous and spectroscopic analysis was influence by this factor. Despite that, MIR spectral comparison between IPro product, PM and pure compounds revealed some differences (Figure 35 (a)), which indicate some type of reaction between Arg and HTZ. Also, MIR spectra of pure Arg, PM and HTZ:Arg system show a non-typical band in the region of 3150 cm^{-1} . Further investigation lead to conclusion that this band corresponds to OH stretching vibrations of water, probable due to atmospheric water absorption of pure arginine. There are no evidences of water in Raman spectra, once water molecules are not Raman active.

However, information is not decisive relatively to cocrystal formation and the system must be further study.



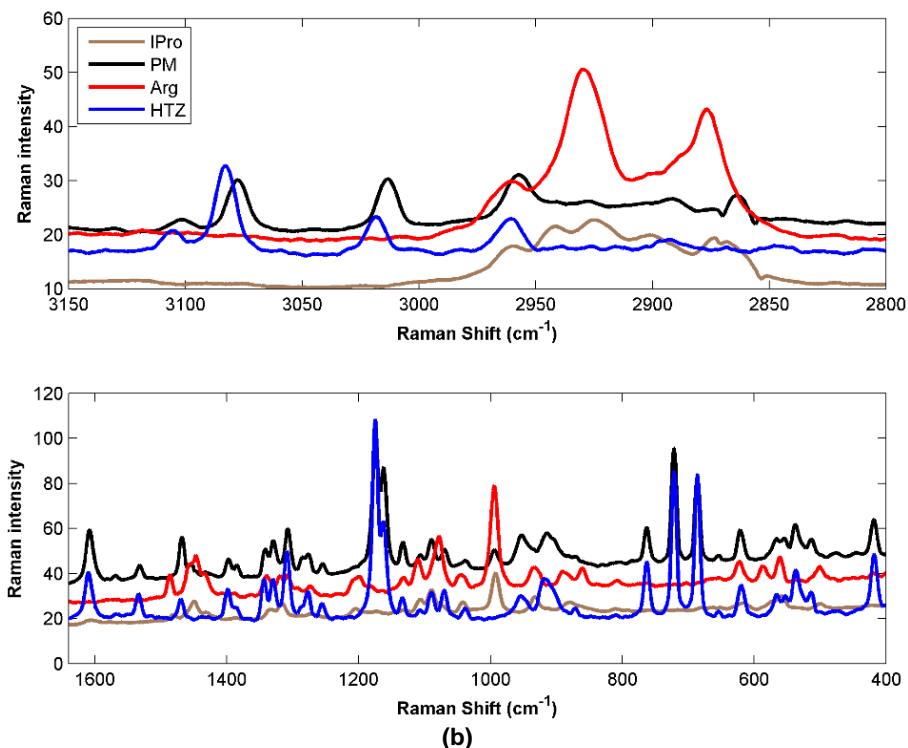


Figure 35: MIR (a) and RMS (b) spectra from the cocrystallization product of HTZ:Arg 1:2 with IPro (brown), PM (black), HTZ (blue) and Arg (red).

ii. Hydrochlorothiazide: nicotinamide systems (HTZ:Nic)

In the case of HTZ:Nic systems, both 1:1 and 1:2 ratios form a product with spectral signatures very different from the PM and similar between ratios, leading to the question, which is the true ratio of the cocrystal.

In order to find cocrystal probable ratio, a detailed analysis of the MIR spectra was done (Figure 36), by comparing the spectra of the products of HTZ:Nic 1:1 and 1:2 systems with the PM, pure HTZ and nicotinamide.

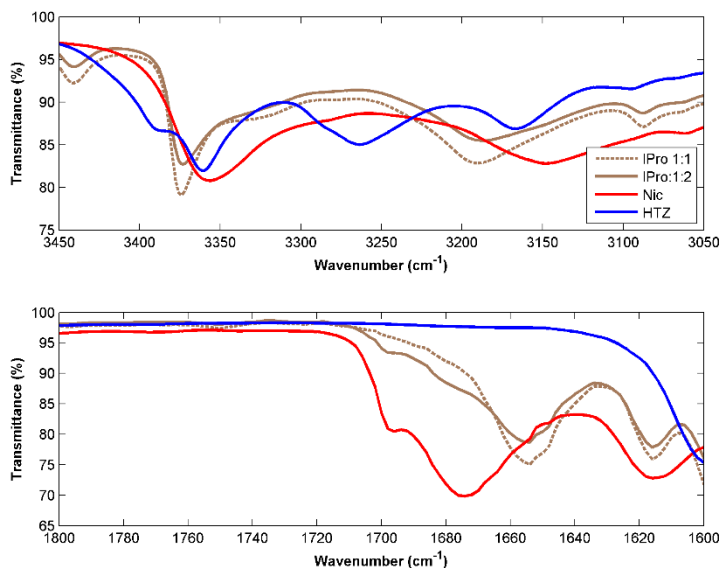


Figure 36: Selected region of MIR spectra from the HTZ:Nic 1:1 IPro (brown dashed), HTZ:Nic 1:2 IPro (brown), pure Nic (red) and pure HTZ (blue).

The analysis showed that the product of the 1:2 ratio have an excess of nicotinamide. This can be concluded by the lack of bands in products' spectra corresponding to HTZ, for example at 3265 cm^{-1} (Figure 36), which confirms the absence of HTZ, which was all used to form the cocrystal. An excess of nicotinamide can be seen in the peak corresponding to the vibration of carboxyl group of nicotinamide at 1700 cm^{-1} (Figure 36). This analysis proves that the ratio of the cocrystal was indeed of 1:1, as published by Sanphui et. al.⁽³⁾ Therefore, a more careful analysis is presented about this ratio.

It was also found that different solvents produced cocrystals with a different degree of purity. HCA was made using the MIR spectra to verify the possibility to group the samples with similar purity (Figure 37). The product obtained with MeOH was the less pure, with a spectrum very similar to the one of the PM, followed by the group of the products formed with Ace and ACN. The purest products were the ones produced with EtOH and IPro.

A very important point must be emphasized, in this specific case, the sample produced without solvent (WS) also reacted, moreover, with a high purity. It is common in this kind of screening procedure to set one line of wells with the parent components without solvent to serve as comparison with the reaction products.^(92, 146, 147) However, care must be taken because if the system is highly reactant this physical mixture can react even without the solvent.

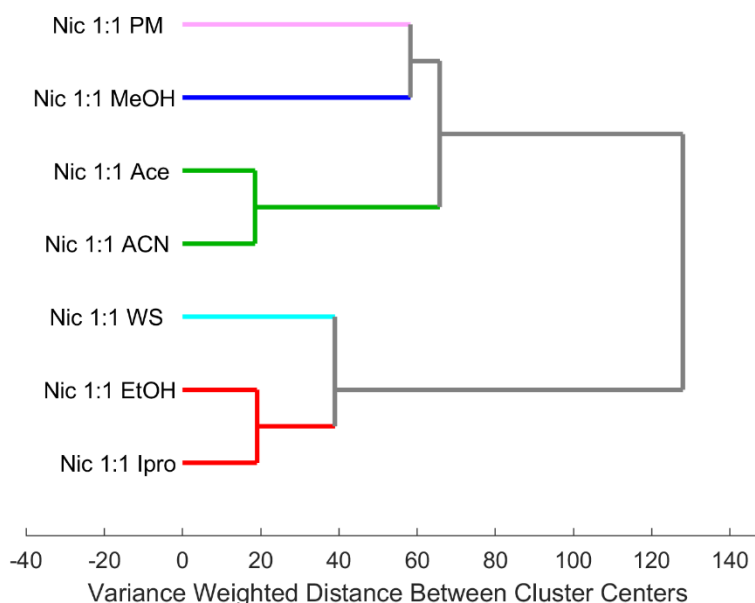


Figure 37: Dendrogram from the HCA performed with the MIR spectra of the systems HTZ:Nic 1:1.

Regarding the groups involved in the formation of the HTZ:Nic 1:1 cocrystal, both spectroscopic techniques show evidences of the formation of hydrogen bonding between the NH of sulfonamide group of HTZ and the carbonyl group of Nic. The replacement of the API sulfonamide catemer hydrogen bond by heterosynthons in the cocrystal is reflected in

the MIR spectra in the SO₂ asymmetric/symmetric (1370, 1320 and 1150 cm⁻¹) and NH stretching frequencies (from 3360 to 3450 cm⁻¹). In the cocrystal spectrum, the Nic carbonyl group vibration between 1700 cm⁻¹ and 1640 cm⁻¹ is completely different when compared with the Nic spectrum (Figure 38 (a) and Figure 36).

The same conclusion can be drawn from the Raman spectra with the main differences in the sulfonamide group vibration at frequencies around 1400 cm⁻¹ and 1300 cm⁻¹ and in the region between 3100 cm⁻¹ and 2900 cm⁻¹ correspondent to the amine group of HTZ (Figure 38 (b)). These deductions are in line with the work by Sanphui et al.⁽³⁾

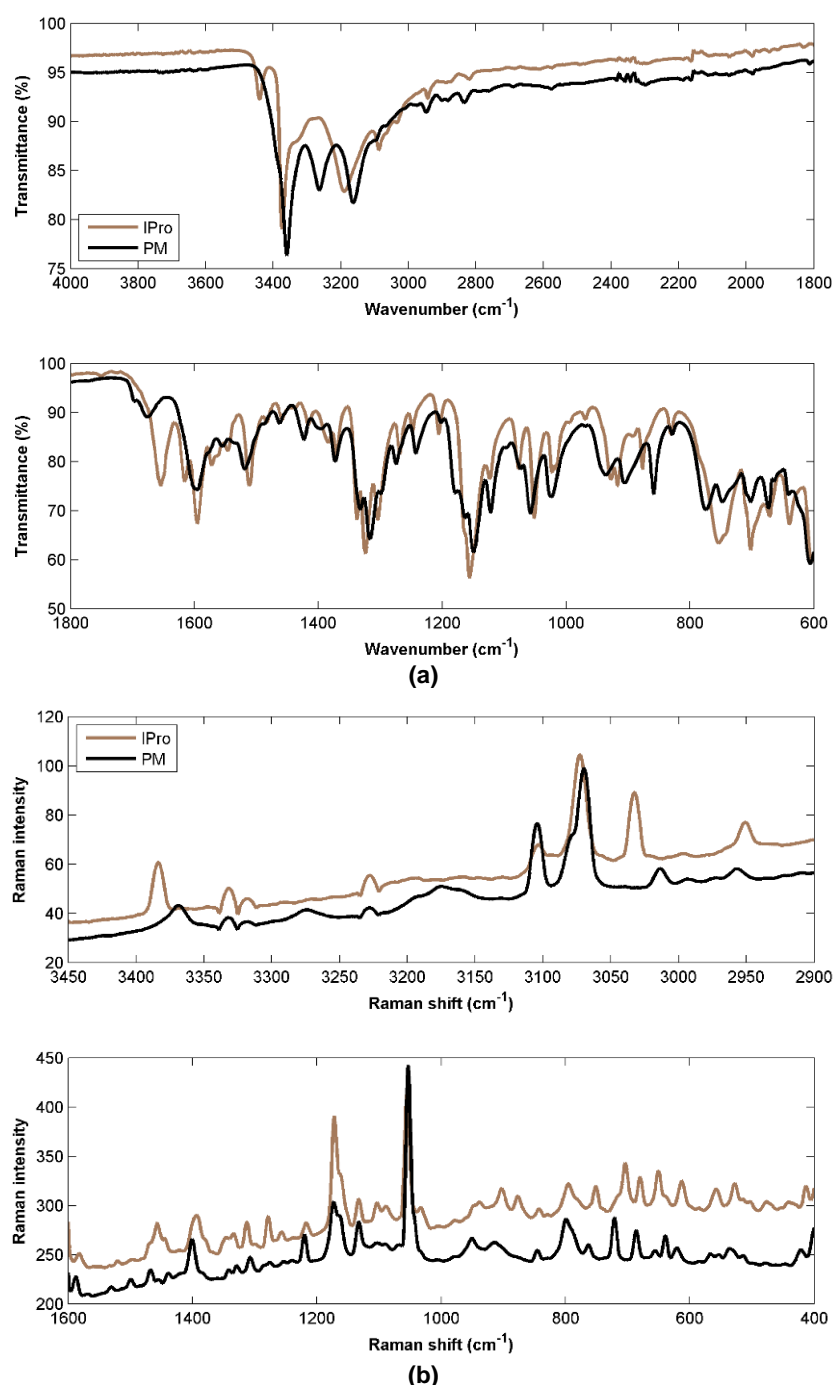


Figure 38: MIR (a) and RMS (b) spectra from the cocrystallization product of HTZ:Nic 1:1 IPro (brown), and respective PM (black) and 1:2 (black).

iii. Hydrochlorothiazide: *p*-aminobenzoic acid systems (HTZ:PABA)

Similar to the HTZ:Nic system, both ratios of the HTZ:PABA system formed a cocrystal with similar spectra, in MIR and Raman techniques. Therefore, the same strategy was used to verify which of the components was in excess. Products from systems with Ace as solvents have no excess of PABA, which can be seen in Figure 39 that shows the absence of the band at 3450 cm^{-1} in products' spectra, a wavenumber of a characteristic band from PABA. However, the band at 3160 cm^{-1} characteristics from HTZ appears slightly in the 1:1 ratio, proving an excess of HTZ and, consequently, confirming the 1:2 as the correct ratio.⁽¹⁴²⁾

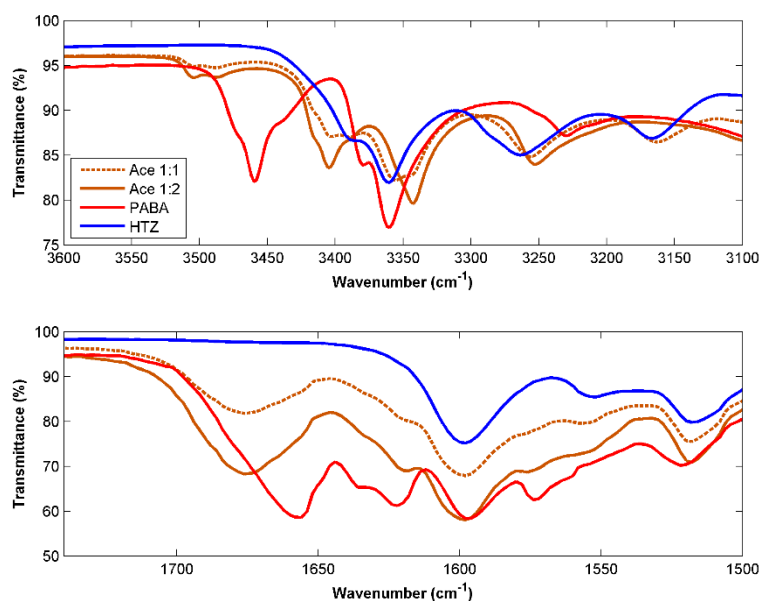


Figure 39: MIR spectra from the cocrystallization product of HTZ:PABA 1:1 Ace (orange dashed), HTZ:PABA 1:2 Ace (orange), pure PABA (red) and pure HTZ (blue).

A HCA was performed with the MIR spectra of the products for both ratios (Figure 40 (a)) confirming that the products of the 1:2 ratio form a cluster with the exception of MeOH that almost did not form the cocrystal.

Cocrystal presents a MIR spectra with several differences when compared to the one from PM (Figure 40 (b)), namely, new bands formation at 3500 cm^{-1} , characteristic region from OH vibrations, differences in spectral regions corresponding to NH stretching vibrations (primary amine) from PABA and HTZ, at 3465 and 3360 cm^{-1} , in characteristic regions of OH stretching from PABA ($3250\text{--}3200\text{ cm}^{-1}$), of C=O stretching of PABA (1655 cm^{-1}), in typical regions of SO₂ symmetric and asymmetric stretching (1319 , 1144 and 1064 cm^{-1}). Therefore, groups involved in cocrystal formation are the carboxylic acid and amine of PABA and the primary and secondary sulfonamide groups. This is consistent with the reported by Sanphui *et al.*, which described cocrystals synthons as type N-H \cdots O, involving the NH group of primary sulfonamide of HTZ and the OH group of the carboxylic acid of

PABA. Also, important interactions for cocrystal structure are reported, involving the NH group of secondary sulfonamide of HTZ and amine group of PABA.⁽³⁾

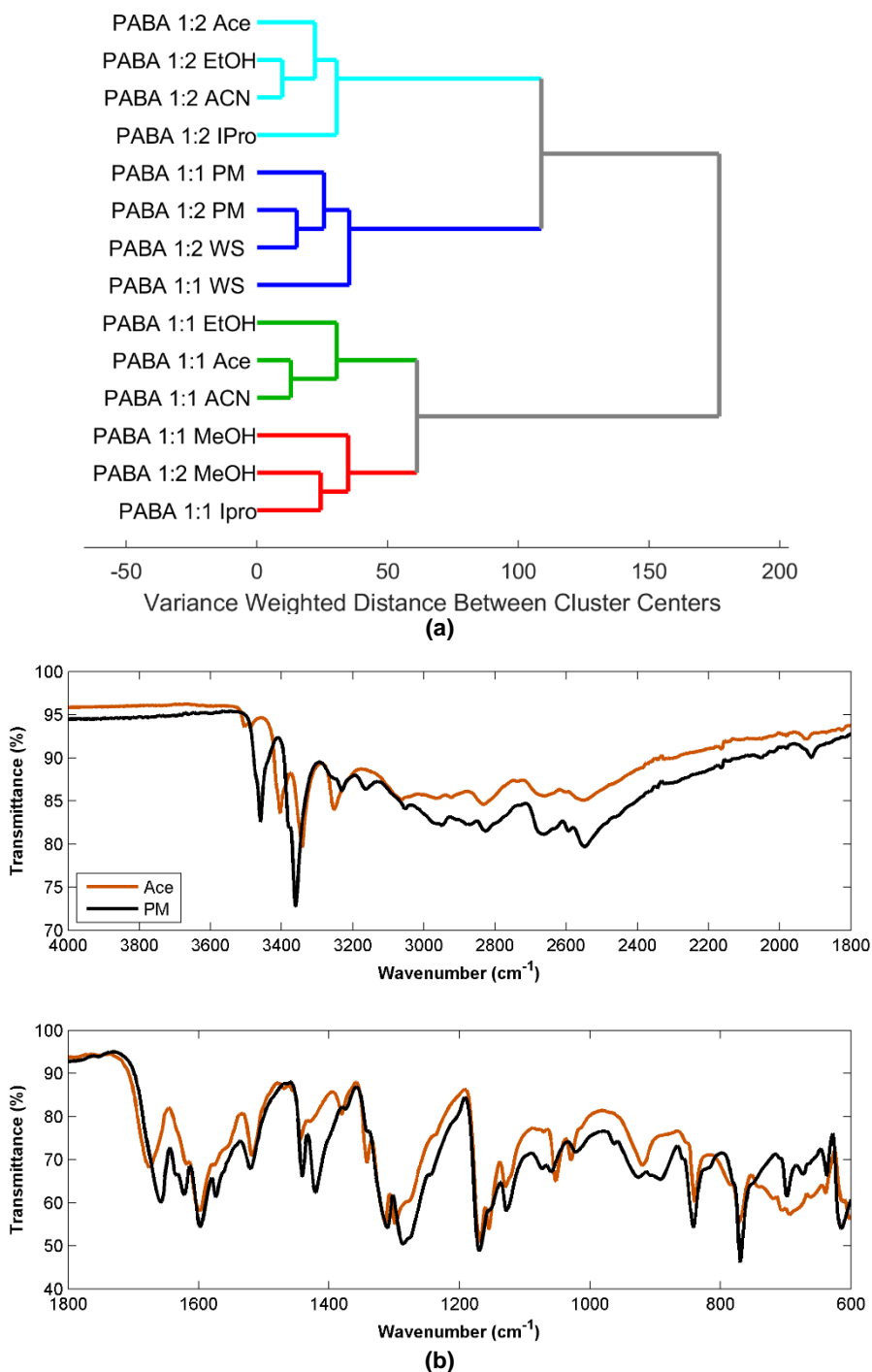


Figure 40: (a) Dendrogram from the HCA made with the MIR spectra of the cocrystallization products of HTZ:PABA systems in both ratios, 1:1 and 1:2. (b) MIR spectra from the cocrystallization product of HTZ:PABA 1:2 Ace (orange), pure PABA (red), pure HTZ (blue) and PM (black).

The intent of the in-situ analysis by Raman microspectroscopy was to analyze the products of cocrystallization in a fast way, without the need to remove the sample from the 96-well plate for analysis. However, some problems arose due to fluorescence. As can be

seen in Figure 41 (a) the Raman spectra of almost all cocrystallization products exhibit fluorescence hiding most Raman peaks. This is particularly problematic for some cases, such as for the product produced with Ace (Figure 41 (b)), where all the spectral features are lost. Therefore, this technique presents no advantage if the products have inherent fluorescence problems. A Raman with a laser of 1064 nm could be used to decrease the effect of fluorescence. However, the intensity of scattering falls off as the reciprocal fourth power of the wavelength, leading to lost in sensibility.^[16]

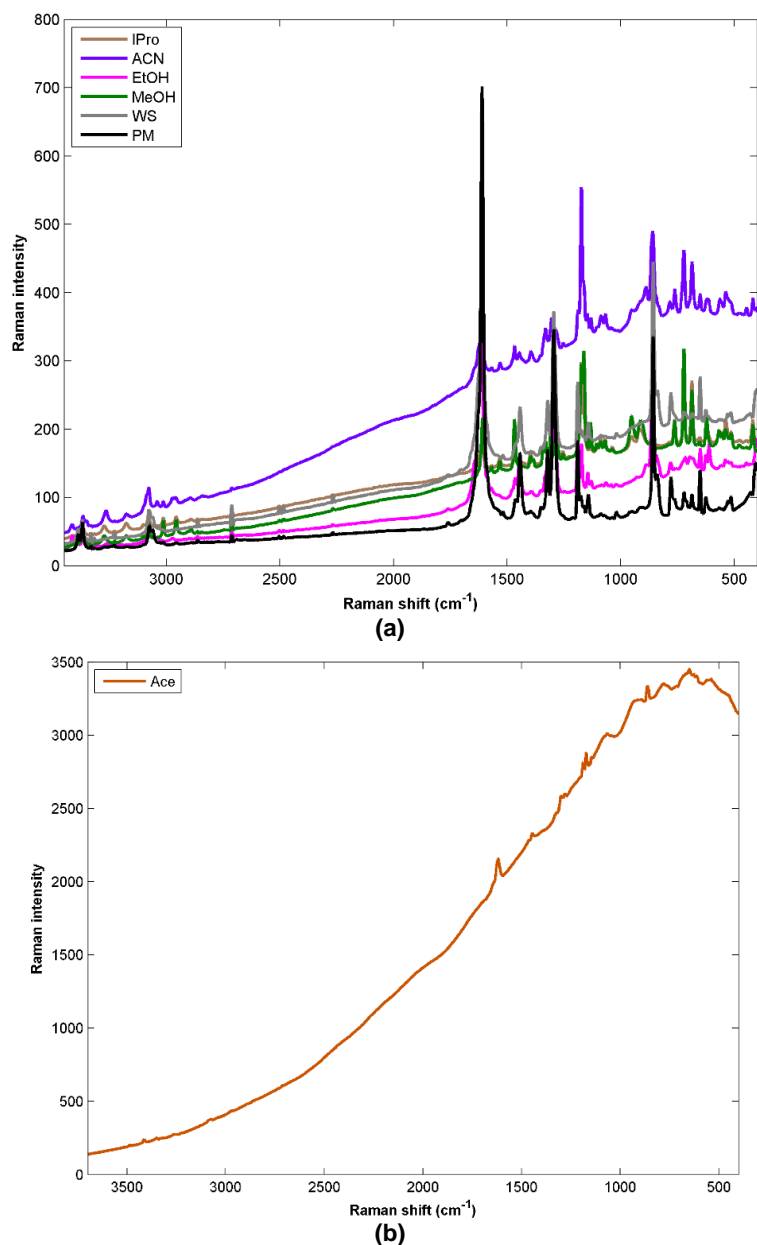


Figure 41: RMS spectra from (a) the products of cocrystallization produced with IPPro (brown), ACN (lilac), EtOH (pink), MeOH (green), WS (grey) and the PM (black); (b) the product of cocrystallization produced with Ace (orange).

iv. Hydrochlorothiazide: citric acid systems (HTZ:Cit)

HTZ:Cit 1:2 system was attempted for the second time, in order to study solvent influence on cocrystal formation. The HCA performed with MIR spectra of the products gives indication that MeOH and Ace were the solvents with the best performance (Figure 42 (a)). New attempted solvents, as IPro, were not efficient. MeOH and Ace were also used in the first plate and comparing both spectra from the first plate and the second plate, differences are not noticeable. Therefore, the same product was formed in the two screening products. As confirmed in Figure 42 (b), groups involved in cocrystal formation were the already referred, namely, NH_2 (differences at 3300 and 3100 cm^{-1}), $\text{S}=\text{O}$ groups of HTZ (1400 and 1100 cm^{-1}) and $\text{C}=\text{O}$ group from citric acid (1700 and 1750 cm^{-1}).

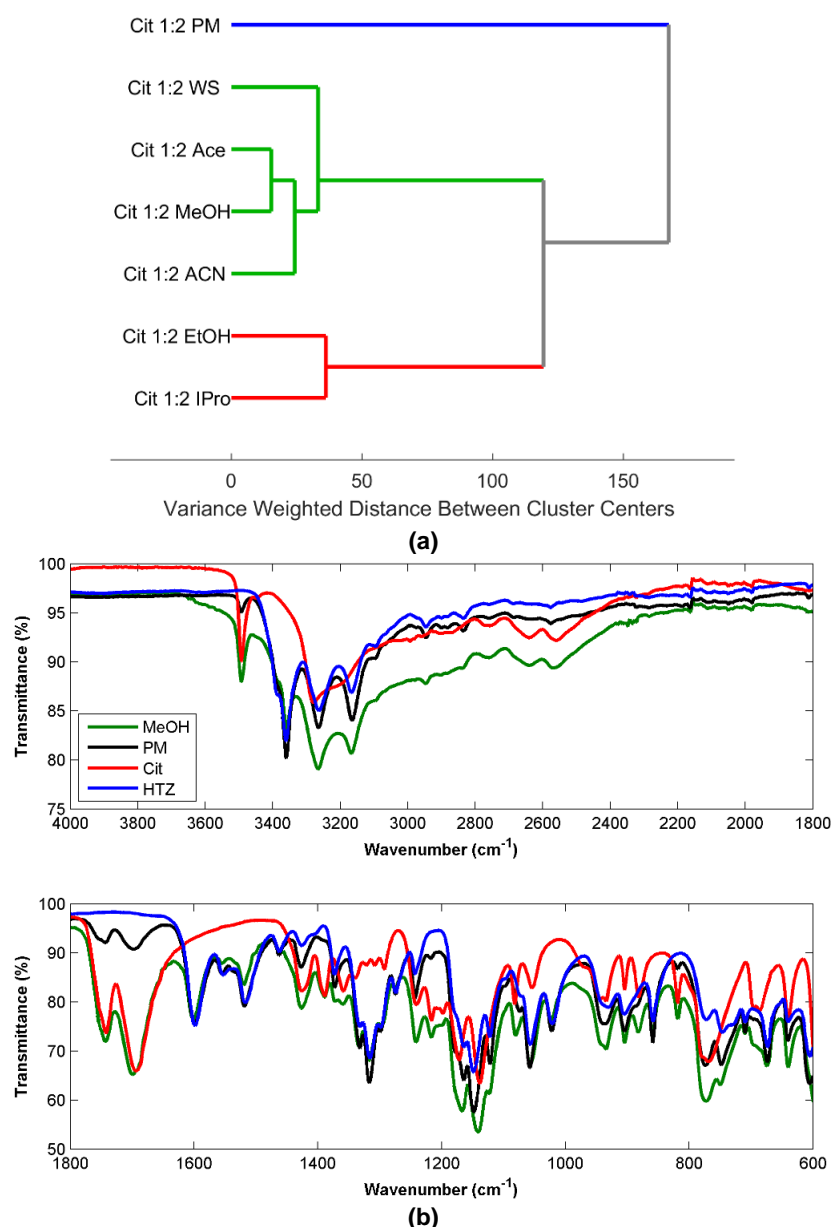


Figure 42: (a) Dendrogram from the HCA made with the MIR spectra of the cocrystallization products of HTZ:Cit 1:2 systems. (b) MIR spectra of HTZ:Cit 1:2 systems with MeOH (green), PM (black), pure citric acid (red) and pure HTZ (blue).

4.1.3. Screening experiments resume

Screening experiments allowed to discriminate systems with ability to form a cocrystal and systems without this propensity. Table 9 presents tested systems and the outcome evaluation relatively to cocrystal formation. Only for the system with coformer L(+)-arginine, a deduction about system suitability to cocrystal formation was not possible. These experiments gave information about groups involved on each cocrystal formation, based in spectra interpretation. Moreover, it was possible to select preferred coformer, ratio and solvents. Hydrochlorothiazide seems to have a preference to 1:2 ratio, once the majority of systems tested were better succeed in 1:2 ratio.

From the solvents analyzed in the first part of the screening, DCM and EtOAc were the ones with more tendency to form a cocrystal in most of the cases, while water and MeOH were the ones with more negative outcomes. Thus, the majority of the systems with HTZ seems to have a tendency to less polar solvents. In the case of the second part of the experiment, this tendency was not evident. IPro and EtOH were the tested solvents that showed a better performance. A deeper study is necessary to the establishment of a correlation between cocrystallization outcome and solvents, considering solvents properties.

Table 9: Resume of screening results in terms of evidences of cocrystal formation. Preferred ratio (HTZ:coformer) and solvent are also presented.

NC: not conclusive.

*polymorph formation.

System	Cocrystal formation	Preferred ratio	Solvent with best performance
HTZ:Ade	No	-	-
HTZ:Arg	NC	NC	IPro, ACN, EtOH
HTZ:Caf	No	-	-
HTZ:Cit	Yes	1:2	DMSO, EtOAc MeOH, Ace
HTZ:Mal	Yes	1:2	DCM, EtOAc
HTZ:Man	Yes	1:2	EtOAc, DCM, MeOH*
HTZ:Nic	Yes	1:1	IPro, EtOH
HTZ:PABA	Yes	1:2	Ace, EtOH, ACN
HTZ:Tris	Yes	1:2	DCM, EtOAc, DMSO
HTZ:Tryp	No	-	-

4.2. Laboratory-scale experiments

From the eleven coformers tested in cocrystal screening phase, citric acid, D(-)-mannitol, DL-malic acid, nicotinamide, *p*-aminobenzoic acid and tromethamine were selected as promising coformers to cocrystal formation. Cocrystallization screening methods and cocrystallization at laboratory-scale are not necessarily the same. Consequently, it is necessary to evaluate the influence of the scale increase in cocrystallization outcome. Therefore, all systems tested in screening experiment were produced in laboratory-scale through a slurry (Table 7), with the solvent(s) selected in screening as the most adequate.

After products characterization through vibrational spectroscopy techniques, it was found that the majority of the products had low purity. Purity is important for solubility assays, which are one the main objectives of this phase. Then, all the systems were submitted to a solvent evaporation method, to achieve products with higher purity (Table 8).

For solvent evaporation cocrystallization, solvent choice was rationally made accordingly to solubility of HTZ and coformer, in order to both achieve complete solubilization.^(10, 11) When that was not possible, a mixture of two solvents were made to achieve the same result.

Table 10 shows all the systems tested in laboratory-scale through a solvent cocrystallization method and the characterization techniques used for each system. Each obtained product was analyzed by NIRS and MIRS, comparing product's spectra with the one from the PM and pure compounds. Spectral analysis allowed to infer about cocrystal formation or not and to select the preferred ratio, analyzing purity of the products. If spectral analysis showed evidence of cocrystal formation with high purity, this cocrystallization products were characterized by DSC and PXRD. In the case of systems with nicotinamide, D(-)-mannitol, *p*-aminobenzoic acid and L(+)-arginine, after spectral analysis dubs about preferred ratio remained, thus, both ratios were characterized.

Cocrystallization products with adenine, L(+)-arginine, citric acid, D(-)-mannitol, nicotinamide, *p*-aminobenzoic acid and tromethamine are different from the respective PM, thus they are presented case by case with corresponding results of each technique. DSC data is specified in Table 11. Systems with caffeine, DL-malic acid and L-tryptophan did not show evidences of a reaction, being identical to the PM. Thus, this system's results are not presented. Results from the systems with DL-malic acid are not consistent with the screening results, since no cocrystal was obtained in laboratory-scale experiments and in screening experiments there were evidences of cocrystal formation. By other side, the system with adenine, which in screening experiments did not present evidences of cocrystal

formation, in laboratory-scale experiments formed a cocrystal. This two cases clearly showed that change process from screening experiments to laboratory-scale production can have impact on cocrystallization outcome. Different products in screening and laboratory-scale experiments are the result of different cocrystallization methods.

Table 10: Systems tested in laboratory-scale through solvent evaporation and techniques used for analyze each product.

System (ratio)	Solvent	Characterization techniques		
		NIRS/ MIRS	DSC	PXRD
HTZ:Ade (1:1)	DMSO	Yes	No	No
HTZ:Ade (1:2)	DMSO	Yes	Yes	Yes
HTZ:Arg (1:1)	EtOH/H ₂ O	Yes	Yes	Yes
HTZ:Arg (1:2)	EtOH/H ₂ O	Yes	Yes	Yes
HTZ:Caf (1:1)	Ace	Yes	No	No
HTZ:Cit (1:1)	DMSO	Yes	No	No
HTZ:Cit (1:2)	DMSO	Yes	No	No
	DCM	Yes	Yes	Yes
	MeOH	Yes	No	No
	Ace	Yes	No	No
HTZ:Mal (1:1)	DCM	Yes	No	No
	MeOH	Yes	Yes	Yes
HTZ:Mal (1:2)	DCM	Yes	No	No
	MeOH	Yes	Yes	Yes
HTZ:Man (1:1)	DMSO	Yes	Yes	Yes
HTZ:Man (1:2)	EtOH/H ₂ O	Yes	Yes	Yes
HTZ:Nic (1:1)	Ace	Yes	Yes	Yes
HTZ:Nic (1:2)	Ace	Yes	Yes	Yes
HTZ:PABA (1:2)	MeOH	Yes	Yes	Yes
HTZ:Tris (1:1)	DMSO	Yes	No	No
	MeOH	Yes	No	No
HTZ:Tris (1:2)	DCM	Yes	No	No
	DMSO	Yes	Yes	Yes
	MeOH	Yes	No	No
HTZ:Tryp (1:2)	EtOH/H ₂ O	Yes	No	No

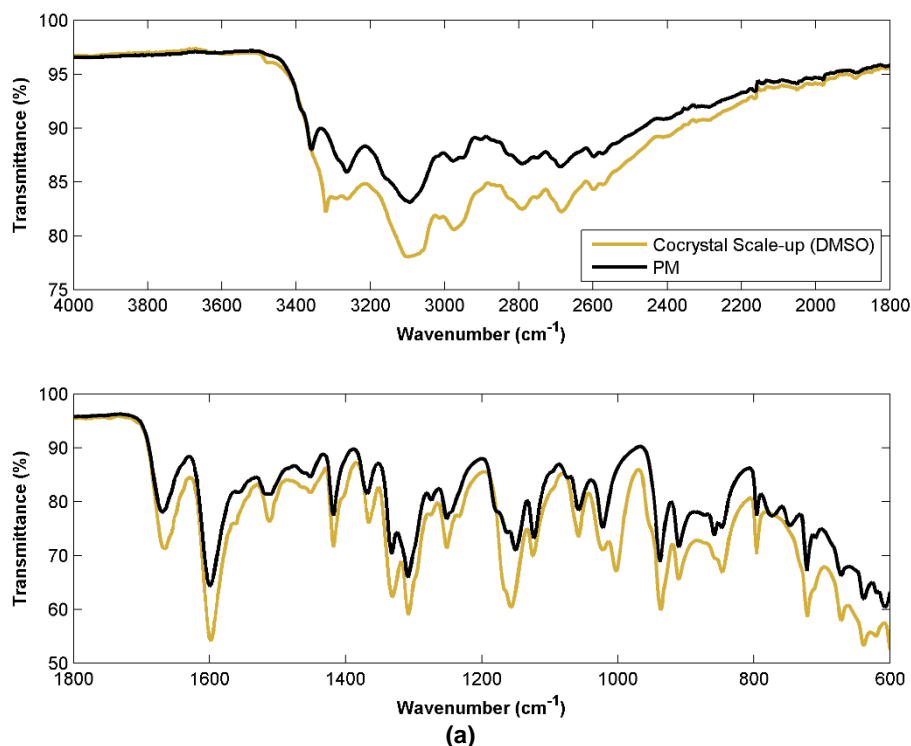
Table 11: Data from DSC analysis with onset temperatures for each endothermic event observed and correspondent enthalpy. In the case of HTZ:Arg 1:1 and 1:2, glass transition temperature (T_g) is presented.

	1 st peak		2 nd peak		3 rd peak		T _g (°C)
	T _{onset} (°C)	ΔH (J.g ⁻¹)	T _{onset} (°C)	ΔH (J.g ⁻¹)	T _{onset} (°C)	ΔH (J.g ⁻¹)	
HTZ	268.45	121.8	-	-	-	-	-
HTZ:Ade system							
HTZ:Ade 1:2 DMSO	103.00	6.732	291.90	30.22	-	-	-
PM	239.10	118.4	295.10	88.12	-	-	-
Ade	-	-	-	-	-	-	-
HTZ:Arg system							
HTZ:Arg 1:1 EtOH/H ₂ O	49.71	5.588	166.13	1.252	-	-	132.08
PM (1:1)	87.50	3.783	175.84	58.63	-	-	-
HTZ:Arg 1:2 EtOH/H ₂ O	46.27	8.852	161.17	5.072	-	-	126.57
PM (1:2)	83.95	3.684	186.85	70.61	-	-	-
Arg	96.76	0.6746	208.31	67.49	-	-	-
HTZ:Cit system							
HTZ:Cit 1:2 DCM	59.400	70.09	137.70	10.53	151.20	14.37	-
PM	152.73	128.7	-	-	-	-	-
Cit	154.43	232.0	-	-	-	-	-
HTZ:Mal system							
HTZ:Mal 1:2 MeOH	123.13	82.48	-	-	-	-	-
PM	128.08	117.3	-	-	-	-	-
Mal	129.23	247.2	-	-	-	-	-
HTZ:Man system							
HTZ:Man 1:1 DMSO	161.90	76.73	-	-	-	-	-
PM (1:1)	164.50	126.5	286.80	13.90	-	-	-
HTZ:Man 1:2 EtOH/H ₂ O	167.33	147.9	-	-	-	-	-
PM (1:2)	163.25	173.6	-	-	-	-	-
Man	164.43	275.9	-	-	-	-	-
HTZ:Nic system							
HTZ:Nic 1:1 Ace	174.27	123.2	-	-	-	-	-
PM (1:1)	113.74	58.35	168.72	6.225	-	-	-
HTZ:Nic 1:2 Ace	118.18	1.691	170.39	96.38	-	-	-
PM (1:2)	113.68	83.23	164.97	1.880	-	-	-
Nic	127.40	220.2	-	-	-	-	-
HTZ:PABA system							
HTZ:PABA 1:2 MeOH	174.66	93.65	-	-	-	-	-
PM	173.70	105.1	-	-	-	-	-
PABA	186.89	177.0	-	-	-	-	-
HTZ:Tris system							
HTZ:Tris 1:2 DMSO	112.7	121.6	-	-	-	-	-
PM	134.69	153.8	-	-	-	-	-
Tris	132.89	255.3	169.68	24.13	-	-	-

4.2.1. Hydrochlorothiazide: adenine system (HTZ:Ade)

When HTZ:Ade system was attempted through the solvent evaporation method, using DMSO and 1:2 ratio, a cocrystal was formed, contrarily to screening experiment, which did not show any indication of cocrystal formation.

NIRS and MIRS show several differences between the spectra of cocrystal and the PM, proving the existence of interaction between API and coformer. In MIRS, main differences are located in the region of amine groups, namely in bands corresponding to NH stretching of HTZ, at 3362 cm^{-1} , and of adenine, at 3320 cm^{-1} . Also, several differences are noticed in bands corresponding to symmetric stretching of SO_2 group of HTZ, at 1164 and 1002 cm^{-1} (Figure 43 (a)). NIRS is consistent with MIRS, presenting main differences at NH first overtone region, from 6835 to 6584 cm^{-1} , and NH combination bands, at 4721 and 4687 cm^{-1} (Figure 43 (b)). Hence, vibrational spectroscopy techniques suggest that groups involved in cocrystal formation are the sulfonamide group of HTZ and amine group of adenine.



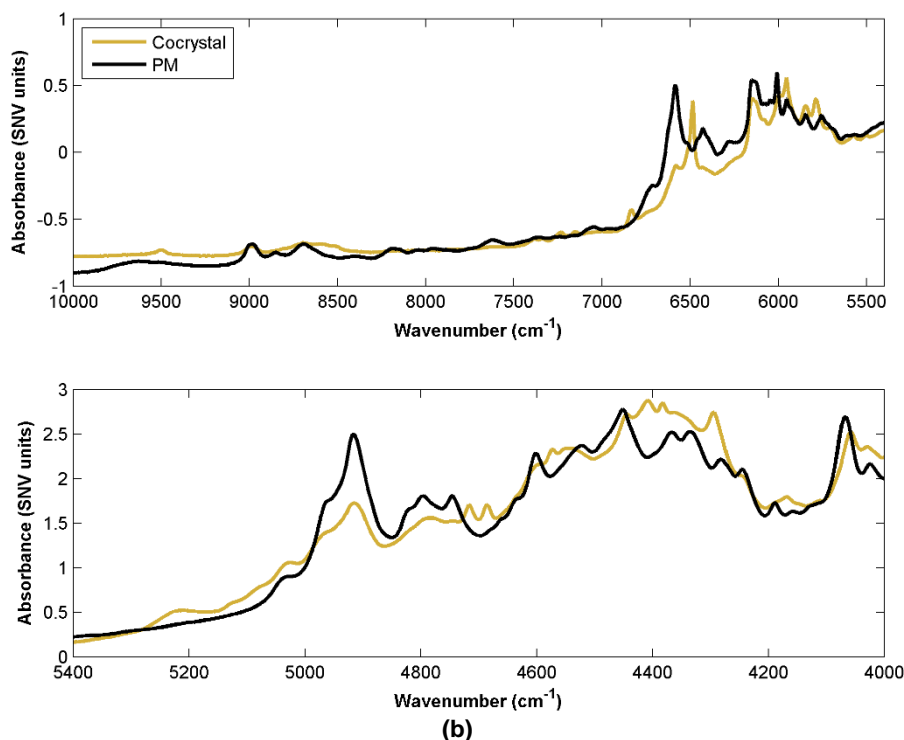


Figure 43: MIR (a) and NIR (b) spectra of HTZ:Ade 1:2 cocrystal produced with DMSO (dark yellow) and the respective PM (black).

PM is thermally characterized by an endothermic peak at 239.10 °C, following an exothermic event and an endothermic peak at 295.10 °C (Figure 44 and Table 11). These three events may correspond to a fusion, a crystallization and a new fusion of the crystallized product. Yamashita *et al.* described a thermal behavior associated to cocrystal formation, consisting in an endothermic peak associated to the eutectic melting of the mixture between the API and the coformer, instantly followed by an exothermic peak and another endothermic peak, corresponding to the cocrystal melting point.^(93, 94) PM thermal behavior seems to correspond to the described one.

Cocrystal's thermogram is presented in Figure 44 and, despite of the curved baseline, it is possible to distinguish an endothermic peak at 103.00 °C, followed by exothermic event close to the one of the PM and an endothermic peak (291.90 °C). Comparing with PM's thermal behavior, these events may correspond to the form I cocrystal fusion, followed by a recrystallization (creating a polymorph) and form II cocrystal fusion. However, to confirm this statements more analysis must be done, for example, by PXRD with temperature, to analyze the product after each thermal event.

PXRD analysis allowed to obtain a diffractogram from the cocrystal, with a crystalline pattern different from the PM diffractogram, proving changes in the crystal lattice. Cocrystal diffractogram presents several new peaks and appear to have a higher total number of peaks (Figure 45). Comparing with pure compounds diffractogram, no excess of API or coformer was notice, so the product was confirmed to be pure.

All characterization techniques are consistent with formation of a HTZ:Ade 1:2 cocrystal, with high levels of purity. This cocrystal is based in hydrogen bonds between sulfonamide groups of HTZ and amine group of adenine.

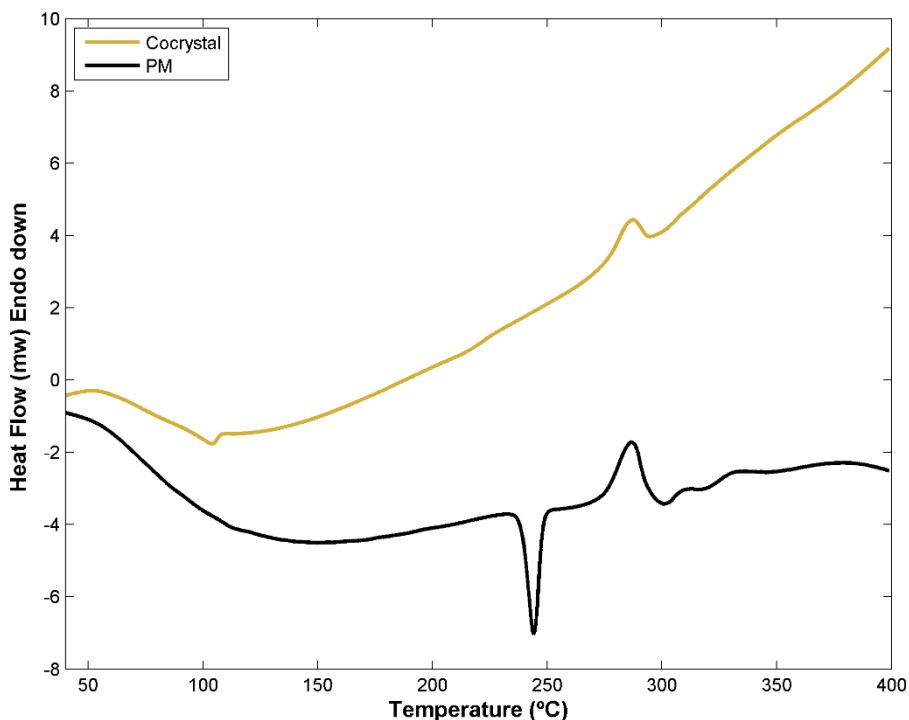


Figure 44: Thermogram of HTZ:Ade 1:2 cocrystal (dark yellow) and the respective PM (black).

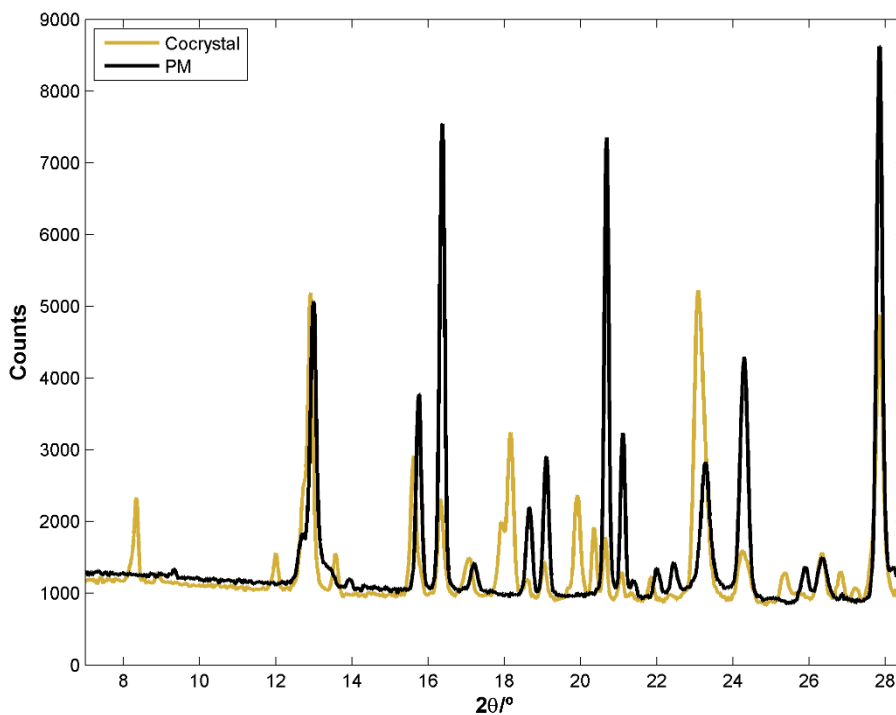


Figure 45: Diffractogram of HTZ:Ade 1:2 cocrystal (dark yellow) and the respective PM (black).

4.2.2. Hydrochlorothiazide: L(+)-arginine system (HTZ:Arg)

HTZ:Arg systems were submitted to a solvent evaporation method, in laboratory-scale experiments. A mixture of two solvents, EtOH and water, was used, in order to achieve complete dissolution.

Thermal behavior of HTZ:Arg system consists in two endothermic events and a glass transition, which is typical of amorphous compounds (Figure 46 and Table 11). Thermogram of HTZ:Arg 1:1 systems presents a glass transition at 132.08 °C and 1:2 systems presents the same event at 126.57 °C. Glass transition event is not present in PM. Each system's thermogram shows an endothermic event (at 166.13 and 161.17 °C respectively) that seems to correspond to a fusion, probably from HTZ.

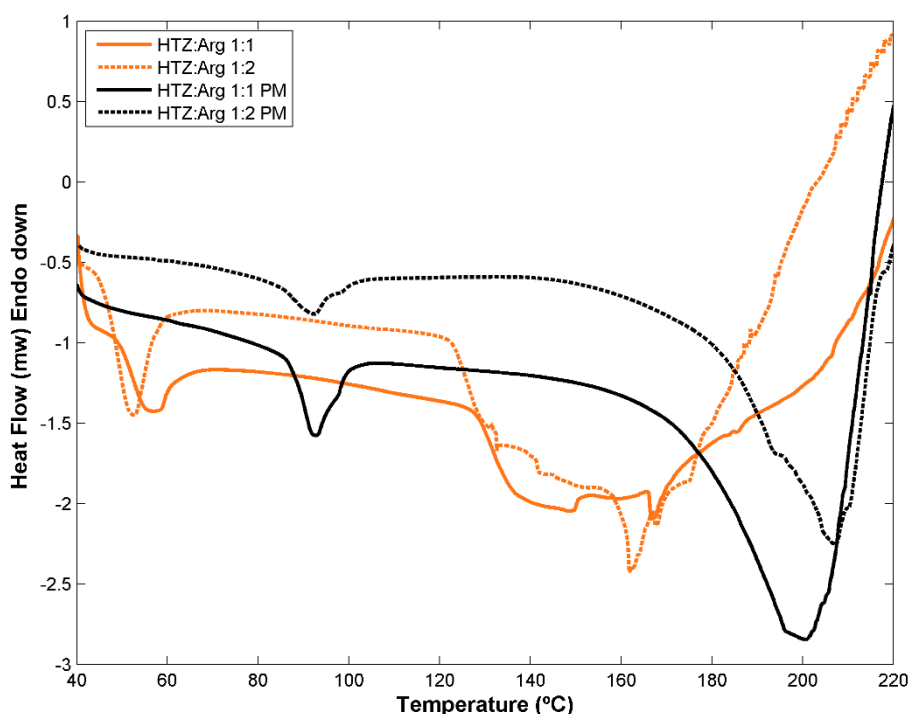


Figure 46: Thermogram of the systems of HTZ:Arg 1:1 (orange) and 1:2 (orange dashed) and PMs of the HTZ:Arg 1:1 (black) and 1:2 (black dashed).

Another endothermic peak appear at 49.71°C in the case of HTZ:Arg 1:1 system and at 46.27 °C in the case of HTZ:Arg 1:2 system. The same event appears in the PM of the system 1:1 at 87.50 °C and in the PM of the system 1:2 at 83.95 °C. This event probably corresponds to water desorption. Arginine absorbed atmospheric water, which explains the endothermic event at 96.76 °C on pure arginine thermogram (see Table 11). In the case of PMs, water desorption happens at similar temperatures and, in the case of HTZ:Arg 1:1 and 1:2 products, water desorption takes place at lower temperature. This can be justified with arginine amorphization. As Presswala *et al.* described, water bonding with arginine is weaker when arginine is in amorphous state, needing less energy to water desorption.⁽¹⁴⁸⁾ Water presence is also proved with MIR spectra of pure arginine and PMs (Figure 47 (a)),

where a broad band can be observed around 3150 cm^{-1} , corresponding to stretching of OH groups of water.

To verify if amorphization happened, crystalline arginine was subject to the same cocrystallization conditions as the ones of HTZ:Arg system. A certain amount of L(+)-arginine was dissolved in a mixture of ethanol/water (80/20) under agitation at 40°C . After dissolution, the solution was left to evaporate in a fume hood at room temperature. The product obtained was a gel like product, and after spectral characterization, it was considered an amorphous phase (Figure 47 (b)).

MIRS analysis corroborate that arginine had suffered a solid state change from crystalline to amorphous form during cocrystallization process (Figure 47). In the MIR spectra of the sample, it is possible to observe peaks attenuation, similar to the one seen in spectrum of amorphous arginine, which has clearly less sharp peaks in comparison to spectrum of crystalline arginine. Löbmann *et al.* had already described peak attenuation due to compound amorphization, resulting in broader peaks.⁽¹⁴⁹⁾

In another work, the main differences between MIR spectra of crystalline and amorphous arginine are described as bands shifts, for example: shift from 1675 cm^{-1} (corresponding to stretching of COO^- and guanidyl groups) to 1668 cm^{-1} , from 1613 cm^{-1} (corresponding to vibration of guanidyl group) to 1632 cm^{-1} , from 1552 cm^{-1} (CN group) to 1540 cm^{-1} , and from 1420 cm^{-1} (COO^- group) to 1405 cm^{-1} .⁽¹⁵⁰⁾ A comparison between MIR spectra of amorphous arginine and the one of crystalline (Figure 47), revealed the same spectral differences described above. Spectrum of HTZ:Arg system is similar to the one of amorphous arginine in several regions ($1680\text{-}1660\text{ cm}^{-1}$, $1450\text{-}1400\text{ cm}^{-1}$ and around 1000 cm^{-1}). Peaks corresponding to HTZ remain similar to pure HTZ.

Diffractionograms of HTZ:Arg systems are equal to the one of pure HTZ (see Figure 48). Amorphous compounds do not present peaks in PXRD thermograms, generally, they present a baseline change from a strict to a curved baseline.⁽¹²²⁾ In this case, HTZ of the system remained crystalline giving origin to the peaks observed in Figure 48 and peaks corresponding to Arg are not present, proving that arginine is in the amorphous state.

Concluding, HTZ:Arg 1:1 and 1:2 systems did not formed a cocrystal and there is no indication of coamorphous formation as well. Results show that a mixture from crystalline HTZ and hydrated amorphous arginine was formed (crystalline-amorphous hydrated mixture).

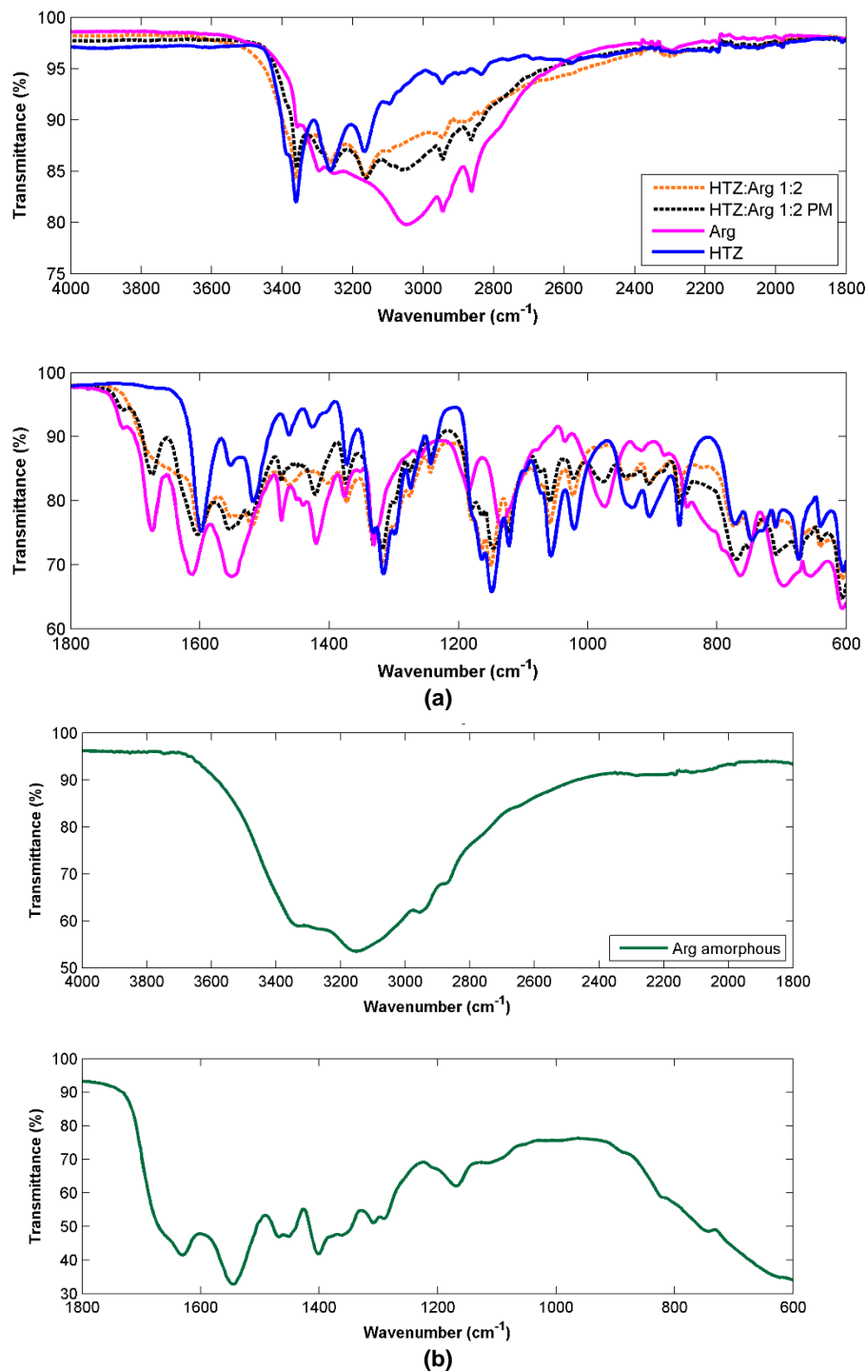


Figure 47: (a) MIR spectra of the product of HTZ:Arg 1:2 system (orange dashed), respective PM (black dashed), crystalline arginine (pink) and HTZ (blue); (b) MIR spectrum of amorphous arginine (green).

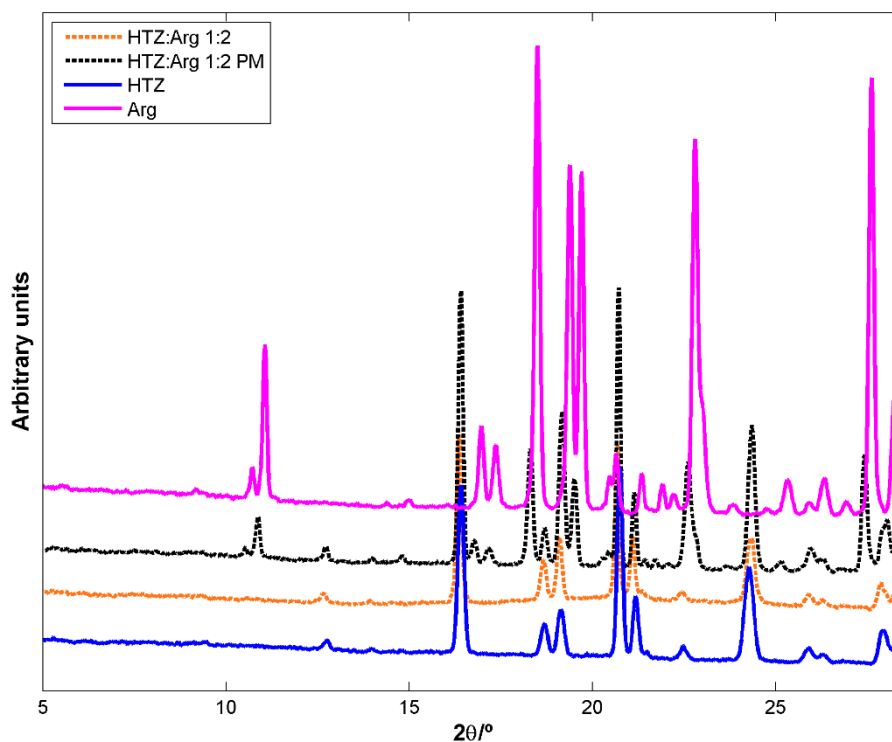


Figure 48: Diffractogram of the HTZ:Arg 1:2 system's product (orange dashed), respective PM (black dashed), pure HTZ (blue) and arginine (pink).

4.2.3. Hydrochlorothiazide: citric acid system (HTZ:Cit)

The cocrystallization was performed with DCM. Comparing MIR spectra of the product from laboratory-scale experiment with the one from screening experiments, some differences are perceived, mainly, a band at 3494 cm^{-1} with very different intensity; from 1750 to 1650 cm^{-1} , where scale up product have three bands and screening product have two bands; around 1400 cm^{-1} and from 1200 to 1100 cm^{-1} , where spectra from laboratory-scale is similar to the one from the PM and different from the one of the screening product (Figure 49 (a)). Thus, laboratory-scale product is different from screening product.

MIR spectrum of the laboratory-scale product presents differences when compared to PM, namely at 3494 cm^{-1} , a band corresponding to stretching vibrations of OH groups of citric acid has different intensity in the two spectra. Between 1750 and 1650 cm^{-1} , which is a region corresponding to stretching vibration of C=O groups of citric acid (Figure 49 (a)). No differences in regions corresponding to bands of HTZ are detected. Also, differences between NIR spectra of the scale up product and the respective PM are restricted to the region between 6500 and 7000 cm^{-1} , characteristic from OH first overtone, and no more differences are distinguished (Figure 49 (b)).

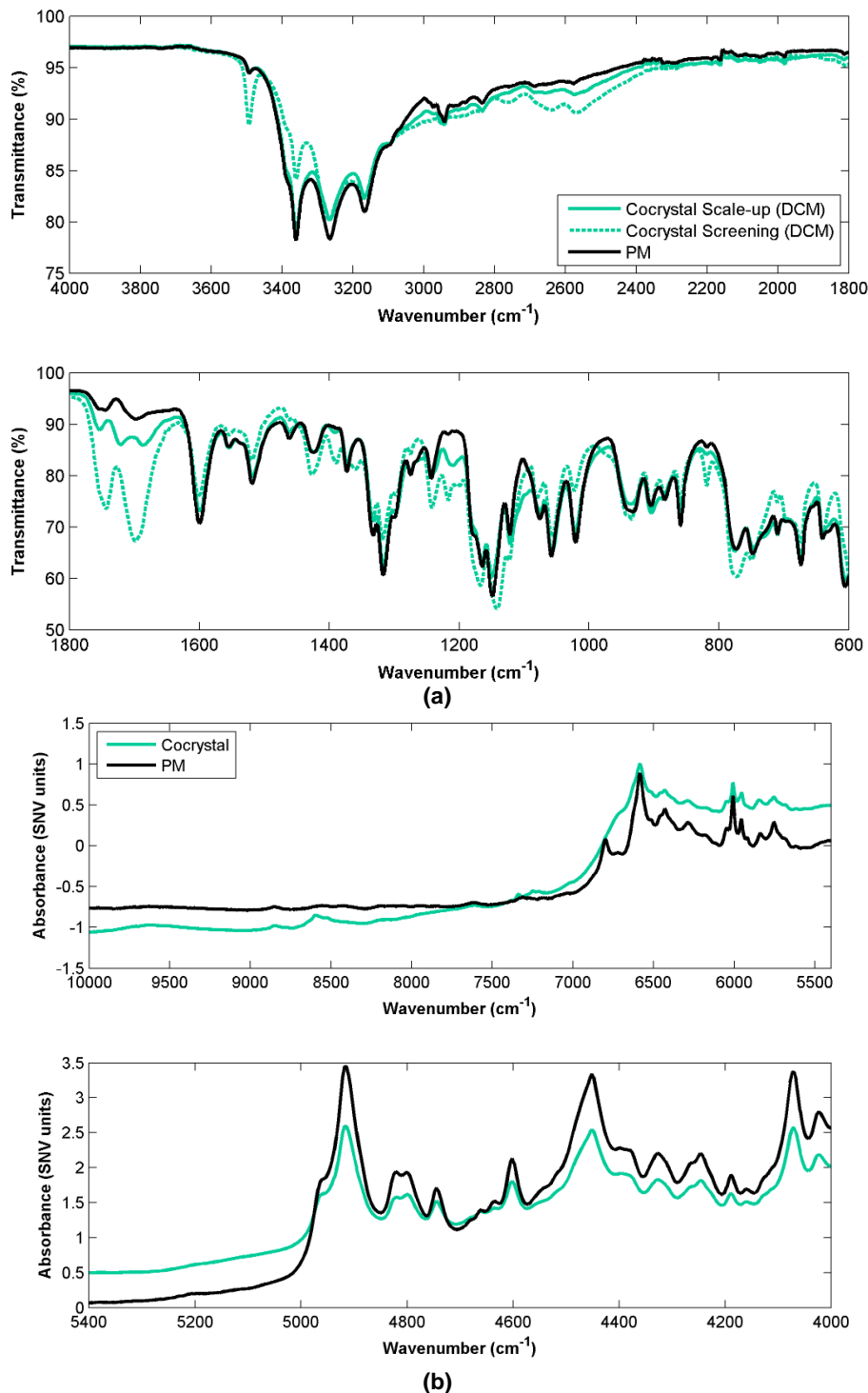


Figure 49: MIR (a) and NIR (b) spectra of scale up product of the HTZ:Cit 1:2 system (green), screening product of the same system (green dashed) and respective PM (black).

Thermogram of PM of HTZ:Cit 1:2 shows an endothermic peak at 152,73 °C, related to PM fusion. HTZ:Cit 1:2 system presents two endothermic peaks that are different from the one of the PM: a broad peak at 59,40 °C, which seems to be water desorption of an hydrated product, or a desolvation of incorporated DCM during cocrystallization, and a sharp peak at 137,70 °C that correspond to systems fusion. The product still have some

unreacted system, once it present a third endothermic event at 151,20 °C, close to PM's fusion temperature (Figure 50 and Table 11).

It is important to understand if a solvate was formed during cocrystallization process. In order to understand if the first endothermic event was caused by solvent desolvation or water desorption, MIR spectra was analyzed to check if bands corresponding to DCM are present. DCM is a solvent with MIR characteristic bands mainly at the following wavenumbers: 3050, 2985, 1425, 1269 (very intense band), 894 and 727 (very intense band) cm^{-1} . Figure 49 (a) presents the spectrum of scale-up cocrystallization product with the solvent DCM. DCM characteristics bands are not perceived in the spectrum, so it is not probable that a solvate was formed in cocrystallization process. However, it is feasible that cocrystallization product had absorbed atmospheric water, since citric acid is a highly hygroscopic compound.⁽¹⁵¹⁾ MIR spectral differences between the scale up product and PM, which were already pinpointed, are consistent with an hydrate formation.

Diffractiongram of the HTZ:Cit 1:2 cocrystal presents several differences from the one of the respective PM, which may be caused by structural differences in the scale up product due to water incorporation (Figure 51). In fact, changes in some peaks (for example around 14, 14 and 22°) are related to hydration of citric acid.⁽¹⁵²⁾

However, it is not possible to understand if the product is a cocrystal hydrate or if citric acid got hydrated and a cocrystal was not formed. More studies are necessary, for example, PXRD with temperature, to verify the form of the product after each thermal event.

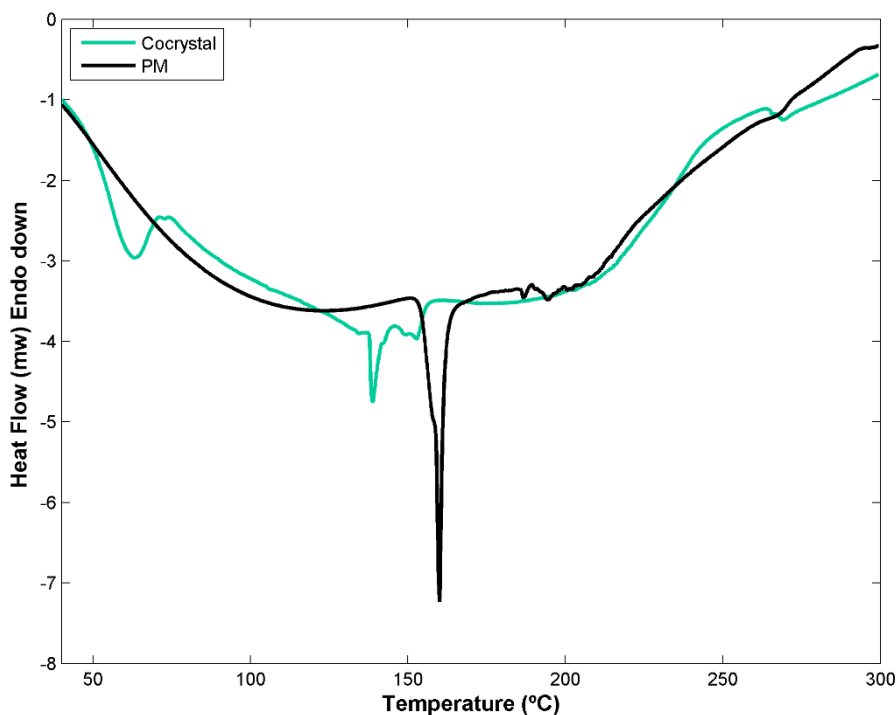


Figure 50: Thermogram of scale up product of the HTZ:Cit 1:2 system (green) and respective PM (black).

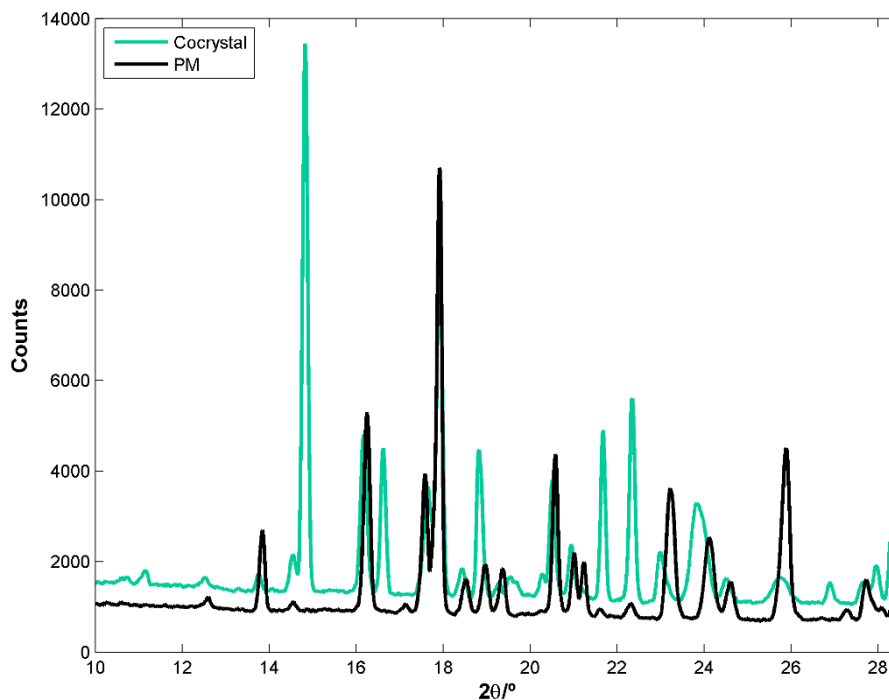


Figure 51: Diffractogram of scale up product of the HTZ:Cit 1:2 system (green) and respective PM (black).

4.2.4. Hydrochlorothiazide: D(-)-mannitol systems (HTZ:Man)

Screening experiment suggested that HTZ:Man systems are able to form a cocrystal. Despite of the similarity between products obtained with the two different ratios, 1:2 ratio was proposed as the most probable to cocrystal formation. Also, two polymorphs were obtained, one with the majority of the solvents and the other one with MeOH.

In laboratory-scale experiments, HTZ:Man systems was submitted to cocrystallization with DMSO in a 1:1 ratio, and with a solvents mixture of EtOH and water in a 1:2 ratio. Since vibrational spectroscopic analysis left doubts relatively to cocrystal ratio, both products were analyzed by DSC and PXRD. Spectroscopic evidences show that the obtained cocrystal was the same as the polymorph obtained in screening phase with the majority of the solvents. Polymorph obtained with the MeOH was not replicated.

Despite of screening had indicated 1:2 has the most suitable ratio, MIR analysis of the laboratory-scale products suggests that 1:1 is the most probable ratio (Figure 52). In spectra of HTZ:Man 1:2 cocrystals and respective PM and pure compounds (Figure 52 (b)), it is possible to detect an excess of the cofomer by peak attenuation in regions where pure Man does not have a big spectral signature: between 1600 and 1500 cm^{-1} , around 1300 cm^{-1} , between 1200 and 1100 cm^{-1} and around 750 cm^{-1} .

Groups involved in cocrystal formation seems to be the same as described in screening experiment, since spectral differences are the same.

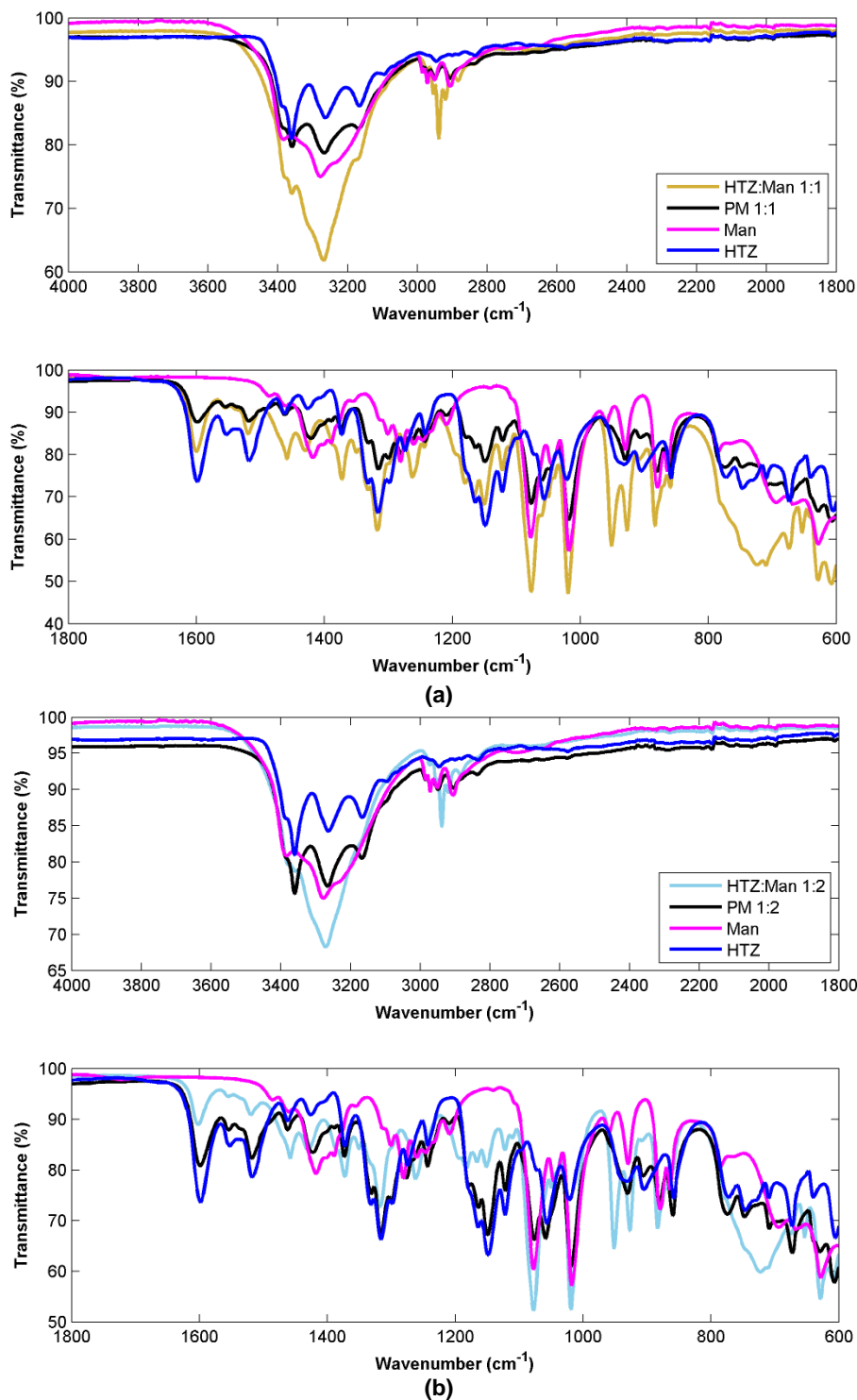


Figure 52: (a) MIRS spectra of the HTZ:Man 1:1 (yellow) cocrystal, PM (black) system, pure D(-)-mannitol (pink) and HTZ (dark blue); (b) MIRS spectra of the HTZ:Man 1:2 (light blue) cocrystal, PM (black) system, pure D(-)-mannitol (pink) and HTZ (dark blue).

Thermal analysis of pure D(-)-mannitol reveal an sharp endothermic peak at 164.43 °C, representing its melting point. PM of HTZ:Man 1:1 systems presents a endothermic event at a similar temperature (164.50 °C), while PM of HTZ:Man 1:2 shows a endothermic peak at lower temperatures (163.25 °C). This last peak is directly succeeded by a small other peak and that can be justified for the partial formation of the cocrystal inside the DSC

capsule, during the thermal analysis. HTZ:Man 1:1 cocrystal has an thermogram with a endothermic peak at 161.90 °C, corresponding to cocrystal melting point, a lower temperature when comparing to the PM and pure compounds. HTZ:Man 1:2 cocrystal have the same thermal event at 167.33 °C, a higher temperature comparing to the PM and pure compound (Figure 53 and Table 11). This technique shows that a cocrystal was formed with both systems, but does not gives clear information about cocrystal real ratio.

Diffractiongrams of systems with 1:1 and 1:2 ratios are different from the ones of the respective PM (Figure 54). Therefore, its proved that a new crystal structure was formed through. Yet, HTZ:Man 1:1 and 1:2 cocrystals show equal diffractiongrams, so it is not possible to infer about cocrystal ratio.

All the techniques are in agreement about the formation of a cocrystal with the HTZ:Man system. DSC and PXRD does not clarify the real ratio of the cocrystal. Only MIRS was able to give indications about the most probable cocrystal ratio, which was 1:1, in opposition on what assumed in screening experiments.

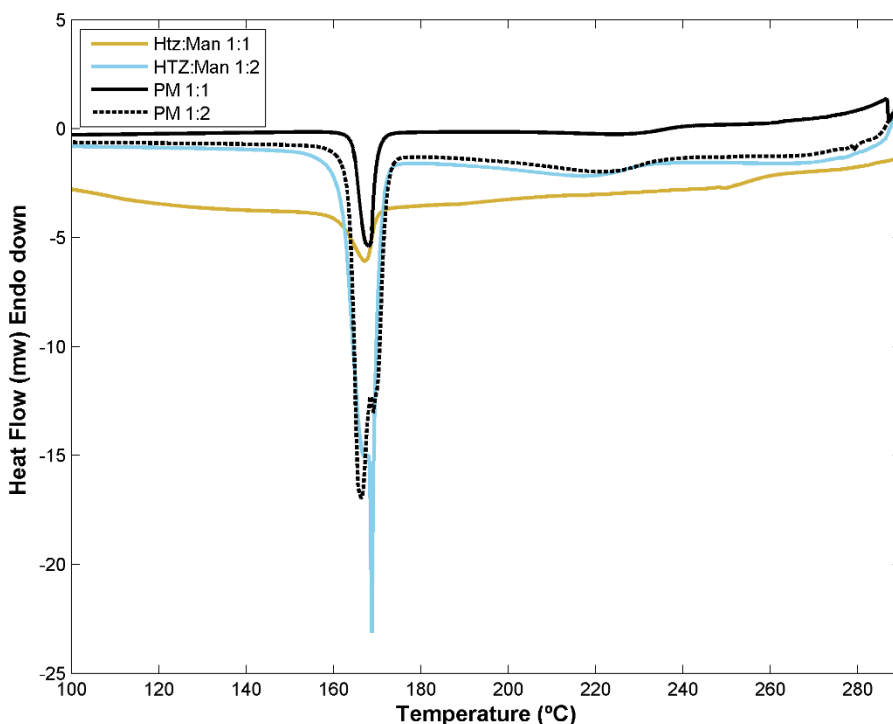


Figure 53: Thermograms of the HTZ:Man 1:1 (yellow) and 1:2 (light blue) cocrystal and PMs of the 1:1 (black) and 1:2 (dashed black) systems.

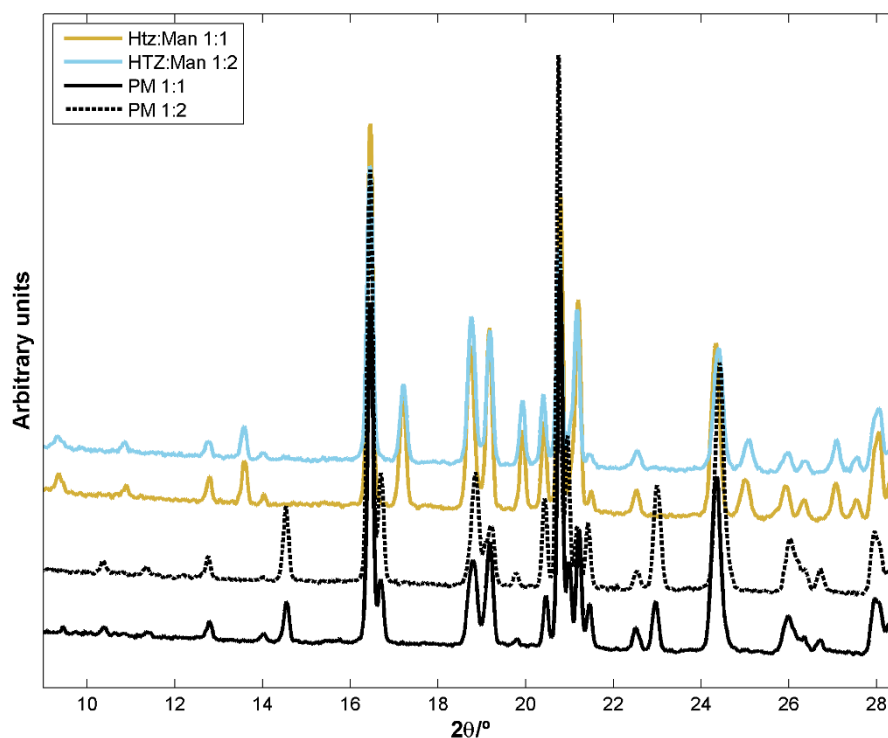


Figure 54: Diffractogram of the HTZ:Man 1:1 (yellow) and 1:2 (light blue) cocrystal and PMs of the 1:1 (black) and 1:2 (dashed black) systems.

4.2.5. Hydrochlorothiazide: nicotinamide systems (HTZ:Nic)

Screening phase showed that both ratios 1:1 and 1:2 from HTZ:Nic system had formed a cocrystal. A deeper spectral analysis suggested that 1:1 ratio is the real ratio of the cocrystal. Both HTZ:Nic 1:1 and 1:2 systems were submitted to cocrystallization with acetone, to confirm screening results.

HTZ:Nic 1:1 cocrystal presents a MIR spectrum similar to the spectrum of the cocrystal obtained in the screening (Figure 55). Consequently, differences comparing to the PM and groups involved in cocrystal formation were already described before.

Comparison of thermal behavior of cocrystals from both ratios allowed to identify that 1:1 was indeed the real cocrystal ratio (Figure 56 and Table 11). Thermogram of the HTZ:Nic 1:2 cocrystal presents an endothermic peak at 170.39 °C, corresponding to cocrystal fusion, and it presents another smaller endothermic event at 118.18 °C, which corresponds to an excess of nicotinamide. This corroborates that HTZ:Nic 1:2 cocrystal is not pure. HTZ:Nic 1:1 cocrystal's thermogram show a unique and sharp endothermic peak at 174.27 °C, corresponding to cocrystal's melting point, indicating that this cocrystal is pure. Obtain cocrystal's melting point value is consistent with the one referred in literature.⁽³⁾

PRXD analysis of the cocrystal shows a different diffractogram from the one of the PM, present several new peaks, indicating a new crystalline structure. Despite of PRXD

being a technique very used to obtain sample purity, when compared diffracting pattern of cocrystal with 1:1 and 1:2 ratios, no differences were visualized (Figure 56).

All techniques were consistent, demonstrating the formation of a high pure HTZ:Nic 1:1 cocrystal, based in hydrogen bonding between the NH of sulfonamide group of HTZ and the carbonyl group of Nic.

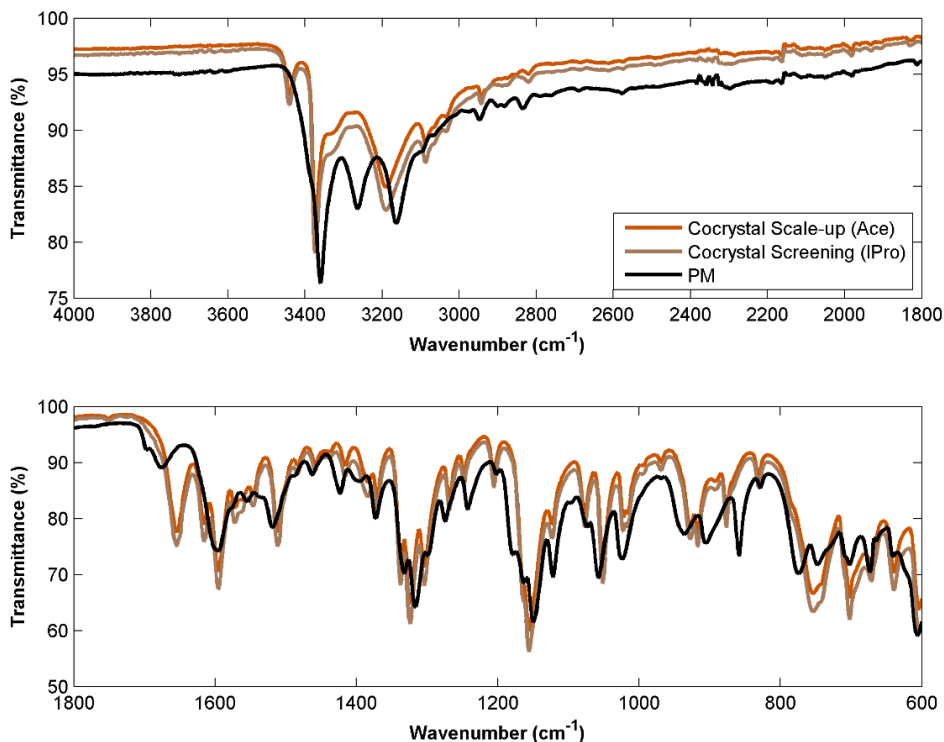


Figure 55: MIR spectrum of HTZ:Nic 1:1 cocrystal produced in scale up (orange), of the same cocrystal produced in screening (brown) and of the PM (black).

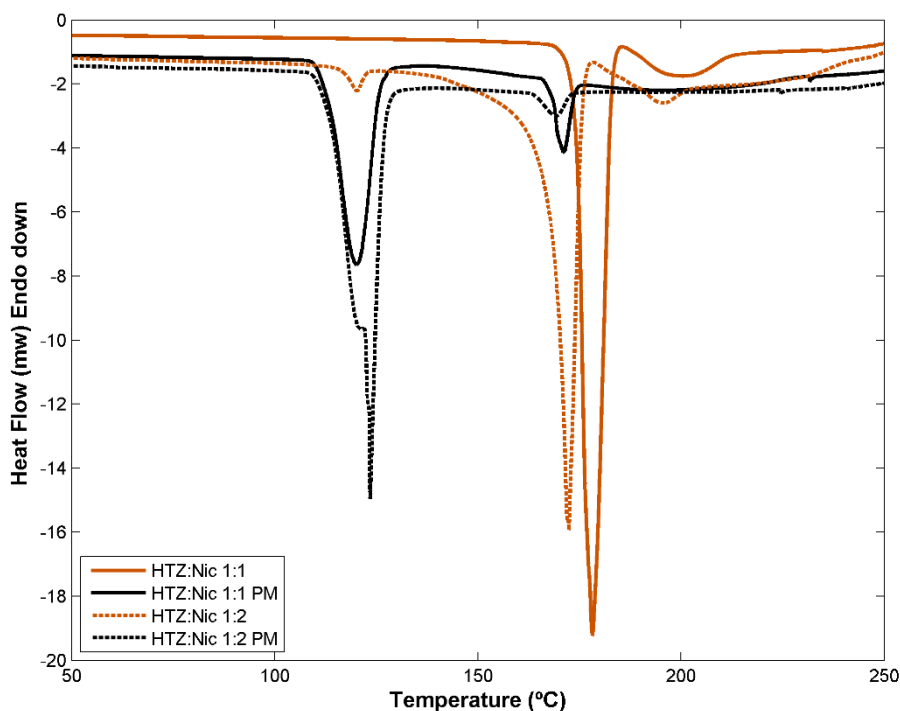


Figure 56: Thermograms of the cocrystal of HTZ:Nic 1:1 (orange), HTZ:Nic 1:2 (orange dashed), PM 1:1 (black) and PM 1:2 (dark dashed).

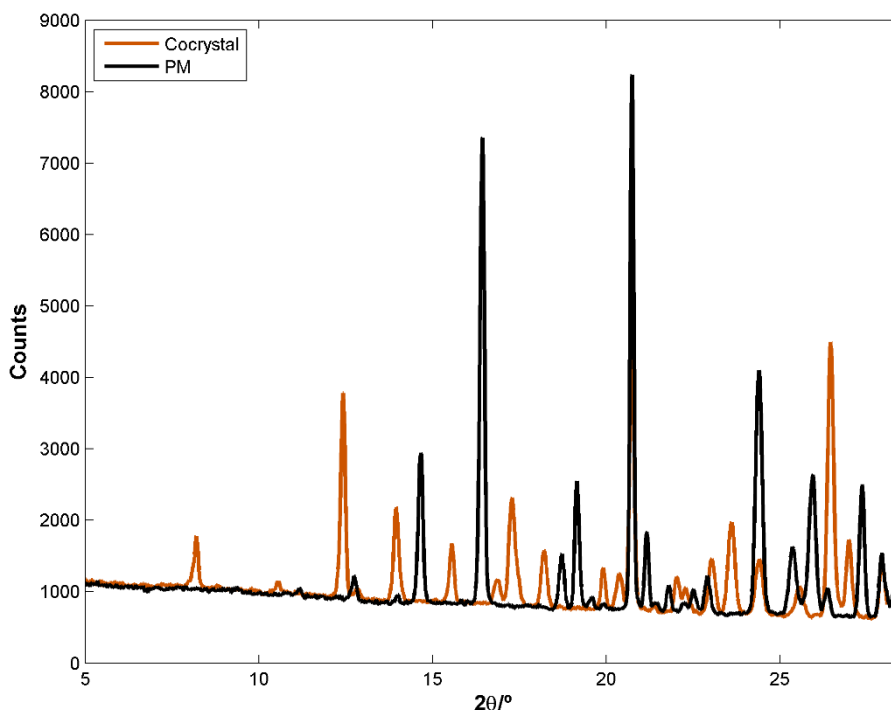


Figure 57: Diffractogram of HTZ:Nic 1:1 cocrystal (orange) and respective PM (black).

4.2.6. Hydrochlorothiazide: *p*-aminobenzoic acid systems (HTZ:PABA)

Screening procedure led to selection of HTZ:PABA 1:2 as promising cocrystal. Laboratory-scale cocrystal was obtained through a solvent evaporation method with methanol, a solvent where both API and coformer are soluble described in the literature.⁽¹⁴²⁾

Cocrystal produced in scale up phase and the one produced in screening are the same, since they present identical MIR spectra, as it can be seen in Figure 58. Therefore, spectral differences to the PM and groups involved in cocrystal are the ones already reported in screening phase cocrystal.

Thermogram of HTZ:PABA 1:2 cocrystal presents a single and sharp endothermic peak, corresponding to cocrystal fusion, at 174.66 °C (Figure 59 and Table 11). This value is in conformation with the one already reported.^(3, 142) PM presents a fusion peak in thermogram at 173.70 °C.

Also, PXRD diffractogram is consistent with a cocrystal formation, showing several differences between cocrystal's diffractogram and the one from PM (Figure 60).

The techniques were consistent with a cocrystal formation with HTZ:PABA 1:2 system, involving the groups NH from primary sulfonamide group of HTZ and OH from the carboxylic acid of PABA.

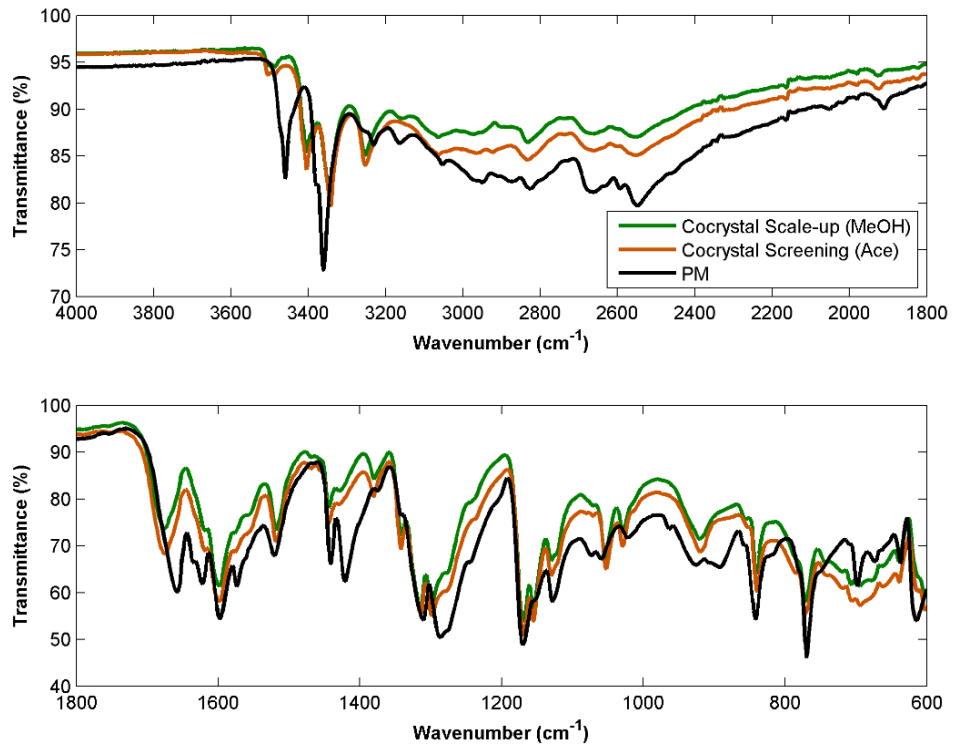


Figure 58: MIR spectra of the HTZ:PABA 1:2 cocrystals produced in scale up (green), produced in the screening (orange) and PM (black).

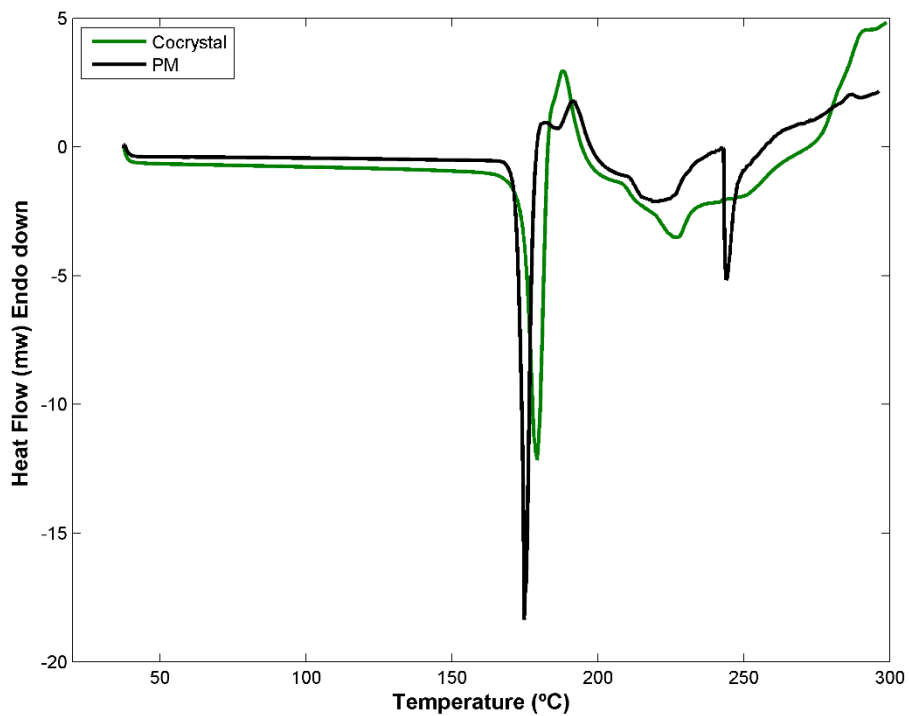


Figure 59: Thermograms of HTZ:PABA 1:2 cocrystal (green) and of the respective PM (black).

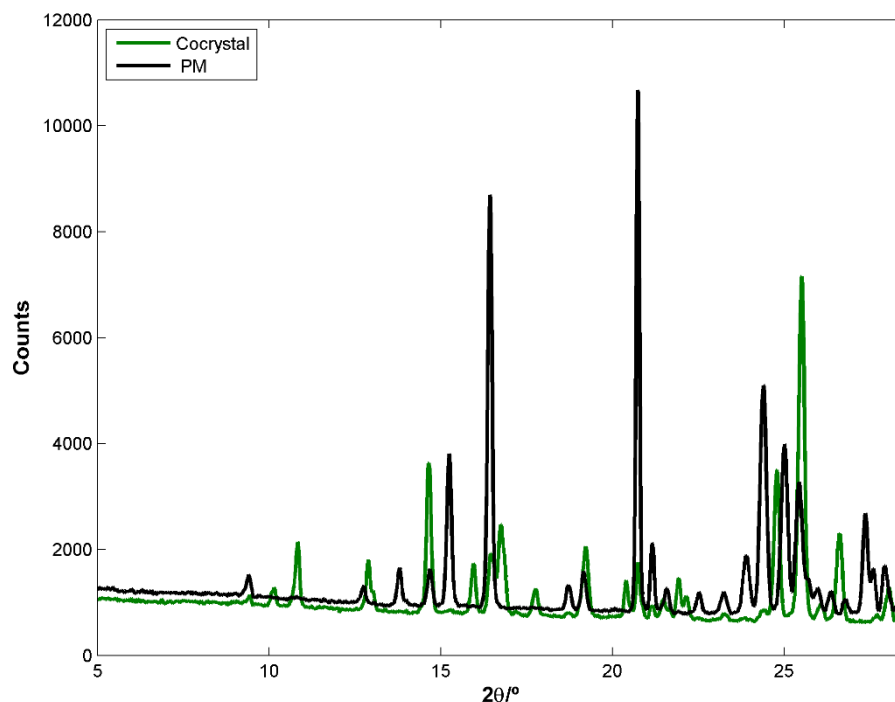


Figure 60: Diffractogram pattern of the HTZ:PABA 1:2 cocrystal (green) and of the respective PM (black).

4.2.7. Hydrochlorothiazide: tromethamine systems (HTZ:Tris)

Screening phase showed that HTZ and tromethamine produced a cocrystal. It was also possible to identify 1:2 ratio as the most probable ratio of the cocrystal and that the groups involved in cocrystal formation are the sulfonamide group of HTZ and the amine group of Tris.

In laboratory-scale experiments, HTZ:Tris 1:2 cocrystal was obtained using DMSO as a solvent.

MIR spectrum of HTZ:Tris 1:2 cocrystal produced in scale-up is different from the spectrum of cocrystal produced in screening with the same solvent (Figure 61). Therefore, products from scale up is not the same than product from screening. The use of different cocrystallization methods is the probable explanation, which may had cause different polymorphs formation. Despite of this differences, a closer MIR analysis suggest that the same groups are involved in cocrystal formation than the ones proposed in screening (sulfonamide group of HTZ and hydroxyl group of Tris). Several differences are identified in regions corresponding to stretching vibration of NH groups of HTZ, at 3325 and 3225 cm^{-1} , and OH bending vibrations of Tris, at 1445 and 1375 cm^{-1} . Bands around 1150 cm^{-1} are completely different and this region corresponds to stretching vibrations of C-O groups of Tris and of SO_2 groups of HTZ. There are also differences on regions of symmetric stretching of SO_2 groups of HTZ, at 1150 and 1080 cm^{-1} .

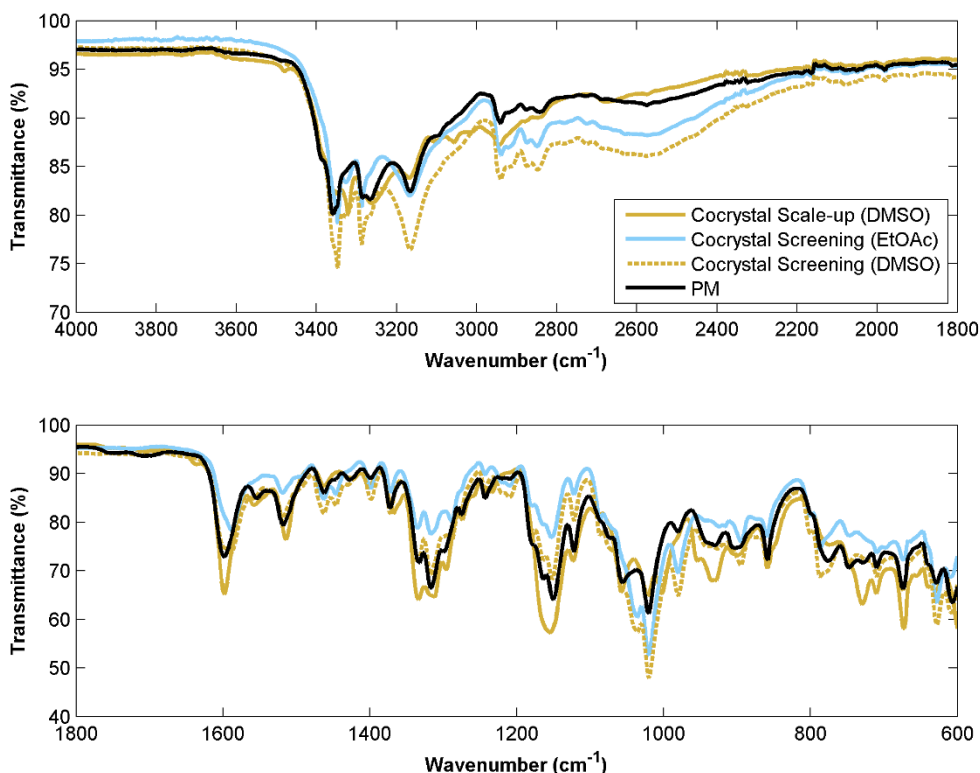


Figure 61: MIR spectra of the HTZ:Tris 1:2 cocrystal produced in scale up phase (dark yellow), of cocrystal produced in screening phase with DMSO (dark yellow dashed) and with EtOAc (blue) and the PM (black).

Thermal behavior of HTZ:Tris cocrystal is different from the one of PM, presenting a endothermic event at 112.70 °C, a different temperature from the endothermic event of the PM (134.69 °C), proving that compounds have a different nature (Figure 62). Cocrystal thermogram is also different from the thermograms of the pure API and Tris. API thermogram presents a fusion peak at 268.45 °C and Tris thermogram shows two endothermic events: at 132.89 °C, corresponding to Tris solid-solid phase transition point; at 169.68 °C, representing Tris melting point (Table 11).

PXRD analysis provided a HTZ:Tris 1:2 cocrystal's diffractogram different from the one of the respective PM, presenting a crystalline pattern with several new peaks. That indicates new crystalline structure formation through cocrystallization (see Figure 63).

All the techniques were consistent with the HTZ:Tris 1:2 cocrystal formation. Vibrational spectroscopy techniques gave information about groups involved in cocrystal formation earlier in screening phase, which was confirmed by spectra of MIR and NIR of scale increase product. DSC technique allowed to demonstrate the formation of a new entity different from the PM and pure components and also to determinate HTZ:Tris 1:2 cocrystal purity. PRXD technique proved a new crystalline structure formation, based in diffractogram comparison.

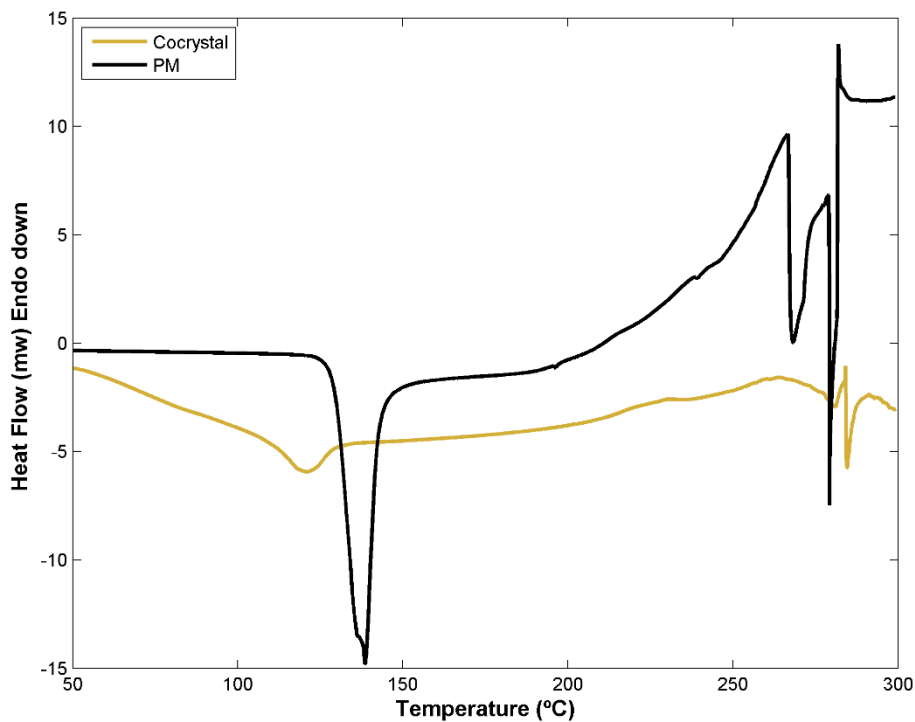


Figure 62: Thermogram of the HTZ:Tris 1:2 cocystal (dark yellow) and of the respective PM (black).

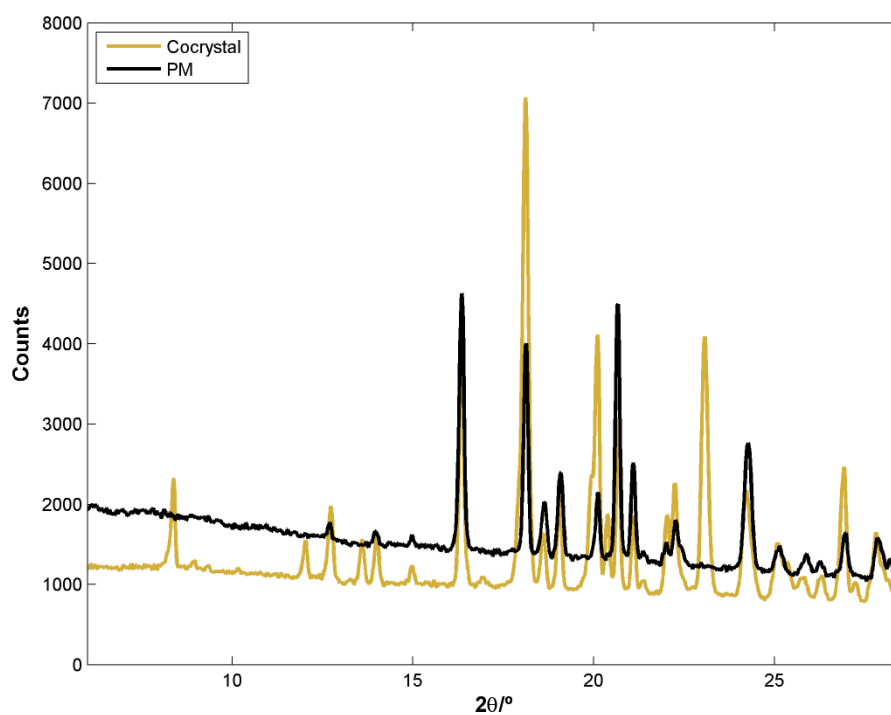


Figure 63: Diffractogram of the HTZ:Tris 1:2 cocystal (dark yellow) and of the respective PM (black).

4.3. Solubility assays

Confirmed cocrystals, including the systems with citric acid in which doubts remain regarding cocrystal formation, were subjected to solubility assays. Additionally, the systems with L(+)-arginine were also studied to verify if Arg have any effect on HTZ solubility. The solubility assays were performed in phosphate buffer pH 7.4 and at 37°C, conditions used to mimic physiologic pH and temperature. The calibration curve used to obtain concentration values of cocrystal in solution is represented in Figure 64.

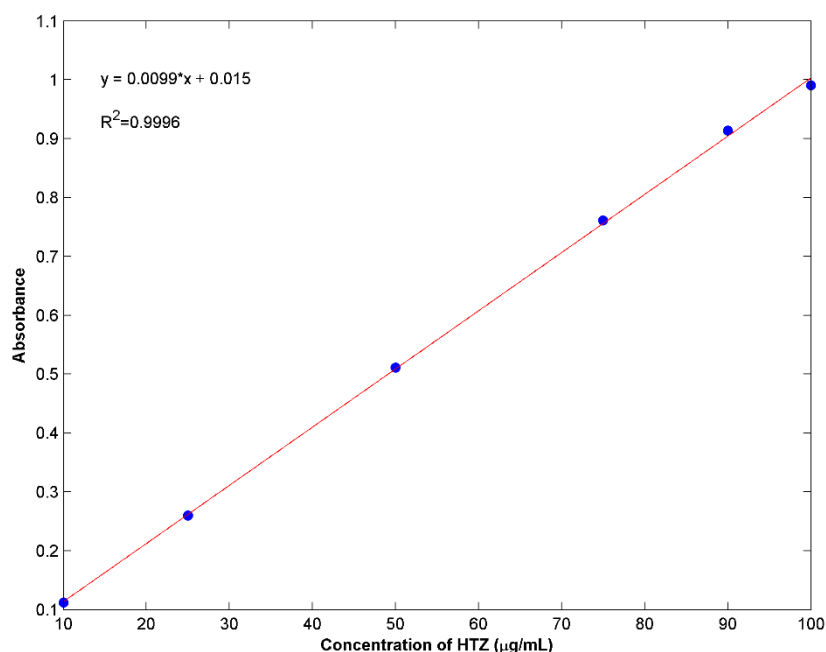


Figure 64: Calibration curve made with six solutions of known HTZ concentration, at the wavelength of 320 nm.

Since half-life of HTZ in human body is 5.6 and 14.8 hours⁽¹³⁸⁾, the experiment was made during 24 hours, as the ideal time to obtain information about cocrystal's stability and solubility. In all the tested systems (except for system with Tris) and in pure HTZ, maximum apparent solubility of the cocrystal was measure at 24 hours of dissolution experiments. From 12 to 24 hours of dissolution, the increase of apparent solubility values was slight, thus, the maximum value at 24 hours was considered close to saturation solubility.

Apparent solubility of HTZ was $1102.34 \mu\text{g}\cdot\text{mL}^{-1}$, reaching this maximum value after 24 hours of dissolution (Figure 65 and Table 12). Theoretical solubility of HTZ in water at 25°C is $722 \text{ mg}\cdot\text{L}^{-1}$.⁽¹³⁷⁾ The difference between experimental value and theoretical value is justified with the different experimental conditions, namely different pH and different temperature. These two factors can highly influence solubility value.^(95, 99)

For each cocrystallization product, thirteen aliquots were taken during the experiment and a plot of the HTZ concentration value at each time was constructed to comparison of the solubility profile of the cocrystals and the HTZ (Figure 65 and Table 12).

All the cocrystallization products present a higher apparent solubility when compared to HTZ and stability over 24 hours in solution, except for the system with citric acid.

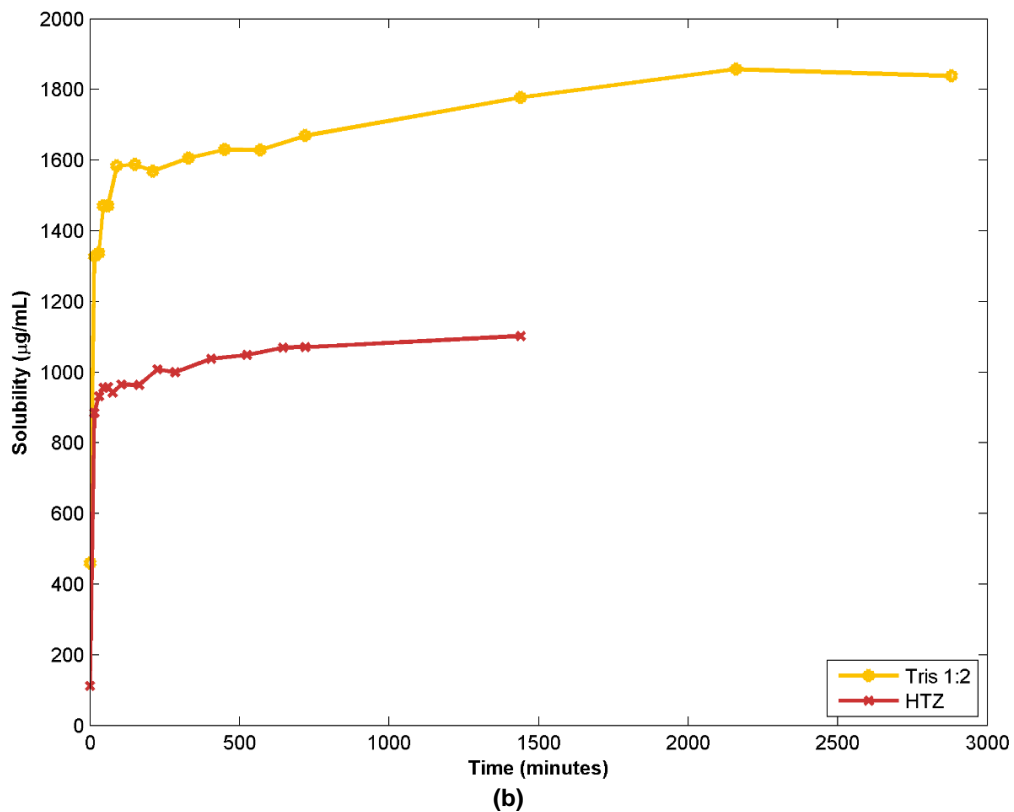
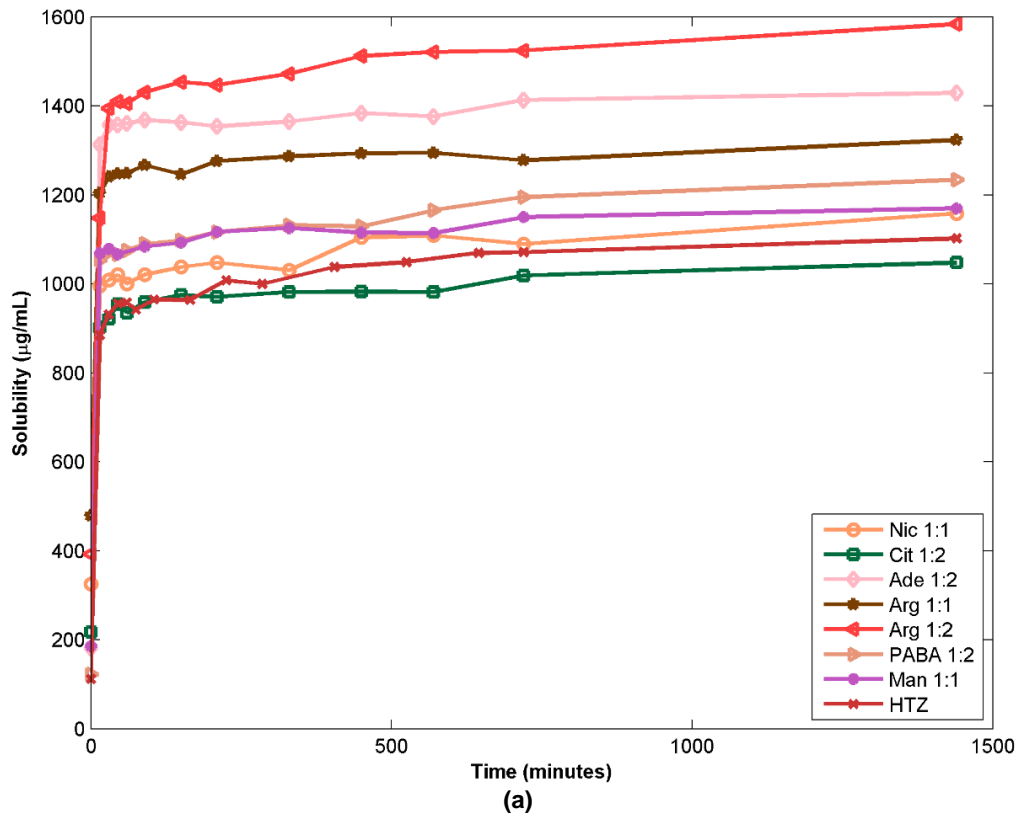


Figure 65 : (a) Solubility profile of all tested products during 24 hours. (b) Solubility profile of HTZ:Tris cocrystal during 48 hours and pure HTZ during 24 hours.

HTZ:Cit system form was not confirmed by characterization techniques, remaining the doubt about a cocrystal formation. The product presents a slightly lower solubility when compared with HTZ, mainly after the 3 hours of dissolution (Figure 65 (a) and Table 12). This may indicate that a cocrystal was not indeed formed, once solubility was not improved. However, a similar solubility behavior is expected when a cocrystal is not stable in solution.

HTZ:Arg system formed a crystalline-amorphous hydrated mixture, which present an improved solubility (Figure 65 (a) and Table 12). In fact, HTZ:Arg 1:2 system increased solubility in 1.4 fold, when compared with pure HTZ, having a maximum apparent solubility of 1583.88 $\mu\text{g}\cdot\text{mL}^{-1}$, after 24 hours of solubility test. Also, HTZ:Arg 1:1 system increased solubility in 1.2 fold, having an maximum apparent solubility of 1323.28 $\mu\text{g}\cdot\text{mL}^{-1}$, also after 24 hours of experiment.

Arginine has been reported as a solubility enhancer.⁽¹⁵³⁻¹⁵⁵⁾ Arginine, when used as cosolute, it is capable to enhance the solute's solubility, becoming the solution environment more favorable to the accommodation of the solute in the solvent (negative values of Gibbs free energy of transfer). Also, this solubility enhancement is promoted by solute-solvent and solute-cosolute interactions.⁽¹⁵⁴⁾ This amino acid can enhance both solubility and stability of an API by stablishing hydrogen bonds with API molecule and forcing a significant desolvation.⁽¹⁵⁵⁾ Guanidinium group of arginine is referred as an important group in solubility enhancement.⁽¹⁵³⁾ This solubility influence is usually achieve with Arg solutions with high concentration. In this case, it is achieved even with low quantities of Arg, as in the ratio of 1:1. A deeper investigation about Arg role in solubility enhancement is necessary. Also, it is essential to understand if Arg amorphization influence solubility, as well as hydration of the product.

HTZ:Nic and HTZ:PABA cocrystals were already reported, as well as their solubility. However, these experimental conditions were never tested. Maximum apparent solubility of HTZ:Nic cocrystal was 1158.46 $\mu\text{g}\cdot\text{mL}^{-1}$, maximum value measured at 24 hours of dissolution. Comparing with pure HTZ, cocrystal increased solubility in 1.1 fold (Figure 65 (a) and Table 12). During the 24 hours of experiment, cocrystal is stable in solution. Reported solubility value for the same cocrystal is 1362.6 $\mu\text{g}\cdot\text{mL}^{-1}$, achieve after 1 hour of experiments, using water as solvent at 37°C. This represents a 1.5 fold increase of solubility, when compared to pure HTZ. Also, in this study, HTZ:Nic cocrystal starts to dissociate after 1 hour in dissolution.⁽³⁾ In this case, HTZ:Nic cocrystal does not dissociate in solution until at least 24 hours, remaining stable. Discrepancy in values can arise from the different pH used in solubility assays, which can influence both pure HTZ and cocrystal's solubility.

HTZ:PABA cocrystal presents an apparent solubility of 1308.11 $\mu\text{g}\cdot\text{mL}^{-1}$, measured at 24 hours of dissolution, when cocrystal reach the maximum solubility. This represents an increase of 1.2 fold when comparing to solubility of pure HTZ (Figure 65 and Table 12).

HTZ:PABA cocrystal is also stable in solution during the 24 hours. One reported value of apparent solubility for HTZ:PABA cocrystal is $5395.7 \mu\text{g}\cdot\text{mL}^{-1}$, at 24 hours of dissolution experiment using water with neutral pH at 37°C . This represents an increase of more than six folds, comparing to pure HTZ. Also, the experiment shows that the cocrystals remains stable during 24h and reach the saturation solubility at 1h.⁽³⁾ This value is superior than the one obtained in this work. Since experimental temperature is the same, solubility differences may arise from differences in pH.

HTZ:Man cocrystal is not referred in literature. Maximum apparent solubility of this cocrystal is $1169.52 \mu\text{g}\cdot\text{mL}^{-1}$, after 24 hours of dissolution. This represents an increase of 1.1 fold when compared to pure HTZ solubility (Figure 65 (a) and Table 12). Cocrystal solubility profile is characterized by a plateau achieved after 3 hours of experiments.

Solubility of HTZ:Ade and HTZ:Tris cocrystal was also never reported. HTZ:Ade cocrystal have an apparent solubility of $1429.30 \mu\text{g}\cdot\text{mL}^{-1}$, measured at 24 hours of experiment, and a solubility increase of 1.3 fold comparing with pure HTZ's solubility (Figure 65 (a) and Table 12).

HTZ:Tris cocrystals present a solubility profile distinct of the others. This cocrystal present the highest solubility values in every point and from 12h to 24h solubility values increased significantly. Therefore, solubility experiment was extended to 48 hours and two more aliquots were taken at 36 and 48 hours (Figure 65 (b) and Table 12). Maximum apparent solubility was $1857.22 \mu\text{g}\cdot\text{mL}^{-1}$ and it was obtained after 36 hours of experiment, when cocrystals achieve its saturation solubility. Solubility was increased in 1.7 fold, when compared to pure HTZ's solubility. This cocrystal have the highest solubility and it is stable in solution during 36 hours, when the cocrystal starts to dissociate.

Table 12: Maximum apparent solubility values of each tested system, time of the measure and solubility increase fold when compared to HTZ solubility value.

System	Product form	Apparent solubility ($\mu\text{g.mL}^{-1}$)	Time (hours)	Solubility increase fold
HTZ	Crystalline	1102.34	24	-
HTZ:Ade 1:2	Cocrystal	1429.30	24	1.3
HTZ:Arg 1:1	Crystalline-amorphous hydrated mixture	1323.28	24	1.2
HTZ:Arg 1:2	Crystalline-amorphous hydrated mixture	1583.88	24	1.4
HTZ:Cit 1:2	Cocrystal hydrate/hydrate	1047.72	24	0.95
HTZ:Man 1:1	Cocrystal	1169.52	24	1.1
HTZ:Nic 1:1	Cocrystal	1158.46	24	1.1
HTZ:PABA 1:2	Cocrystal	1308.11	24	1.2
HTZ:Tris 1:2	Cocrystal	1857.22	36	1.7

5. CONCLUSION AND FUTURE PERSPECTIVES

The main objective of this dissertation was to study and develop a high-throughput screening procedure to find new cocrystals, applying vibrational spectroscopic techniques to evaluate cocrystal formation, purity and preferred ratio and solvent.

Cocrystal screening was performed with 96-well plates, testing several coformers and solvents at the same time applying different vibrational spectroscopy techniques: MIRS, NIRS, RS and RMS. The use of 96-well plates in this type of procedures, for example polymorphs screening, is not new, but its combination with several vibrational spectroscopic techniques was important, providing information about the most appropriate technique applicable to high-throughput screening methods for cocrystals.

The experiments allowed test a total of eleven coformers, nine solvents and two different API:coformer ratios (1:1 and 1:2). From all tested coformers, citric acid, D(-)-mannitol, DL-malic acid, nicotinamide, *p*-aminobenzoic acid and tromethamine were selected as promising coformers to cocrystal formation. Also, in the case of the system with L(+)-arginine, spectroscopic techniques showed evidences of a reaction, but more conclusions about cocrystal formation and cocrystal ratio were not possible. In the case of D(-)-mannitol, two different polymorphs were detected, demonstrating the capability of this method to identify different cocrystal polymorphs.

All vibrational spectroscopic techniques used in the first part of screening experiments (MIRS, NIRS and RS) prove to be able to detect cocrystal formation. With PCA, it was possible to infer about the purity of the different cocrystallization products, selecting the solvent with the best performance. From the three vibrational spectroscopy techniques, MIRS provided the most relevant information about cocrystal formation and about chemical groups involved in cocrystallization. NIRS also contributed with important information about cocrystal formation, but not so significant information about groups involved. NIRS does not provide available information about the vibration of the S=O groups of HTZ and, in this particular case, that can be a disadvantage of the technique, since this group was involved in the cocrystal formation in all cases. Concerning Raman spectroscopy, and because the used spectrometer did not span the region between 4000 cm^{-1} and 1850 cm^{-1} (a region with information on the amine and alcohol groups), it was considered to be less informative when compared with MIRS.

Regarding to the second part of screening, MIRS and RMS were compared relatively to the ability of detect cocrystal formation and products purity. One of the objectives of this work was to use *in-situ* Raman microspectroscopy to perform the analysis. However, problems with fluorescence eliminate, in some way, the advantage of using an *in-situ*

technique. The MIR analysis done at-line provided considerably more information about the cocrystal formation and groups involved on that process. The possibility of defining the correct ratio of the cocrystal using only MIR is also of importance since the spectroscopic technique is simple and fast and with a single spectrum it can be detected cocrystal formation and which was the ratio API:coformer. By using multivariate data analysis, e.g. HCA, the purity of the cocrystallization products can be easily accessed using MIR. This analysis also helps to understand how the solvent affect the cocrystallization.

In this type of experiments, commonly spectral comparison is performed between the product of each well and the respective physical mixture from the plate (WS). PM of one of the systems (nicotinamide) also reacted. Consequently, it is important to compare the products of reaction with a PM that was not subjected to the cocrystallization conditions.

Among the coformers tested in screening experiments, adenine, caffeine and tryptophan were the ones not forming a cocrystal with hydrochlorothiazide. In the most part of the cases, it was demonstrated that the ratio 1:1 is able to form the cocrystal but with a lower yield than the 1:2 ratio, except nicotinamide systems, which seems to prefer 1:1 ratio. Hydrochlorothiazide seems to have a preference to form 1:2 ratio cocrystals, possibly due to the presence of two sulfonamide groups capable of hydrogen bonding with the coformers. However, it is not possible to claim that the cocrystal ratio was truly 1:2 since in the screening procedure the compounds were not dissolved, and therefore the ratio may not be the one present in the well. To determine the real ratio of the cocrystal, new experiments should be done (e.g., high performance liquid chromatography, Single crystal X-ray diffraction).

Globally, screening experiments showed that, with the equipment used, vibrational spectroscopic techniques can be useful to analyze the outcome of a cocrystal screening procedure, allowing to confirm the cocrystal formation, purity and eventual presence of polymorphs. These methods allow this analysis in a very simple and rapid manner, extremely important for the cocrystal screening task.

To verify screening results and to analyze the effect of increasing the scale of the experiments on the cocrystallization outcome, all the systems were submitted to cocrystallization in a laboratory-scale. Scale increase production led to the production of five confirmed cocrystals, two of them (HTZ:Nic 1:1 and HTZ:PABA 1:2) are already reported in literature and the remain three (HTZ:Ade 1:2, HTZ:Man 1:1 and HTZ:Tris 1:2) are new forms.

System with adenine did not reacted in screening experiments, and when produced in the laboratory-scale, it gave origin to a cocrystal. Also, DL-malic acid was selected as a potential coformer to cocrystal formation in screening experiments, although, in laboratory-scale experiments, DL-malic acid did not react with HTZ. The change from screening

experiments to laboratory-scale products, generally, involves different cocrystallization methods. This case shows clearly that different cocrystallization methods led to different outcomes, since some cocrystallization methods are more or less appropriate for each system. This shows a drawback of screening experiments, which is important to overcome with the development of more accurate screening experiments.

Screening experiments suggested cocrystal formation with the cofomers Nic, PABA, Man and Tris, which was confirmed with the laboratory-scale productions. Also, the results in terms of groups involved are consistent.

Citric acid was considered a potential cofomer for cocrystal formation in screening experiments, with spectral evidences of a reaction between citric acid and HTZ. Laboratory-scale experiment lead to the formation of a different product from the one of the screening phase. Evidences suggest the formation of a hydrate. However, doubts about cocrystal formation were not clarified. More studies on this system are necessary, to understand if the product is a cocrystal hydrate or a citric acid hydrate in a mixture with HTZ.

Screening also showed that L(+)-arginine had reacted somehow with HTZ. When the system was produced in laboratory-scale experiments, a crystalline-amorphous hydrated mixture was formed, where L(+)-arginine is amorphous and hydrated and HTZ remained crystalline.

High-throughput screening experiments were successfully performed, applying vibrational spectroscopy techniques as an effective way to detect cocrystal formation, to give indications about the preferred ratio and the preferred solvent and to suggest groups involved in cocrystal formation. MIRS was the technique that provide a more complete information. The work also allowed to pinpoint some drawbacks of this type of experiment, showing that is essential compare results from the plate with a PM that was not subjected to cocrystallization conditions and that results interpretation is essential to understand what type of spectral differences are indicative of cocrystal formation or not. Also, it was showed that different cocrystallization methods can give origin to different products, one of the biggest problems of passing from screening experiments to cocrystal product in higher scale. It is important to correct these drawbacks and to develop more accurate methods, applicable to a wider range of systems.

Solubility assays show that all produced cocrystals improved API's solubility, demonstrating the capability of cocrystals to improve API's properties. More studies must be done, namely dissolution and stability studies, to conclude about the more advantageous cocrystal in terms of improvement of physical and chemical properties.

Cocrystal with the cofomer tromethamine presents the higher apparent solubility, followed by cocrystals with adenine, *p*-aminobenzoic acid, D(-)-mannitol and nicotinamide.

Despite of not having formed a cocrystal, the crystalline-amorphous hydrated mixture with L(+)-arginine presents one of the highest apparent solubility values. This system must be study to a better understanding about the solid form nature and its ability to improve API's properties, namely on how L(+)-arginine influence solubility of the API, which type of interactions are on the basis of this influence and if amorphization also have impact on API's properties.

Concluding, a deeper characterization of the new cocrystals is essential, since these solid forms are advantageous in terms of improvement of API's properties. Techniques as single crystal X-ray diffraction must be done to provide information about molecular structure and interactions. Stability and dissolution assays are crucial to a greater comprehension on improvement of properties. HTZ is a BSC class IV drug, thus it has low solubility and permeability. The cocrystals produced in this work were design to improve solubility. Formulation studies should be performed to study and improve permeability of the new forms.

6. REFERENCES

1. Gopi SP, Banik M, Desiraju GR. New Cocrystals of Hydrochlorothiazide: Optimizing Solubility and Membrane Diffusivity. *Crystal Growth & Design*. 2017;17(1):308-16.
2. Ranjan S, Devarapalli R, Kundu S, Vangala VR, Ghosh A, Reddy CM. Three new hydrochlorothiazide cocrystals: Structural analyses and solubility studies. *Journal of Molecular Structure*. 2017;1133:405-10.
3. Sanphui P, Rajput L. Tuning solubility and stability of hydrochlorothiazide cocrystals. *Acta Crystallographica Section B-Structural Science Crystal Engineering and Materials*. 2014;70:81-90.
4. McNamara DP, Childs SL, Giordano J, Iarriccio A, Cassidy J, Shet MS, et al. Use of a glutaric acid cocrystal to improve oral bioavailability of a low solubility API. *Pharmaceutical Research*. 2006;23(8):1888-97.
5. Trask AV, Motherwell WDS, Jones W. Physical stability enhancement of theophylline via cocrystallization. *International Journal of Pharmaceutics*. 2006;320(1-2):114-23.
6. Bevill MJ, Vlahova PI, Smit JP. Polymorphic Cocrystals of Nutraceutical Compound p-Coumaric Acid with Nicotinamide: Characterization, Relative Solid-State Stability, and Conversion to Alternate Stoichiometries. *Crystal Growth & Design*. 2014;14(3):1438-48.
7. Schultheiss N, Bethune S, Henck JO. Nutraceutical cocrystals: utilizing pterostilbene as a cocrystal former. *CrystEngComm*. 2010;12(8):2436-42.
8. Lee MJ, Wang IC, Kim MJ, Kim P, Song KH, Chun NH, et al. Controlling the polymorphism of carbamazepine-saccharin cocrystals formed during antisolvent cocrystallization using kinetic parameters. *Korean Journal of Chemical Engineering*. 2015;32(9):1910-7.
9. Lange L, Heisel S, Sadowski G. Predicting the Solubility of Pharmaceutical Cocrystals in Solvent/Anti-Solvent Mixtures. *Molecules*. 2016;21(5):593.
10. Holan J, Stepanek F, Billot P, Ridvan L. The construction, prediction and measurement of co-crystal ternary phase diagrams as a tool for solvent selection. *European Journal of Pharmaceutical Sciences*. 2014;63:124-31.
11. Childs SL, Rodriguez-Hornedo N, Reddy LS, Jayasankar A, Maheshwari C, McCausland L, et al. Screening strategies based on solubility and solution composition generate pharmaceutically acceptable cocrystals of carbamazepine. *CrystEngComm*. 2008;10(7):856-64.

12. Sarraguca MC, Ribeiro PR, Santos AO, Silva MC, Lopes JA. A PAT approach for the on-line monitoring of pharmaceutical co-crystals formation with near infrared spectroscopy. *International Journal of Pharmaceutics*. 2014;471(1-2):478-84.
13. Sarraguca MC, Ribeiro PRS, Dos Santos AO, Lopes JA. Batch Statistical Process Monitoring Approach to a Cocrystallization Process. *Journal of Pharmaceutical Sciences*. 2015;104(12):4099-108.
14. Sarraguca MC, Paisana M, Pinto J, Lopes JA. Real-time monitoring of cocrystallization processes by solvent evaporation: A near infrared study. *European Journal of Pharmaceutical Sciences*. 2016;90:76-84.
15. Moradiya H, Islam MT, Woollam GR, Slipper IJ, Halsey S, Snowden MJ, et al. Continuous Cocrystallization for Dissolution Rate Optimization of a Poorly Water-Soluble Drug. *Crystal Growth & Design*. 2014;14(1):189-98.
16. do Amaral LH, do Carmo FA, Amaro MI, de Sousa VP, da Silva LCRP, de Almeida GS, et al. Development and Characterization of Dapsone Cocrystal Prepared by Scalable Production Methods. *American Association of Pharmaceutical Scientists*. 2018;19(6):2687-99.
17. Sarkar A, Rohani S. Cocrystals of acyclovir with promising physicochemical properties. *Journal of Pharmaceutical Sciences*. 2015;104(1):98-105.
18. Wright JD. *Molecular crystals*. 2 ed. Cambridge ; New York: Cambridge University Press; 1995. 221 p.
19. Aitipamula S, Banerjee R, Bansal AK, Biradha K, Cheney ML, Choudhury AR, et al. Polymorphs, Salts, and Cocrystals: What's in a Name? *Crystal Growth & Design*. 2012;12(5):2147-52.
20. ANDAs: Pharmaceutical Solid Polymorphism. Food and Drug Administration; 2007.
21. Stahly GP. Diversity in single- and multiple-component crystals. The search for and prevalence of polymorphs and cocrystals. *Crystal Growth & Design*. 2007;7(6):1007-26.
22. Schultheiss N, Newman A. Pharmaceutical Cocrystals and Their Physicochemical Properties. *Crystal Growth & Design*. 2009;9(6):2950-67.
23. Reflection paper on the use of cocrystals of active substances in medicinal products. European Medicines Agency, CHMP; 2015.
24. Guidance for industry: Regulatory classification of pharmaceutical co-crystals. Food and Drug Administration; 2013.
25. Aitipamula S, Chow PS, Tan RBH. Polymorphs and Solvates of a Cocrystal Involving an Analgesic Drug, Ethenzamide, and 3,5-Dinitrobenzoic Acid. *Crystal Growth & Design*. 2010;10(5):2229-38.

26. Stahly GP. A Survey of Cocrystals Reported Prior to 2000. *Crystal Growth & Design*. 2009;9(10):4212-29.
27. Haneef J, Chadha R. Drug-Drug Multicomponent Solid Forms: Cocrystal, Coamorphous and Eutectic of Three Poorly Soluble Antihypertensive Drugs Using Mechanochemical Approach. *American Association of Pharmaceutical Scientists*. 2017;18(6):2279-90.
28. Guidance for industry: Regulatory Classification of Pharmaceutical Co-Crystals. Food and Drug Administration; 2016.
29. Aakeroy CB, Fasulo ME, Desper J. Cocrystal or salt: Does it really matter? *Molecular Pharmaceutics*. 2007;4(3):317-22.
30. Desiraju GR. Supramolecular Synthons in Crystal Engineering - a New Organic-Synthesis. *Angewandte Chemie International Edition*. 1995;34(21):2311-27.
31. Hemamalini M, Loh WS, Quah CK, Fun HK. Investigation of supramolecular synthons and structural characterisation of aminopyridine-carboxylic acid derivatives. *Chemistry Central Journal*. 2014;8.
32. Qiao N, Li M, Schlindwein W, Malek N, Davies A, Trappitt G. Pharmaceutical cocrystals: an overview. *International Journal of Pharmaceutics*. 2011;419(1-2):1-11.
33. Karki S, Friscic T, Jones W. Control and interconversion of cocrystal stoichiometry in grinding: stepwise mechanism for the formation of a hydrogen-bonded cocrystal. *CrystEngComm*. 2009;11(3):470-81.
34. He GW, Jacob C, Guo LF, Chow PS, Tan RBH. Screening for cocrystallization tendency: The role of intermolecular interactions. *Journal of Physical Chemistry B*. 2008;112(32):9890-5.
35. Etter MC, Reutzel SM. Hydrogen-Bond Directed Cocrystallization and Molecular Recognition Properties of Acyclic Imides. *Journal of the American Chemical Society*. 1991;113(7):2586-98.
36. Regulatory Classification of Pharmaceutical Co-Crystals Guidance for Industry. Food and Drug Administration; 2018.
37. Assessment report - Entresto. European Medicines Agency, CHMP; 2015. Report No.: EMEA/H/C/004062/0000.
38. Assessment report - Odomzo. European Medicines Agency, CHMP; 2015. Contract No.: EMEA/H/C/002839/0000.
39. Assessment report - Steglatro European Medicines Agency, CHMP; 2018. Contract No.: EMEA/H/C/004315/0000.
40. Assessment report - Segluromet European Medicines Agency, CHMP; 2018. Contract No.: EMEA/H/C/004314/0000.

41. Assessment report - Steglujan. European Medicines Agency, CHMP; 2018. Contract No.: EMEA/H/C/004313/0000.
42. Moradiya HG, Islam MT, Halsey S, Maniruzzaman M, Chowdhry BZ, Snowden MJ, et al. Continuous cocrystallisation of carbamazepine and trans-cinnamic acid via melt extrusion processing. *CrystEngComm*. 2014;16(17):3573-83.
43. Moradiya HG, Islam MT, Scoutaris N, Halsey SA, Chowdhry BZ, Douroumis D. Continuous Manufacturing of High Quality Pharmaceutical Cocrystals Integrated with Process Analytical Tools for In-Line Process Control. *Crystal Growth & Design*. 2016;16(6):3425-34.
44. Duarte I, Andrade R, Pinto JF, Temtem M. Green production of cocrystals using a new solvent-free approach by spray congealing. *International Journal of Pharmaceutics*. 2016;506(1-2):68-78.
45. Hasa D, Carlino E, Jones W. Polymer-Assisted Grinding, a Versatile Method for Polymorph Control of Cocrystallization. *Crystal Growth & Design*. 2016;16(3):1772-9.
46. Qiu S, Li MZ. Effects of coformers on phase transformation and release profiles of carbamazepine cocrystals in hydroxypropyl methylcellulose based matrix tablets. *International Journal of Pharmaceutics*. 2015;479:118-28.
47. IUPAC. Compendium of Chemical Terminology - Gold Book. 2.3.3 ed 2014.
48. Braga D, Giaffreda SL, Grepioni F, Pettersen A, Maini L, Curzi M, et al. Mechanochemical preparation of molecular and supramolecular organometallic materials and coordination networks. *Dalton Transactions*. 2006(10):1249-63.
49. Weyna DR, Shattock T, Vishweshwar P, Zaworotko MJ. Synthesis and Structural Characterization of Cocrystals and Pharmaceutical Cocrystals: Mechanochemistry vs Slow Evaporation from Solution. *Crystal Growth & Design*. 2009;9(2):1106-23.
50. Rodriguez-Hornedo N, Nehm SJ, Seefeldt KF, Pagan-Torres Y, Falkiewicz CJ. Reaction crystallization of pharmaceutical molecular complexes. *Molecular Pharmaceutics*. 2006;3(3):362-7.
51. He GW, Chow PS, Tan RBH. Investigating the Intermolecular Interactions in Concentration-Dependent Solution Cocrystallization of Caffeine and p-Hydroxybenzoic Acid. *Crystal Growth & Design*. 2010;10(8):3763-9.
52. Sheikh AY, Rahim SA, Hammond RB, Roberts KJ. Scalable solution cocrystallization: case of carbamazepine-nicotinamide I. *CrystEngComm*. 2009;11(3):501-9.
53. Wang IC, Lee MJ, Sim SJ, Kim WS, Chun NH, Choi GJ. Anti-solvent cocrystallization of carbamazepine and saccharin. *International Journal of Pharmaceutics*. 2013;450(1-2):311-22.

54. Lee MJ, Chun NH, Kim MJ, Kim P, Song KH, Choi GJ. In Situ Monitoring of Antisolvent Cocrystallization by Combining Near-Infrared and Raman Spectroscopies. *Crystal Growth & Design*. 2015;15(9):4385-93.
55. Padrela L, Rodrigues MA, Tiago J, Velaga SP, Matos HA, de Azevedo EG. Tuning physicochemical properties of theophylline by cocrystallization using the supercritical fluid enhanced atomization technique. *Journal of Supercritical Fluids*. 2014;86:129-36.
56. Padrela L, Rodrigues MA, Velaga SP, Fernandes AC, Matos HA, de Azevedo EG. Screening for pharmaceutical cocrystals using the supercritical fluid enhanced atomization process. *Journal of Supercritical Fluids*. 2010;53(1-3):156-64.
57. Padrela L, Rodrigues MA, Velaga SR, Matos HA, de Azevedo EG. Formation of indomethacin-saccharin cocrystals using supercritical fluid technology. *European Journal of Pharmaceutical Sciences*. 2009;38(1):9-17.
58. Soares FLF, Carneiro RL. In-line monitoring of cocrystallization process and quantification of carbamazepine-nicotinamide cocrystal using Raman spectroscopy and chemometric tools. *Spectrochimica Acta Part A: Molecular and Biomolecular Spectroscopy*. 2017;180:1-8.
59. Zhang GGZ, Henry RF, Borchardt TB, Lou XC. Efficient co-crystal screening using solution-mediated phase transformation. *Journal of Pharmaceutical Sciences*. 2007;96(5):990-5.
60. Aher S, Dhumal R, Mahadik K, Paradkar A, York P. Ultrasound assisted cocrystallization from solution (USSC) containing a non-congruently soluble cocrystal component pair: Caffeine/maleic acid. *European Journal of Pharmaceutical Sciences*. 2010;41(5):597-602.
61. Friscic T, Childs SL, Rizvi SAA, Jones W. The role of solvent in mechanochemical and sonochemical cocrystal formation: a solubility-based approach for predicting cocrystallisation outcome. *CrystEngComm*. 2009;11(3):418-26.
62. Eddleston MD, Patel B, Day GM, Jones W. Cocrystallization by Freeze-Drying: Preparation of Novel Multicomponent Crystal Forms. *Crystal Growth & Design*. 2013;13(10):4599-606.
63. Grossjohann C, Serrano DR, Paluch KJ, O'Connell P, Vella-Zarb L, Manesiotis P, et al. Polymorphism in Sulfadimidine/4-Aminosalicylic Acid Cocrystals: Solid-State Characterization and Physicochemical Properties. *Journal of Pharmaceutical Sciences*. 2015;104(4):1385-98.
64. Patil SP, Modi SR, Bansal AK. Generation of 1:1 Carbamazepine:Nicotinamide cocrystals by spray drying. *European Journal of Pharmaceutical Sciences*. 2014;62:251-7.

65. Sarcevic I, Orola L, Nartowski KP, Khimyak YZ, Round AN, Fabian L. Mechanistic and Kinetic Insight into Spontaneous Cocrystallization of Isoniazid and Benzoic Acid. *Molecular Pharmaceutics*. 2015;12(8):2981-92.
66. Fernandez-Ronco MP, Kluge J, Mazzotti M. High Pressure Homogenization as a Novel Approach for the Preparation of Co-Crystals. *Crystal Growth & Design*. 2013;13(5):2013-24.
67. Rehder S, Christensen NPA, Rantanen J, Rades T, Leopold CS. High-shear granulation as a manufacturing method for cocrystal granules. *European Journal of Pharmaceutics and Biopharmaceutics*. 2013;85(3):1019-30.
68. Rehder S, Klukkert M, Lobmann KA, Strachan CJ, Sakmann A, Gordon K, et al. Investigation of the Formation Process of Two Piracetam Cocrystals during Grinding. *Pharmaceutics*. 2011;3(4):706-22.
69. Chieng N, Hubert M, Saville D, Rades T, Aaltonen J. Formation Kinetics and Stability of Carbamazepine-Nicotinamide Cocrystals Prepared by Mechanical Activation. *Crystal Growth & Design*. 2009;9(5):2377-86.
70. Chadwick K, Davey R, Cross W. How does grinding produce co-crystals? Insights from the case of benzophenone and diphenylamine. *CrystEngComm*. 2007;9(9):732-4.
71. Jayasankar A, Somwangthanaroj A, Shao ZJ, Rodriguez-Hornedo N. Cocrystal formation during cogrinding and storage is mediated by amorphous phase. *Pharmaceutical Research*. 2006;23(10):2381-92.
72. Nguyen KL, Friscic T, Day GM, Gladden LF, Jones W. Terahertz time-domain spectroscopy and the quantitative monitoring of mechanochemical cocrystal formation. *Nature Materials*. 2007;6(3):206-9.
73. Shan N, Toda F, Jones W. Mechanochemistry and co-crystal formation: effect of solvent on reaction kinetics. *Chemical Communications*. 2002(20):2372-3.
74. Friscic T, Trask AV, Motherwell WDS, Jones W. Guest-directed assembly of caffeine and succinic acid into topologically different heteromolecular host networks upon grinding. *Crystal Growth & Design*. 2008;8(5):1605-9.
75. Friscic T, Trask AV, Jones W, Motherwell WDS. Screening for inclusion compounds and systematic construction of three-component solids by liquid-assisted grinding. *Angewandte Chemie International Edition*. 2006;45(45):7546-50.
76. Hasa D, Rauber GS, Voinovich D, Jones W. Cocrystal Formation through Mechanochemistry: from Neat and Liquid-Assisted Grinding to Polymer-Assisted Grinding. *Angewandte Chemie International Edition*. 2015;54(25):7371-5.

77. Dhumal RS, Kelly AL, York P, Coates PD, Paradkar A. Cocrystalization and Simultaneous Agglomeration Using Hot Melt Extrusion. *Pharmaceutical Research*. 2010;27(12):2725-33.
78. Boksa K, Otte A, Pinal R. Matrix-Assisted Cocrystallization (MAC) Simultaneous Production and Formulation of Pharmaceutical Cocrystals by Hot-Melt Extrusion. *Journal of Pharmaceutical Sciences*. 2014;103(9):2904-10.
79. Berry DJ, Seaton CC, Clegg W, Harrington RW, Coles SJ, Horton PN, et al. Applying hot-stage microscopy to co-crystal screening: A study of nicotinamide with seven active pharmaceutical ingredients. *Crystal Growth & Design*. 2008;8(5):1697-712.
80. Yan Y, Chen JM, Lu TB. Thermodynamics and preliminary pharmaceutical characterization of a melatonin-pimelic acid cocrystal prepared by a melt crystallization method. *CrystEngComm*. 2015;17(3):612-20.
81. Fucke K, Myz SA, Shakhtshneider TP, Boldyreva EV, Griesser UJ. How good are the crystallisation methods for co-crystals? A comparative study of piroxicam. *New Journal of Chemistry*. 2012;36(10):1969-77.
82. Pagire S, Korde S, Ambardekar R, Deshmukh S, Dash RC, Dhumal R, et al. Microwave assisted synthesis of caffeine/maleic acid co-crystals: the role of the dielectric and physicochemical properties of the solvent. *CrystEngComm*. 2013;15(18):3705-10.
83. Apshingekar PP, Aher S, Kelly AL, Brown EC, Paradkar A. Synthesis of Caffeine/Maleic Acid Co-crystal by Ultrasound-assisted Slurry Co-crystallization. *Journal of Pharmaceutical Sciences*. 2017;106(1):66-70.
84. Duggirala NK, Perry ML, Almarsson O, Zaworotko MJ. Pharmaceutical cocrystals: along the path to improved medicines. *Chemical Communications*. 2016;52(4):640-55.
85. Aljohani M, Pallipurath AR, McArdle P, Erxleben A. A Comprehensive Cocrystal Screening Study of Chlorothiazide. *Crystal Growth & Design*. 2017;17(10):5223-32.
86. Etter MC. Encoding and Decoding Hydrogen-Bond Patterns of Organic-Compounds. *Accounts of Chemical Research*. 1990;23(4):120-6.
87. Wang JR, Ye CJ, Mei XF. Structural and physicochemical aspects of hydrochlorothiazide co-crystals. *CrystEngComm*. 2014;16(30):6996-7003.
88. Mohammad MA, Alhalaweh A, Velaga SP. Hansen solubility parameter as a tool to predict cocrystal formation. *International Journal of Pharmaceutics*. 2011;407(1-2):63-71.
89. Ma K, Zhang Y, Kan H, Cheng L, Luo L, Su Q, et al. Thermodynamic and kinetic investigation on the crucial factors affecting adefovir dipivoxil-saccharin cocrystallization. *Pharmaceutical Research*. 2014;31(7):1766-78.

90. Gibson M. *Pharmaceutical Preformulation and Formulation: A Practical Guide from Candidate Drug Selection to Commercial Dosage Form*. Second ed: CRC Press; 2009.
91. Childs SL, Mouglin P, Stahly BC, inventors; Center For Innovative Food Technology (United States), assignee. Screening for solid forms by ultrasound crystallization and cocrystallization using ultrasound. 2005.
92. Leung DH, Lohani S, Ball RG, Canfield N, Wang YL, Rhodes T, et al. Two Novel Pharmaceutical Cocrystals of a Development Compound - Screening, Scale-up, and Characterization. *Crystal Growth & Design*. 2012;12(3):1254-62.
93. Yamashita H, Hirakura Y, Yuda M, Terada K. Cofomer Screening Using Thermal Analysis Based on Binary Phase Diagrams. *Pharmaceutical Research*. 2014;31(8):1946-57.
94. Yamashita H, Hirakura Y, Yuda M, Teramura T, Terada K. Detection of Cocrystal Formation Based on Binary Phase Diagrams Using Thermal Analysis. *Pharmaceutical Research*. 2013;30(1):70-80.
95. Sanphui P, Devi VK, Clara D, Malviya N, Ganguly S, Desiraju GR. Cocrystals of Hydrochlorothiazide: Solubility and Diffusion/Permeability Enhancements through Drug-Cofomer Interactions. *Molecular Pharmaceutics*. 2015;12(5):1615-22.
96. Guidance for Industry - Waiver of In Vivo Bioavailability and Bioequivalence Studies for Immediate-Release Solid Oral Dosage Forms Based on a Biopharmaceutics Classification System. Food and Drug Administration; 2015.
97. Guideline on the investigation of bioequivalence. European Medicines Agency CHMP; 2010.
98. IUPAC. *Compendium of Chemical Terminology (the "Gold Book")*. 2 ed. Oxford: Blackwell Scientific Publications; 1997.
99. Alhalaweh A, Roy L, Rodriguez-Hornedo N, Velaga SP. pH-Dependent Solubility of Indomethacin-Saccharin and Carbamazepine-Saccharin Cocrystals in Aqueous Media. *Molecular Pharmaceutics*. 2012;9(9):2605-12.
100. Drozd KV, Manin AN, Churakov AV, Perlovich GL. Drug-drug cocrystals of antituberculous 4-aminosalicylic acid: Screening, crystal structures, thermochemical and solubility studies. *European Journal of Pharmaceutical Sciences*. 2017;99:228-39.
101. Samie A, Desiraju GR, Banik M. Salts and Cocrystals of the Antidiabetic Drugs Gliclazide, Tolbutamide, and Glipizide: Solubility Enhancements through Drug Cofomer Interactions. *Crystal Growth & Design*. 2017;17(5):2406-17.

102. Arenas-Garcia JI, Herrera-Ruiz D, Morales-Rojas H, Hopfl H. Interrelation of the dissolution behavior and solid-state features of acetazolamide cocrystals. *European Journal of Pharmaceutical Sciences*. 2017;96:299-308.
103. Higuchi T, Connors KA. Phase-solubility techniques. . *Advances in Analytical Chemistry and Instrumentation*. 1965;4:117–212.
104. Childs SL, Kandi P, Lingireddy SR. Formulation of a Danazol Cocrystal with Controlled Supersaturation Plays an Essential Role in Improving Bioavailability. *Molecular Pharmaceutics*. 2013;10(8):3112-27.
105. Leitao MLP, Canotilho J, Cruz MSC, Pereira JC, Sousa AT, Redinha JS. Study of polymorphism from DSC melting curves - Polymorphs of terfenadine. *Journal of Thermal Analysis and Calorimetry*. 2002;68(2):397-412.
106. Stevens JS, Byard SJ, Schroeder SLM. Salt or Co-Crystal? Determination of Protonation State by X-Ray Photoelectron Spectroscopy (XPS). *Journal of Pharmaceutical Sciences*. 2010;99(11):4453-7.
107. Settle FA. *Handbook of Instrumental Techniques for Analytical Chemistry*. Universidade de Michigan: Prentice Hall PTR; 1997. 995 p.
108. Larkin P. *Infrared and raman spectroscopy : principles and spectral interpretation*. 1 ed: Elsevier; 2011. 230 p.
109. Bakeev KA. *Process analytical technology - spectroscopic tools and implementation strategies for the chemical and pharmaceutical industries*. Second ed: Wiley; 2010.
110. Blanco M, Villarroya I. NIR spectroscopy: a rapid-response analytical tool. *Trac-Trends in Analytical Chemistry*. 2002;21(4):240-50.
111. Wartewig S. *IR and Raman Spectroscopy: Fundamental Processing*. Weinheim: Wiley-VCH; 2003. 191 p.
112. McGoverin CM, Rades T, Gordon KC. Recent Pharmaceutical Applications of Raman and Terahertz Spectroscopies. *Journal of Pharmaceutical Sciences*. 2008;97(11):4598-621.
113. Eliasson C, Macleod NA, Jayes LC, Clarke FC, Hammond SV, Smith MR, et al. Non-invasive quantitative assessment of the content of pharmaceutical capsules using transmission Raman spectroscopy. *Journal of Pharmaceutical and Biomedical Analysis*. 2008;47(2):221-9.
114. Turrell G, Corset J. *Raman Microscopy - Developments and Applications*: Academic Press; 1996. 463 p.
115. Ali HRH, Alhalaweh A, Mendes NFC, Ribeiro-Claro P, Velaga SP. Solid-state vibrational spectroscopic investigation of cocrystals and salt of indomethacin. *CrystEngComm*. 2012;14(20):6665-74.

116. Limwikrant W, Nagai A, Hagiwara Y, Higashi K, Yamamoto K, Moribe K. Formation mechanism of a new carbamazepine/malonic acid cocrystal polymorph. *International Journal of Pharmaceutics*. 2012;431(1-2):237-40.
117. Liu X, Michalchuk AAL, Pulham CR, Boldyreva EV. An acetonitrile-solvated cocrystal of piroxicam and succinic acid with co-existing zwitterionic and non-ionized piroxicam molecules. *Acta Crystallographica Section C-Structural Chemistry*. 2019;75(Pt 1):29-37.
118. Guidance for Industry: Q8(R2) Pharmaceutical Development. Food and Drug Administration; 2009.
119. Guidance for Industry PAT — A Framework for Innovative Pharmaceutical Development, Manufacturing, and Quality Assurance. Food and Drug Administration; 2004.
120. Simone E, Zhang W, Nagy ZK. Application of Process Analytical Technology-Based Feedback Control Strategies To Improve Purity and Size Distribution in Biopharmaceutical Crystallization. *Crystal Growth & Design*. 2015;15(6):2908-19.
121. Zhang T, Yu QS, Li XR, Ma XX. Preparation of 2:1 urea-succinic acid cocrystals by sublimation. *Journal of Crystal Growth*. 2017;469:114-8.
122. Font-Bardia M, Alcobé X. X-ray single crystal and powder diffraction: possibilities and applications. In: Barcelona CCiTUD, editor. *Handbook of instrumental techniques for materials 2012*.
123. Elbagerma MA, Edwards HGM, Munshi T, Hargreaves MD, Matousek P, Scowen IJ. Characterization of New Cocrystals by Raman Spectroscopy, Powder X-ray Diffraction, Differential Scanning Calorimetry, and Transmission Raman Spectroscopy. *Crystal Growth & Design*. 2010;10(5):2360-71.
124. Padrela L, de Azevedo EG, Velaga SP. Powder X-ray diffraction method for the quantification of cocrystals in the crystallization mixture. *Drug Development and Industrial Pharmacy*. 2012;38(8):923-9.
125. Garbacz P, Wesolowski M. DSC, FTIR and Raman Spectroscopy Coupled with Multivariate Analysis in a Study of Co-Crystals of Pharmaceutical Interest. *Molecules*. 2018;23(9).
126. Næs T. A user-friendly guide to multivariate calibration and classification. Chichester, UK: NIR Publications; 2004. 344 p.
127. Jolliffe IT. *Principal component analysis*. 2nd ed. New York: Springer; 2002. xxix, 487 p. p.
128. Jolliffe IT. *Principal Component Analysis*. Second ed. New York: Springer-Verlag; 2002.

129. Lee I, Yang J. Common clustering algorithms, reference module in chemistry. *Molecular Sciences and Chemical Engineering*. 2009;2:577-618.
130. Ward JH. Hierarchical Grouping to Optimize an Objective Function. *Journal of the American Statistical Association*. 1963;58(301):236-44.
131. DrugBank. Hydrochlorothiazide 2005 [cited 2018 10 october]. Available from: <https://www.drugbank.ca/drugs/DB00999>.
132. Kester M, Karpa KD, Vrana KE. Renal System. *Elsevier's Integrated Review Pharmacology*. second ed: Elsevier; 2012. p. 153-60.
133. Kester M, Karpa KD, Vrana KE. 9 - Renal System. In: Kester M, Karpa KD, Vrana KE, editors. *Elsevier's Integrated Review Pharmacology*. Second Edition ed2012. p. 153-60.
134. A global brief on hypertension. World Health Organization; 2013.
135. Duarte JD, Cooper-DeHoff RM. Mechanisms for blood pressure lowering and metabolic effects of thiazide and thiazide-like diuretics. *Expert Rev Cardiovasc Ther*. 2010;8(6):793-802.
136. Pickkers P, Hughes AD, Russel FGM, Thien T, Smits P. Thiazide-induced vasodilation in humans is mediated by potassium channel activation. *Hypertension*. 1998;32(6):1071-6.
137. Deppeler HP. Hydrochlorothiazide. In: Florey K, editor. *Analytical profiles of drug substances*. 101981. p. 405–41.
138. Beermann B, Groschinskygrind M, Rosen A. Absorption, Metabolism, and Excretion of Hydrochlorothiazide. *Clinical Pharmacology & Therapeutics*. 1976;19(5):531-7.
139. PubChem [cited 2019 July 1]. Available from: <https://pubchem.ncbi.nlm.nih.gov/>.
140. El-Gizawy SA, Osman MA, Arafa MF, El Maghraby GM. Aerosil as a novel co-crystal co-former for improving the dissolution rate of hydrochlorothiazide. *International Journal of Pharmaceutics*. 2015;478(2):773-8.
141. Arafa MF, El-Gizawy SA, Osman MA, El Maghraby GM. Sucralose as co-crystal co-former for hydrochlorothiazide: development of oral disintegrating tablets. *Drug Development and Industrial Pharmacy*. 2016;42(8):1225-33.
142. Silva AFT, Sarraguca MC, Ribeiro PR, Santos AO, De Beer T, Lopes JA. Statistical process control of cocrystallization processes: A comparison between OPLS and PLS. *International Journal of Pharmaceutics*. 2017;520(1-2):29-38.
143. Clarke HD, Arora KK, Bass H, Kavuru P, Ong TT, Pujari T, et al. Structure-Stability Relationships in Cocrystal Hydrates: Does the Promiscuity of Water Make Crystalline Hydrates the Nemesis of Crystal Engineering? *Crystal Growth & Design*. 2010;10(5):2152-67.

144. Rager T, Hilfiker R. Cocrystal Formation from Solvent Mixtures. *Crystal Growth & Design*. 2010;10(7):3237-41.
145. Cares-Pacheco MG, Vaca-Medina G, Calvet R, Espitalier F, Letourneau JJ, Rouilly A, et al. Physicochemical characterization of D-mannitol polymorphs: The challenging surface energy determination by inverse gas chromatography in the infinite dilution region. *International Journal of Pharmaceutics*. 2014;475(1-2):69-81.
146. Luu V, Jona J, Stanton MK, Peterson ML, Morrison HG, Nagapudi K, et al. High-throughput 96-well solvent mediated sonic blending synthesis and on-plate solid/solution stability characterization of pharmaceutical cocrystals. *International Journal of Pharmaceutics*. 2013;441(1-2):356-64.
147. Kojima T, Tsutsumi S, Yamamoto K, Ikeda Y, Moriwaki T. High-throughput cocrystal slurry screening by use of in situ Raman microscopy and multi-well plate. *International Journal of Pharmaceutics*. 2010;399(1-2):52-9.
148. Presswala L, Matthews ME, Atkinson I, Najjar O, Gerhardstein N, Moran J, et al. Discovery of bound and unbound waters in crystalline amino acids revealed by thermal analysis. *Journal of Thermal Analysis and Calorimetry*. 2008;93(1):295-300.
149. Lobmann K, Laitinen R, Grohganz H, Strachan C, Rades T, Gordon KC. A theoretical and spectroscopic study of co-amorphous naproxen and indomethacin. *International Journal of Pharmaceutics*. 2013;453(1):80-7.
150. Lobmann K, Laitinen R, Strachan C, Rades T, Grohganz H. Amino acids as co-amorphous stabilizers for poorly water-soluble drugs - Part 2: Molecular interactions. *European Journal of Pharmaceutics and Biopharmaceutics*. 2013;85(3):882-8.
151. Peng CG, Chow AHL, Chan CK. Hygroscopic study of glucose, citric acid, and sorbitol using an electrodynamic balance: Comparison with UNIFAC predictions. *Aerosol Science and Technology*. 2001;35(3):753-8.
152. Lafontaine A, Sanselme M, Cartigny Y, Cardinael P, Coquerel G. Characterization of the transition between the monohydrate and the anhydrous citric acid. *Journal of Thermal Analysis and Calorimetry*. 2013;112(1):307-15.
153. Hirano A, Kameda T, Arakawa T, Shiraki K. Arginine-Assisted Solubilization System for Drug Substances: Solubility Experiment and Simulation. *Journal of Physical Chemistry B*. 2010;114(42):13455-62.
154. Affandi MMRMM, Tripathy M, Shah YAA, Majeed ABA. Solubility enhancement of simvastatin by arginine: thermodynamics, solute-solvent interactions, and spectral analysis. *Drug Design Development and Therapy*. 2016;10:959-69.
155. Figueiras A, Sarraguca JMG, Pais AACC, Carvalho RA, Veiga JF. The Role of L-arginine in Inclusion Complexes of Omeprazole with Cyclodextrins. *American Association of Pharmaceutical Scientists*. 2010;11(1):233-40.